Polygenic risk for schizophrenia converges on alternative polyadenylation as molecular mechanism underlying synaptic impairment

Florian J. Raabe[1,2,3,22], Anna Hausruckinger[1,4,22], Miriam Gagliardi[4,5,22], Ruhel Ahmad[1], Valeria Almeida[2,6], Sabrina Galinski[2,7] Anke Hoffmann[8], Liesa Weigert[1], Christine K. Rummel[1,3], Vanessa Murek[1], Lucia Trastulla[1], Laura Jimenez-Barron[1], Alessia Atella[4,5], Susanne Maidl[1], Danusa Menegaz[9], Barbara Hauger[9], Eva-Maria Wagner[9], Nadia Gabellini[2], Beate Kauschat[2], Sara Riccardo[10,11], Marcella Cesana[10,12], Sergi Papiol[2,9,13], Vincenza Sportelli[8], Monika Rex-Haffner[8], Sebastian J. Stolte[2], Michael C. Wehr[2,7], Tatiana Oviedo Salcedo[2], Irina Papazova[14], Sevilla Detera-Wadleigh[15], Francis J McMahon[15], Andrea Schmitt[2,16], Peter Falkai[2,9], Alkomiet Hasan[14], Davide Cacchiarelli[10,17,18], Udo Dannlowski[19], Igor Nenadić[20], Tilo Kircher[20], Volker Scheuss[2,21], Matthias Eder[9], Elisabeth B. Binder[8], Dietmar Spengler[8], Moritz J. Rossner[2]*, and Michael J. Ziller[1,4,5]*

Affiliations

[1]Lab for Genomics of Complex Diseases, Max Planck Institute of Psychiatry, 80804 Munich, Germany

[2]Department of Psychiatry and Psychotherapy, LMU University Hospital, LMU Munich, 80336 Munich, Germany

[3]International Max Planck Research School for Translational Psychiatry (IMPRS-TP), 80804 Munich, Germany

[4]Department of Psychiatry, University of Münster, 48149 Münster, Germany

[5]Center for Soft Nanoscience, University of Münster, 48149 Münster, Germany

[6]Institute of Biology, University of Campinas (UNICAMP), Campinas, São Paulo, Brazil.

[7]Systasy Bioscience GmbH, 81669 Munich, Germany

[8]Department of Translational Research in Psychiatry, Max Planck Institute of Psychiatry, 80804 Munich, Germany

[9]Max Planck Institute of Psychiatry, 80804 Munich, Germany

[10]Telethon Institute of Genetics and Medicine (TIGEM), Armenise/Harvard Laboratory of Integrative Genomics, Pozzuoli, Italy

[11]NEGEDIA (Next Generation Diagnostic), Pozzuoli, Italy

[12]Department of Advanced Biomedical Sciences, University of Naples "Federico II", Naples, Italy

[13]Institute of Psychiatric Phenomics and Genomics (IPPG), University Hospital, LMU Munich, 80336 Munich, Germany

[14]Department of Psychiatry, Psychotherapy, and Psychosomatics, Medical Faculty, University of Augsburg, 86156 Augsburg, Germany

[15]Human Genetics Branch, National Institute of Mental Health Intramural Research Program (NIMH-IRP), Bethesda, MD, 20892, USA

[16]Laboratory of Neuroscience (LIM27), Institute of Psychiatry, University of São Paulo, São Paulo-SP 05403-903, Brazil

[17]School for Advanced Studies, Genomics and Experimental Medicine Program, University of Naples "Federico II", Naples, Italy

[18]Department of Translational Medicine, University of Naples "Federico II", Naples, Italy
[19]Institute for Translational Psychiatry, University of Münster, 48149 Münster, Germany
[20]Department of Psychiatry and Psychotherapy, Philipps-University and University Hospital Marburg, UKGM, 35039 Marburg, Germany
[21]MSH Medical School Hamburg, Hamburg, Germany
[22]these authors contributed equally
*Corresponding authors: ziller@uni-muenster.de, moritz.rossner@med.uni-muenchen.de

Abstract

Schizophrenia (SCZ) is a genetically heterogenous psychiatric disorder of highly polygenic nature. Correlative evidence from genetic studies indicate that the aggregated effects of distinct genetic risk factor combinations found in each patient converge onto common molecular mechanisms. To prove this on a functional level, we employed a reductionistic cellular model system for polygenic risk by differentiating induced pluripotent stem cells (iPSCs) from 104 individuals with high polygenic risk load and controls into cortical glutamatergic neurons (iNs). Multi-omics profiling identified widespread differences in alternative polyadenylation (APA) in the 3' untranslated region of many synaptic transcripts between iNs from SCZ patients and healthy donors. On the cellular level, 3'APA was associated with a reduction in synaptic density of iNs. Importantly, differential APA was largely conserved between postmortem human prefrontal cortex from SCZ patients and healthy donors, and strongly enriched for transcripts related to synapse biology. 3'APA was highly correlated with SCZ polygenic risk and affected genes were significantly enriched for SCZ associated common genetic variation. Integrative functional genomic analysis identified the RNA binding protein and SCZ GWAS risk gene PTBP2 as a critical trans-acting factor mediating 3'APA of synaptic genes in SCZ subjects. Functional characterization of PTBP2 in iNs confirmed its key role in 3'APA of synaptic transcripts and regulation of synapse density. Jointly, our findings show that the aggregated effects of polygenic risk converge on 3'APA as one common molecular mechanism that underlies synaptic impairments in SCZ.

Introduction

Schizophrenia (SCZ) is a highly debilitating psychiatric disorder originating from the complex interplay of genetic and environmental factors[1]. Genetics has offered a compelling handle on the biological basis of SCZ due its overall high heritability of 79%[2]. Genome Wide Association Studies (GWAS) identified more than 270 common[3] and 32 rare genetic risk factors[4], underscoring the highly polygenic architecture of disease risk in SCZ. Similar results have been obtained for other psychiatric disorders such as major depression (MDD)[5] and bipolar disorder (BD)[6]. Genomic and pathway level annotation studies based on the biological role of the genes within these risk loci implicated synapse, immune and transcriptional control as key processes altered in SCZ and other psychiatric diseases[7,8]. Moreover, scRNAseq from post-mortem brains showed that the expression of SCZ risk genes was highly enriched in excitatory and inhibitory neurons of the cortex[3,4].

However, the molecular mechanisms underlying the de-regulation of these genes in disease as well as their contribution to disease etiology at the functional level remain largely unknown.

To address the former challenge, previous studies focused on the functional characterization of individual common variants (CVs) and the associated genes identified in GWA studies[9,10]. These analyses revealed how disease associated variants alter the regulation of individual genes in *cis*, including modulation of gene expression levels, the chromatin state of regulatory elements or

alterations of gene splicing patterns, effectively acting as quantitative trait loci (QTL)[11-13]. Jointly, these molecular mechanisms are currently estimated to modulate 20-30% of disease associated GWAS loci[11,12,14], indicating the presence of additional yet unknown molecular mechanisms contributing to impairment of gene function.

Such variant and gene-centric studies greatly improved our understanding of the biological function of individual genetic variants. However, their impact on our understanding how these individual variant effects converge on common molecular mechanisms contributing to the etiology of mental illness remains limited.

This limitation is rooted in the high prevalence of common disease associated genetic variants in the general population. Therefore, each variant individually contributes only minimally to overall disease risk and is in isolation not capable to drive disease relevant alterations in molecular and cellular processes. Instead, its disease relevant biological function is highly dependent on the presence of other genetic risk variants. Moreover, due to the highly polygenic architecture of disease risk in SCZ, the patient population is characterized by an extreme heterogeneity in genetic risk variant distribution, leaving almost every patient with an individual genetic risk factor profile.

Thus, in a complementary line of research, large cohort studies sought to pinpoint the aggregated effects of genetic risk factors as well as life and treatment history on postmortem brain samples from individuals with psychiatric disorders and neurotypical controls[11,13]. Although these analyses identified widespread changes in gene expression and splicing patterns in the prefrontal cortex (PFC) of adult individuals with SCZ, BD or ASD, associations between transcriptional changes with common genetic risk factors and in particular polygenic risk were modest to small. The latter observation likely reflects a strong impact of a lifelong disease history on the transcriptome as well as the relevance of additional molecular mechanisms in mediating the converging effect of polygenic risk factors in mental illness. In this respect, post-transcriptional mRNA regulation constitutes an additional disease relevant molecular mechanism potentially mediating polygenic risk factor effects, given its prominent role in neuronal physiology[15] and complex genetic regulation[16,17].

Here, we sought to translate the effects of highly heterogenous polygenic risk across individuals into common molecular mechanisms underlying the etiology in SCZ. Therefore, we set out to pinpoint the joint functional effects of genetic risk factors on a wide array of molecular and cellular phenotypes in a genetic model system relevant to mental illness.

Therefore, we leveraged the unique feature of iPSCs to capture the polygenetic risk architecture of each individual and assessed the aggregated functional consequences of these genetic risk factors on molecular and cellular endophenotypes in the absence of patient level environmental confounders.

Consistent with previous studies, these analyses identified moderate changes in the transcriptome and epigenome of neuronal cells from individuals with SCZ (ISCZ) and the absence of association with polygenic risk. In stark contrast, analysis of post-transcriptional alterations revealed that highly heterogeneous polygenic risk converges on the alternative polyadenylation of the 3' untranslated region (3'APA) of many key synaptic genes. Moreover, we identify de-regulation of the trans-acting RNA binding protein and SCZ risk gene *PTBP2* as one critical contributor to 3'APA in SCZ and demonstrate its role in modulating synaptic density as disease relevant cellular endophenotype.

A comprehensive iPSC cohort from patients with mental illness

We assembled a large cohort of individuals from European ancestry with major psychiatric disorders as well as healthy controls from several research cohorts[18-21] (**Fig. 1a**). Given that SCZ

genetically correlates with bipolar disorder (BD) and unipolar major depressive disorder (MDD)[22,23], we also included individuals with these diseases to evaluate the specificity of polygenically driven effects. This cohort (n=104) comprised neurotypical (healthy) controls (HC, n = 38), and individuals with SCZ (ISCZ, n=38), BD (n = 20) and MDD (n = 8) (**Supplementary Table 1**) with a mean age of onset in the late 20s adolescence (mean 28.5/27.1/29.1 SCZ/BD/MDD).

Importantly, ISCZ exhibited increased polygenic risk scores for SCZ (PRS-SCZ) (p= 0.0045, two-sided Wilcoxon-Test; **Fig. 1b**) concomitant with the general absence of copy number variations previously associated with SCZ (**Extended Data Fig. 1a**). Moreover, all individuals were characterized by a highly heterogeneous distribution of genetic risk factors for SCZ based on common genetic variants identified by GWAS (**Extended Data Fig. 1b**), implying private genetic risk factor profiles. In contrast, no difference in PRS for BD or MDD was detected between any diagnosis group (**Extended Data Fig. 1c,d**). Finally, our cohort also encompasses a set of 4 ISCZ whose cells have been investigated in many pioneering/previous iPSC studies on SCZ as additional points of comparison[25].

We generated 106 iPSC lines from the present cohort and previous set[25] and subjected them to comprehensive quality control (**Fig. 1a**) including digital karyotyping (**Supplementary Data 1**), analysis of pluripotency (**Supplementary Data 2**), differentiation potential and lineage marker analysis (**Extended Data Fig. 1e-l**).

All iPSC lines passing quality control and devoid of genetic aberrations were differentiated into iNs over a timeline of 49 days, relying on lentiviral transduction of Neurogenin-2 (*Ngn2*) in conjunction with small molecule application[26] (**Fig. 1a**). To facilitate cross-lab reproducibility, the iPSC cohort was split in two groups and differentiation experiments were performed at two distinct sites (**Fig. 1a**). For iN analysis, we established a comprehensive multi-layered endophenotype pipeline including deep molecular phenotyping by RNA-Seq and alternative polyadenylation analysis (n=93 donors), ATAC-Seq (n=96 donors) as well as subsets for microRNA-Seq (n=85 donors) followed by high content imaging (n=20 donors) for synaptic density assessment (**Fig. 1a**).

Molecular characteristics of iNs from patients with psychiatric disorders

RNA-Seq and immunocytochemistry (ICC) based analysis confirmed differentiation into well-matured excitatory iNs (**Extended Data Fig. 2a-c)** in line with previous reports[26]. Single cell RNA-Seq (scRNA-Seq) analysis of iNs from 4 donors confirmed bulk and ICC measurements, revealing 7 distinct clusters, mostly differing by excitatory neuron subtype marker expression and/or maturation stage (**Extended Data Fig. 2d-f)**. *In silico* deconvolution of iN bulk RNA-Seq profiles using marker gene sets derived from each cluster of the scRNA-Seq iN data[27] revealed uniform differentiation across the lines with little variation in cellular composition for BD iNs and no difference between iNs from HC and ISCZ (**Extended Data Fig. 2g**). These results underscore the absence of gross differences in cellular identity and distribution or developmental trajectory among iNs from cases and controls. Similarly, basic electrophysiological properties were comparable between neurons from different diagnosis groups and comparable to mature primary human or mouse neurons[28] except for differences in input resistance (**Extended Data Fig. 2h-i**). In line with these findings and iN marker expression (**Extended Data Fig. 2a**), iNs most closely cluster with excitatory neurons of progressed post-natal development (P7) (**Extended Data Fig. 2j**) based on previously published transcriptomic signatures of the developing mouse cortex[29]. Finally, principal component analyses of the RNA-Seq, ATAC-Seq and microRNA-Seq datasets revealed no clustering by diagnostic group in either of the modalities (**Fig. 1c-e**). Instead,

diagnostic groups were highly interspersed, indicating no fundamental differences in cellular state between the diagnosis groups.

QTL mapping across molecular features identifies multi-layered mechanisms of cis-acting genetic variation contributing to polygenic risk in SCZ

Gene expression, open chromatin and microRNA expression levels constitute a critical substrate of psychiatric disorder associated genetic variation[30,31]. Therefore, we sought to pinpoint *cis*-acting variants driving alterations in these molecular layers in iNs across patients and healthy donors. The quantitative trait locus (QTL) analysis identified 1,331 genes (eQTLs), 4,904 open chromatin peaks (caQTLs), 6 microRNAs (miQTLs) subject to modulation by genetic variants in *cis* (**Fig. 1f-h**). Importantly, 55.4% of the identified eQTLs overlapped with eQTLs identified in adult human tissue from the prefrontal cortex (PFC)[11], supporting their *in vivo* relevance (**Fig. 1f** and **Supplementary Table 2**). For open chromatin and microRNAs, no large publicly available reference datasets from relevant primary tissues are currently available to confirm their overlap. Nevertheless, 21.7% of the identified open chromatin peaks associated with caQTLs overlapped with eQTLs detected in bulk PFC. (**Fig. 1g** and **Supplementary Table 2**).

Interestingly, the overlap of QTLs across molecular features in iNs was limited, with 24.9% of eQTL overlapping with caQTLs (**Fig. 1l** and **Supplementary Table 2**). These observations support the notion that distinct *cis* acting variations affect different molecular layers with likely distinct downstream effects. Moreover, 28 genes, 78 peaks and no microRNA with e/ca/miQTLs overlapped with GWAS risk loci for SCZ (**Fig. 1f-h** and **Supplementary Table 2**).

Among the identified QTLs co-localizing with SCZ GWAS risk loci was a caQTL at the *SNX19* and the *KCNQ2* locus (both also observed in PFC) (**Fig. 1j-n**) as well as multiple multiple caQTL in intronic regions of *NRXN1* (**Extended Data Fig. 3a**). This is of particular interest as one of these caQTLs is located in an alternative promoter of *NRXN1* and thus potentially contributes to the previously reported isoform abundance diversity of *NRXN1* in ISCZ[32].

In summary, these observations underscore the capacity of iNs to capture a substantial fraction of the functional effects of genetic variation on disease relevant molecular layers from human PFC. Moreover, these findings also reveal a substantial diversity in the affected molecular features in *cis*, as distinct common variants modulate gene expression, microRNA expression or chromatin accessibility.

Identification of differentially regulated molecular features in iNs from ISCZ

Going beyond individual *cis*-mediated genetic effects, we next leveraged the unique feature of iNs to assess the aggregated functional consequences of distinct polygenic risk profiles in SCZ (**Figures 1b, Extended Data Fig. 1a,b**) in the absence of medication and environmental confounders. To that end, we investigated an array of molecular layers in iNs from HC and ISCZ, including gene expression, microRNA expression, open chromatin marks and alternative polyadenylation as post-transcriptional regulatory mechanism.

Following a detailed power evaluation (**Extended Data Fig. 3b-d**), we performed differential expression analysis and identified 467 transcripts (365 protein coding and 102 non-coding transcripts) (FDR≤0.01, $|\log_2 FC|\geq 0.4$; **Fig. 2a** and **Extended Data Fig. 3e,** and **Supplementary Table 3**), henceforth referred to as DEGs as well as 67 micro RNAs (FDR≤0.05; **Fig. 2b** and **Supplementary Table 3)**. For open chromatin regions, no peaks with differential accessibility were detected significant after multiple testing correction (FDR≤0.05; **Extended Data Fig. 3f**) despite high reproducibility of the generated profiles (**Extended Data Fig. 3g**). This might reflect overall lower sensitivity of the ATAC based data.

Among the differentially expressed microRNAs, we identified several miRs that have been implicated previously in SCZ by GWAS (e.g. miR-135a, miR-137, miR-1180)[33] and/or with their targetome connected to SCZ risk genes (e.g. miRNA-1, miR-7-5p, mir-9-5p)[34,35]. Moreover, several differentially expressed microRNAs in iNs were also found to be differentially present in peripheral blood of SCZ patients (e.g. let-7g, miR-7, miR-34a-5p, miR-218-5p, miR-132)[36,37] (**Fig. 2b)**, suggesting their trans-tissue and potentially diagnostic relevance.

The set of DEGs included 39 SCZ GWAS risk genes while 18 were associated with eQTLs and 36 with caQTL in iNs (**Fig. 2a).** Moreover, 36 DEGs overlapped with DEGs from human PFC comparing neurotypical controls and ISCZ (**Fig. 2a**). However, mean expression of DEGs across samples did not associate with SCZ-PRS (p=0.13, r2=-0.169). Lastly, we note a high disease specificity of DEGs in the SCZ (n=467) and the BD/MDD (n=11 genes) cohorts compared to the neurotypical group with only 1 gene (*PPIAP11*) being shared among the two psychiatric disorders (**Extended Data Fig. 3h**). Notably, we also detected expression differences in multiple genes critical for synaptic function and neuronal activity[38] such as *NLGN2, SHANK3, RAB21, RAB27B, ADAM10, CACNA1A and SCNN1D* to be downregulated in iNs from ISCZ (**Fig. 2a**). Pathway level enrichment did not yield any significant results for genes up-regulated in ISCZ and implicated protein metabolism related processes for down-regulated genes. Consistent with previous reports[13], most of the DEGs, including those with roles in synaptic and neuronal activity, do not harbor any association signal in SCZ or BD GWAS in *cis* range.

Widespread 3'APA of synaptic genes in ISCZ

Going beyond previously investigated molecular traits, we next assessed post-transcriptional mRNA regulation as potential mechanism mediating polygenic risk effects in SCZ. We focused on alternative polyadenylation of the 3' untranslated region (UTR) as the non-protein coding section of the messenger RNA that follows the stop codon. This region contains numerous RNA cis-regulatory elements relevant for the post-transcriptional regulation of the mRNA, modulating RNA stability, translation rates and subcellular localization[39]. Thus, alternative length and composition of the 3'UTR can have a profound impact on these properties of the mRNA, resulting in a critical role in neuronal physiology and synapse biology[15].

We mapped polyadenylation sites (PAS) in iNs from ISCZ using 3'RNA-Seq and identified a total of 19,960 PAS of which 7,812 were not previously detected (**Fig. 3a,b**). Subsequently, we leveraged this library of PAS in combination with our iNs RNA-Seq dataset to identify differential 3'UTR APA events between HC and ISCZ[40].

This analysis revealed widespread differences in APA, identifying 628 differential APA (dAPA) events (**Fig. 3c** and **Supplementary Table 3**) that resulted from an increased usage of either the distal or the proximal PAS to similar degree (14.29% of all genes with more than 1 polyadenylation site). In agreement with the sequencing data, qPCR confirmed dAPA for *SORT1* and *SCN8A* (**Fig. 3d**), two genes with a critical role in synapse function. In contrast, we detected virtually none dAPA events between HC and BD/MDD iNs (**Extended Data Fig. 4a**).

In order to probe the relevance of differential APA under *in vivo* conditions, we repeated the same analysis using previously published bulk RNA-Seq samples from human DLPFC in 291 controls and 275 ISCZ[11]. Consistent with the observations in iNs, this analysis confirmed widespread dAPA in postmortem PFC from ISCZ (**Fig. 3e** and **Supplementary Table 3**) as well as substantial overlap with dAPA in iNs (**Fig. 3f**). Interestingly, dAPA in iNs from ISCZ showed considerable overlap with transcripts subject to dAPA over the course of cortical development and maturation in the mouse (**Fig. 3g** and **Extended Data Fig. 4b**), suggesting a critical role of APA as one mechanism contributing to the neurodevelopmental origins of SCZ.

Strikingly, genes subject to dAPA in ISCZ were strongly enriched for synapse related processes such as glutamatergic neurotransmission, synaptic membrane components, synaptic plasticity or vesicle biology in both iNs and human PFC (**Fig. 4a**,**b**, and **Supplementary Table 3**). In particular, dAPA affected key synaptic genes such as the glutamate receptor subunits *GRIA1*, *SNCA*, *DLG3* as well as *CPLX2* critical for synaptic vesicle fusion in the forebrain[41], the sodium channel *SCN8A* or *SORT1* involved in subcellular trafficking[42] (**Fig. 3a** and **3e**).

To assess the functional relevance of these SCZ specific changes in APA for synapse biology, we measured synapse density by high content imaging across 20 donors (**Fig. 4c**). This analysis identified a significant reduction in synapse density (**Fig. 4d**; p-value=0.0052, LMM) between iNs derived from HC (N=10 donors) and ISCZ (N=10 donors). These results were further confirmed by quantitative western blot, revealing a discrete but significant reduction PSD95 abundance in iNs from ISCZ (**Fig. 4e,f**; p=0.0024, LMM). Jointly, these observations implicate APA as a novel mechanism contributing to alterations in synapse biology in SCZ. Importantly, consistent changes in APA across iNs and PFC suggests genetic origins of differential APA in SCZ, and support that iPSC-based models faithfully capture well-known (e.g. eQTLs) as well as until now unknown (e.g. dAPA) functional consequences of genetic factors.

Polygenic control of differential 3'UTR APA in SCZ

To probe the link between dAPA and genetic risk in more detail, we evaluated whether or not the gene loci subject to dAPA in SCZ were enriched for SCZ associated common risk variants using partition heritability analysis[43]. This analysis revealed a significant and specific enrichment of genes affected by dAPA in iNs as well as in PFC for SCZ risk, implying a close link of APA to the genetic risk for SCZ (**Fig. 5a**).

Based on these observations, we tested the hypothesis that overall APA is a polygenically driven mechanism in SCZ, resulting from the joint action of distinct *cis*- and *trans*-acting variants. Therefore, we determined the association of cumulated APA in individual donor iN across all transcripts subject to dAPA between HC and SCZ with the respective individual polygenic risk for SCZ, BD or MDD. This analysis revealed a significant association between SCZ PRS and cumulative APA (**Fig. 5b**; r=0.26, p=0.02) but not BD or MDD PRS (**Extended Data Fig. 4c,d**), suggesting polygenic origins of dAPA consistent with overall GWAS signal enrichment (**Fig. 5a**). In contrast, association of cumulated APA across transcripts subject to dAPA between HC and BD/MDD using relaxed statistical inclusion criteria (q-value≤0.1) did not show any association with any PRS (**Extended Data Fig. 4e-g).**

To pinpoint specific genetic variants contributing to dAPA, we evaluated *cis*-acting common SNPs for their potential to operate as APA qTLs. This analysis revealed no associations, likely due to lack of power. Given the importance of *trans*-acting factors as potential amplifiers of *cis*-regulatory variants and the previously reported role of RNA binding proteins (RBPs) in the genetic basis of mental disorders[17], we sought to identify de-regulated RBPs as potential causes of dAPA in iNs from ISCZ. RBP motif analysis in the UTRs of transcripts subject to dAPA identified numerous expressed RBPs with critical roles for neuronal biology such as QKI, ELAVL and RBM proteins (**Fig. 5c** and **Supplementary Table 3**). However, only PTBP2 and PCBP2 were also differentially expressed between iNs from HC and ISCZ. PTBP2 had previously been implicated in APA[44] and differential expression in iNs ($p=3.24x10^{-5}$; **Fig. 5d**) extended to postmortem PFC (p=0.018) when comparing HC and ISCZ. Importantly, PTBP2 expression showed a high correlation to APA of transcripts subject to dAPA in iNs (**Fig. 5e**, blue) compared to APA of randomly selected transcripts (**Fig. 5e**, grey, and **Extended Data Fig. 5**).

In addition, PTBP2 is located in a SCZ GWAS risk locus (**Extended Data Fig. 5a)** which harbors multiple regulatory elements in iNs and PFC and exhibits a significant eQTL in both iNs and PFC (**Fig. 5f**), indicating de-regulation of PTBP2 by *cis*-acting SCZ associated genetic variation (**Extended Data Fig. 5b**). However, in light of the low difference in risk allele frequency distribution of the PTBP2 eQTL, *cis*-acting genetic effects can only explain a fraction of PTBP2 de-regulation in SCZ ($R^2_{rs72721996}$ =0.065). However, in addition to cis-acting genetic variation, PTBP2 mRNA was predicted to be targeted by the SCZ associated microRNA let-7-5p[45] (**Fig. 2b**) acting in trans. In line with this prediction, we observe an anti-correlation of PTBP2 expression with miR-let-7-5p ($R_{Pearson}$=-0.318) and a significant increase in explained variance of overall PTBP2 expression ($R^2_{rs72721996+let\text{-}7\text{-}5p}$= 0.1901) based on a linear model incorporating donor genotype and let-7-5p expression (p=0.00257, **Extended Data Fig. 5c).** Jointly, these observations support the notion that multifactorial de-regulation of PTBP2 expression levels partially mediates dAPA in neuronal cells from ISCZ.

Based on these findings, we evaluated whether or not PTBP2 contributes to dAPA in iNs from ISCZ through shRNA mediated acute knockdown (**Fig. 6a**,**b**). RNA-Seq based assessment of dAPA between PTBP2^{KD} and scramble control in iNs revealed widespread dAPA (**Fig. 6c**; n=546), biased towards usage of the more proximal polyadenylation site in the KD condition (n=432 vs n=114). Affected transcripts showed substantial overlap with dAPA between HC and ISCZ in iNs as well as PFC (**Fig. 6d**), suggesting a contribution of PTBP2 to dAPA in these conditions. Similar to the conditions in iNs and PFC from ISCZ, transcripts affected by dAPA upon PTBP2 knockdown were enriched for various synapse related processes (**Fig. 6e**).

Subsequent assessment of synaptic density in PTBP2^{KD} iNs revealed a significant increase in synapse density (**Fig. 6f**) and PSD-95 protein level (**Fig. 6g**). These results corroborate a decrease in synaptic density and PSD-95 levels upon higher expression of PTBP2 in iNs and PFC from ISCZ, supporting a causal role of PTBP2 in mediating APA dependent changes in synaptic components.

Jointly, these findings establish dAPA as molecular mechanism through which diverse SCZ associated genetic variants contribute to synaptic changes in disease relevant glutamatergic neurons of the brain. Moreover, our results demonstrate convergence of diverse *cis*- and *trans*-acting genetic variants specific to SCZ on one common molecular mechanism.

Discussion

In this study, we tested the hypothesis whether polygenic and heterogenous genetic risk for psychiatric disease does <u>functionally converge</u> across patients onto common molecular mechanisms that regulate genes with a central role in disease relevant processes.

To that end, we employed the largest iPSC cohort in the field of psychiatry until today to unravel the functional consequences of distinct polygenic risk factor combinations. This endeavor identified numerous new as well as previously implicated genes and microRNAs associated with SCZ or BD in iPSC-derived neurons.

However, the majority of the identified genes are not located in loci identified by SCZ GWAS and do not seem to be modulated by single *cis*-acting regulators. Instead, the expression of these genes is rather governed by a complex matrix of multiple *cis*- and *trans*-acting factors. Given the minimal differences in disease associated allele frequency of GWAS hits and corresponding heterogeneity in genetic risk factor combinations across the patient population, this is not surprising. Against this background, it is highly unlikely to observe consistently altered genes in GWAS loci, if their effect is expected to be caused predominantly by *cis* acting CVs.

In this study, diagnosis associated changes in gene expression, microRNA expression and open chromatin in iNs showed limited enrichment for specific biological processes or genetic risk. Instead, we identify APA as new mechanism contributing to the molecular basis of SCZ, particularly affecting synaptic genes. Importantly, APA in iNs and PM is significantly associated with SCZ polygenic risk, suggesting a substantial *cis*-acting contribution of genetic risk from common variants to dAPA. Moreover, the consistent alteration of many transcripts across donors with diverse polygenic risk factor combinations implies the presence of functional convergence of these risk factors through dAPA. One potential mechanism that can mediate such functional convergence is the de-regulation of a *trans*-acting regulator of APA such as PTBP2. In this context, the alteration of PTBP2 expression can be driven by various causes such as *cis*-acting SCZ associated genetic variation or other *trans*-acting mechanisms (e.g. microRNAs) depending on the complex genetic background of each donor. The functional consequences of its de-regulation however result in the consistent APA of many synaptic transcripts across ISCZ, partially explaining the observed variation in APA in iNs and PFC.

We show that PTBP2 de-regulation directly impacts synapse density in iNs, with the directional effect consistent with the observation in ISCZ as one functional consequence of APA. It is well established that APA plays a key role in modulating mRNA half lifetime, translation efficiency as well as subcellular localization. Thus, given the large number and diversity of transcripts affected by APA, we hypothesize that APA in ISCZ leads to alterations in distinct physiological properties of neuronal cells, both in the adult brain and over the course of development.

Overall, our findings suggest that distinct genetic risk factor combinations in ISCZ control *cis*- and *trans*-acting regulators that converge on 3'UTR APA as one critical molecular mechanism that drives de-regulations of downstream effector genes with a prominent role in synaptic function. In perspective, our findings also offer conceptual insight into the long-standing question of how heterogeneous patient populations can share clinical diagnosis based on converging molecular psychopathology.

While this study focuses on SCZ, we further propose that deep phenotyping of well-powered iPSC studies can provide in general new insights into those molecular mechanisms, downstream effector genes, and biological processes on which polygenic risk converge and translates into phenotypic states. Such insights will be critical to narrow today's gap in genotype-phenotype relationships in complex diseases and to identify new therapeutic entry points.

Figures

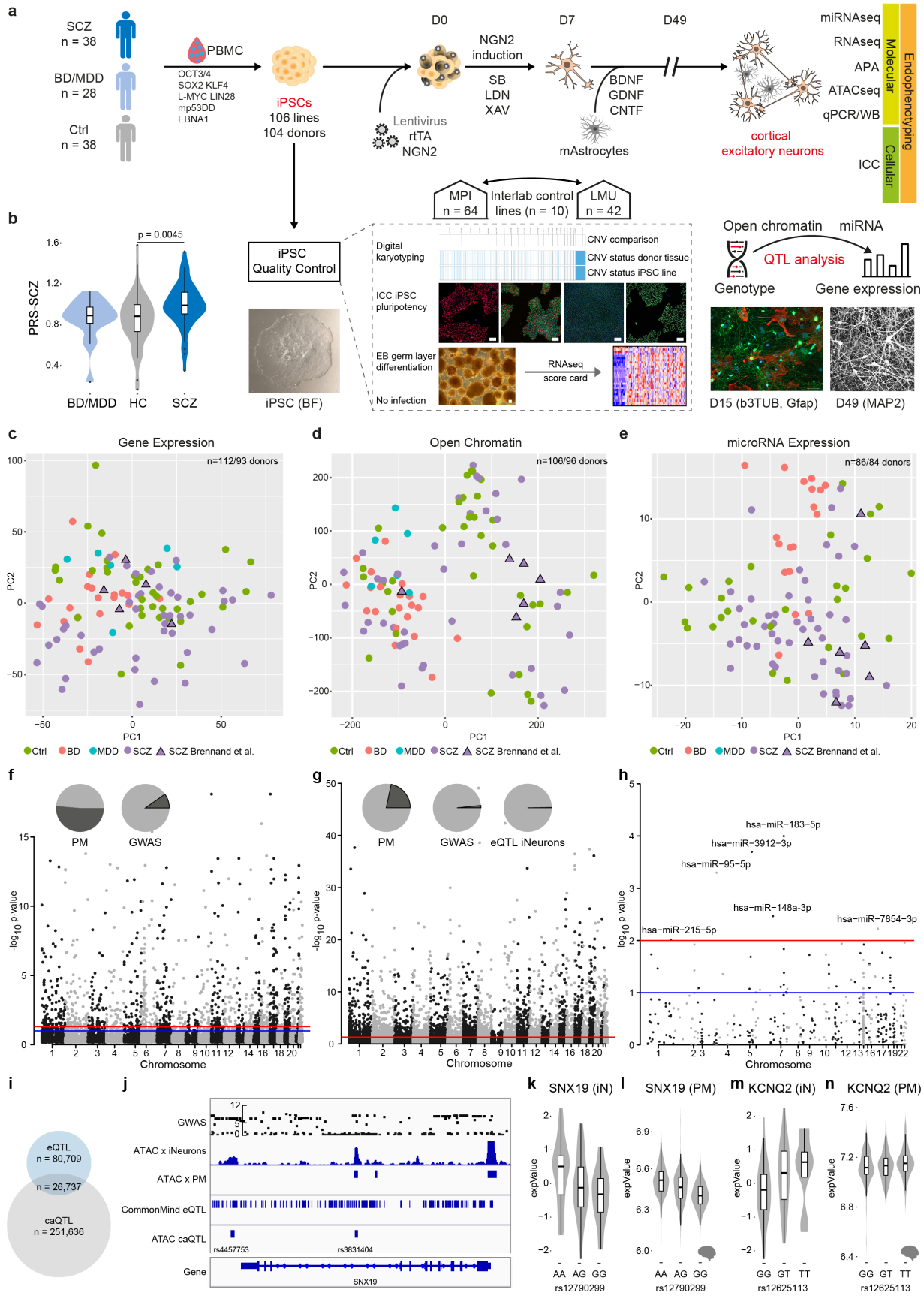
a
SCZ
n = 38
BD/MDD
n = 28
Ctrl
n = 38
PBMC
OCT3/4
SOX2 KLF4
L-MYC LIN28
mp53DD
EBNA1
iPSCs
106 lines
104 donors
Lentivirus
rtTA
NGN2
D0
NGN2
induction
SB
LDN
XAV
D7
BDNF
GDNF
CNTF
mAstrocytes
D49
cortical
excitatory neurons
miRNAseq
RNAseq
APA
ATACseq
qPCR/WB
ICC
Molecular
Cellular
Endophenotyping
MPI
n = 64
Interlab control
lines (n = 10)
LMU
n = 42
b
p = 0.0045
PRS-SCZ
BD/MDD
HC
SCZ
iPSC
Quality Control
iPSC (BF)
Digital
karyotyping
CNV comparison
CNV status donor tissue
CNV status iPSC line
ICC iPSC
pluripotency
EB germ layer
differentiation
RNAseq
score card
No infection
Open chromatin
miRNA
QTL analysis
Genotype
Gene expression
D15 (b3TUB, Gfap)
D49 (MAP2)
c
Gene Expression
n=112/93 donors
PC1
PC2
d
Open Chromatin
n=106/96 donors
e
microRNA Expression
n=86/84 donors
Ctrl
BD
MDD
SCZ
SCZ Brennand et al.
f
PM
GWAS
-log10 p-value
Chromosome
g
eQTL iNeurons
h
hsa-miR-183-5p
hsa-miR-3912-3p
hsa-miR-95-5p
hsa-miR-148a-3p
hsa-miR-7854-3p
hsa-miR-215-5p
i
eQTL
n = 80,709
n = 26,737
caQTL
n = 251,636
j
GWAS
ATAC x iNeurons
ATAC x PM
CommonMind eQTL
ATAC caQTL
rs4457753
rs3831404
Gene
SNX19
k
SNX19 (iN)
l
SNX19 (PM)
m
KCNQ2 (iN)
n
KCNQ2 (PM)
expValue
AA AG GG
rs12790299
GG GT TT
rs12625113

391

Fig. 1. Multi-omic profiling of iNeuron mental health cohort and quantitative trait analysis for gene expression, open chromatin and microRNA expression.

a, Schematic overview of iPSC line generation and differentiation to NGN2-directed cortical excitatory neurons (iNs), co-culturing with murine Astrocytes, and multi-modal endophenotyping after 49 days of differentiation which includes RNAseq, ATACseq, miRNAseq, qPCR, Western Blot (WB) on the molecular level, immunocytochemistry (ICC), fluorescence in situ hybridization (FISH) and electrophysiology by patch-clamp on a cellular level as well as multielectrode arrays (MEA) on the (micro)circuit level in a multicenter approach in order to perform a case-control study with patients affected with schizophrenia (SCZ), unipolar major depressive disorder (MDD), bipolar disorder (BD) and healthy controls (HC) to perform QTL analysis. iPSC characterization pipeline includes digital karyotyping using microarrays, immunocytochemistry (ICC) analysis of key pluripotency markers, and assessment of differentiation potential by embryoid body (EB) generation followed by RNA-Seq to perform score card assessment of the expressed germ layer signature. Infections with HIV, HCV, CMV and mycoplasma were excluded. Scale bars indicate 50µm.

b, Distribution of the individual polygenic risk score for schizophrenia (PGC3 SCZ) for the different diagnosis groups of hiPSC donors. P-value based on two-sided Wilcoxon-Test.

c, Principal component analysis of RNA-Seq based gene expression profiles across iN samples from 93 distinct donors at day 49. Different colors indicate diagnosis group and triangles highlight iPSC line donors originally employed by Brennand and colleagues and subsequently used in many investigations in the field for reference. The latter were re-derived from the same families for this study.

d, Principal component analysis of ATAC-Seq based open chromatin profiles across iN samples from 96 distinct donors at day 49. Different colors indicate diagnosis group and triangles highlight iPSC line donors originally employed by Brennand and colleagues for reference.

e, Principal component analysis of microRNA-Seq based profiles across 86 iNs samples from 86 distinct donors at day 49. Different colors indicate diagnosis group and triangles highlight iPSC line donors originally employed by Brennand and colleagues for reference.

f, Manhatten plot of eQTL association strength (y-axis) across all chromosomes (x-axis). Red line indicates global significance level after multiple testing correction, identifying 1,331 genes with at least one eQTL (FDR≤0.05). Pie charts indicate overlap (dark grey) of identified SNPs with eQTLs found in human post mortem DLPFC (left) or overlapping with SCZ GWAS risk loci (right).

g, Manhatten plot of caQTL association strength (y-axis) across all chromosomes (x-axis). Red line indicates global significance level after multiple testing correction, identifying 4,904 peaks with at least one caQTL (Bonferroni corrected p-value ≤ 0.01). Pie charts indicate overlap (dark grey) of identified SNPs with eQTLs found in human post mortem DLPFC (left), overlapping with SCZ GWAS risk loci (middle) or with eQTLs identified in iNs (right).

h, Manhatten plot of mirQTL association strength (y-axis) across all chromosomes (x-axis). Red line indicates global significance of permutation based p-value, identifying 6 microRNAs (p-value ≤ 0.01) with at least one mirQTL.

i, Venn diagram showing the overlap of SNPs identified as eQTL and caQTL associated SNPs.

j, Representative example of genomic annotations and distinct QTL types at the sorting nexin 19 (*SNX19)* locus, left: from top to bottom: Association strength of imputed SNPs at the locus with SCZ based on SCZ GWAS from Ripke et al. 2013, ATAC-Seq profile of representative iNs at day 49 and post mortem cortex, eQTLs detected at the locus in iNs, caQTLs detected at the locus co-localizing with open chromatin regions.

k, Distribution of normalized gene expression level of SNX19 in iNs (y-axis) by allele status (x-axis).
l, Distribution of normalized gene expression level of SNX19 (y-axis) in human post mortem DLPFC by allele status (x-axis).
m, Distribution of normalized gene expression level of the voltage gate potassium channel, subfamily Q, member 2 (*KCNQ2* y-axis) in iNs by allele status.
n, Distribution of normalized gene expression level of *KCNQ2* (y-axis) in human post mortem DLPFC by allele status (x-axis).

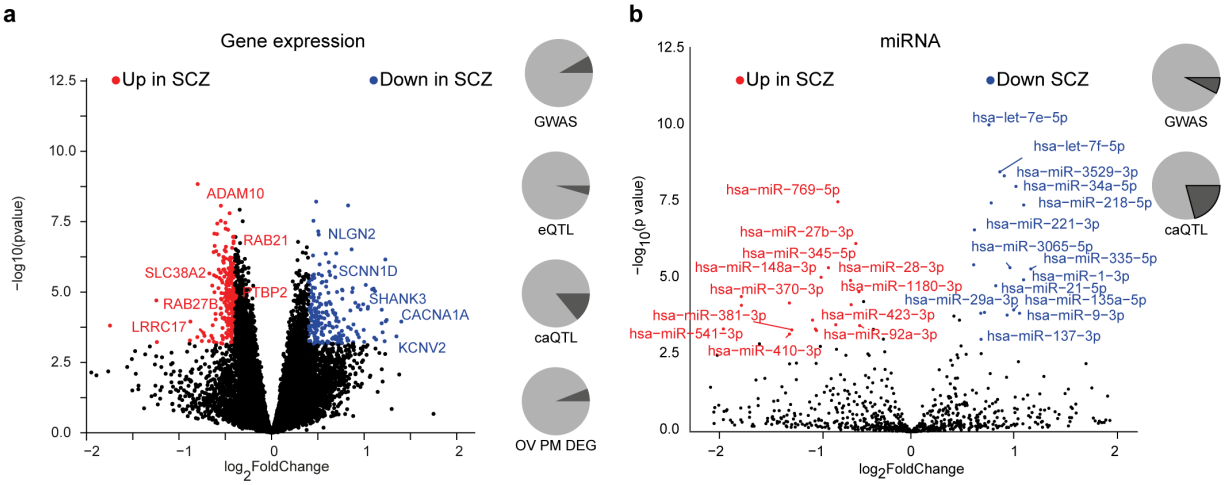

Fig. 2. Differential molecular feature analysis between SCZ and HC iPSC-derived neurons. **a**, Volcano plot showing the $\log_2$ fold-change (x-axis) and significance ($-\log_{10}$ p-value, y-axis) of differentially expressed genes (DEGs) between SCZ and HC iNs at day 49. Positive fold-changes indicate lower expression in SCZ. Red/blue dots indicate significance (FDR≤0.01) and minimal fold-change (|fc|=≥0.4) cutoffs to define DEGs. Text highlights selected genes differentially expressed. Pie charts from top to bottom show: overlap (dark grey) of DEGs with GWAS associated genes, iNs-based eQTLs, iNs-based caQTLs within 100kb and fraction of genes detected as also differentially expressed between HC and SCZ PFC postmortem (p-value ≤ 0.01). **b**, Volcano plot showing the $\log_2$ fold-change and significance of differential microRNA expression between SCZ and HC iNs at day 49. Positive fold-changes indicate lower expression in SCZ. Red/blue dots indicate significance (FDR≤0.01) and minimal fold-change (|fc|≥0.5) cutoffs to define DE microRNAs. Text highlights selected microRNAs DE. Pie charts show overlap (dark grey) of DE microRNAs with GWAS associated genes and iNs-based caQTLs within 200kb.

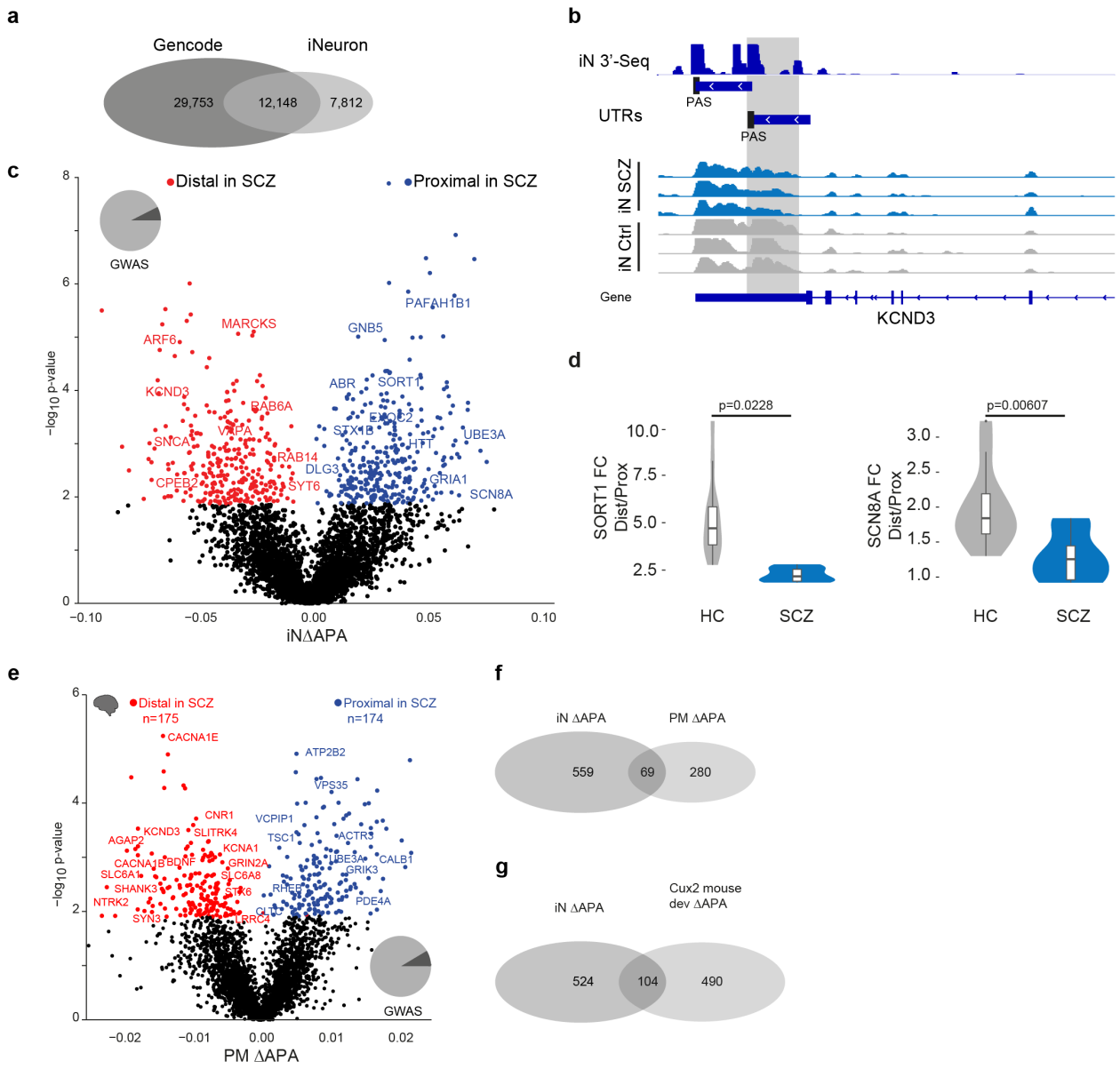

Fig. 3: Alternative 3'UTR polyadenylation in schizophrenia.

a, Overlap of known polyadenylation sites based on the Gencode annotation of the human genome and new polyadenylation sites identified in iNs based on 3'RNA-Seq.

b, Example locus representation of alternative polyadenylation site detection in iNs based on 3'RNA-Seq at the KCND3 locus. From top to bottom: Read count histogram of 3'RNA-Seq in iNs cumulated across 11 donors, detected distinct UTR regions and detected proximal and distal polyadenylation sties (PAS), Read count histograms across individuals iN samples from ISCZ and HC.

c, Volcano plot showing the difference (ΔAPA, x-axis) and significance (y-axis) of differential in 3'APA between ISCZ and HC derived iNs at day 49. Red dots indicate transcripts with a significant (FDR≤0.05) increase in usage of the distal UTR region in ISCZ, whereas blue dots delineate transcripts with a significantly higher usage of the distal UTR in the HC (higher usage of the proximal UTR in SCZ). Text highlights selected genes with dAPA

d, Relative expression values based on qPCR for selected transcripts subjects to dAPA in n=6 iNs from ISCZ and n=6 HC samples in 2 replicates. P-values indicate significance based on LMM t-test.

e, Volcano plot showing the difference (ΔAPA, x-axis) and significance (y-axis) of differential in 3'APA between ISCZ (n=275) and HC (n=291) in adult human postmortem PFC based on bulk RNA-Seq. Red dots indicate transcripts with a significant (FDR≤0.1) increase in usage of the distal UTR region in ISCZ, whereas blue dots delineate transcripts with a significantly higher usage of the distal UTR in the HC.

f, Overlap of transcripts subject to dAPA between ISCZ and HC in iNs and adult PFC.

g, Overlap of transcripts subject to dAPA between ISCZ and HC in iNs and over the course of mouse callosal projection neuron (Cux2 positive) development and maturation.

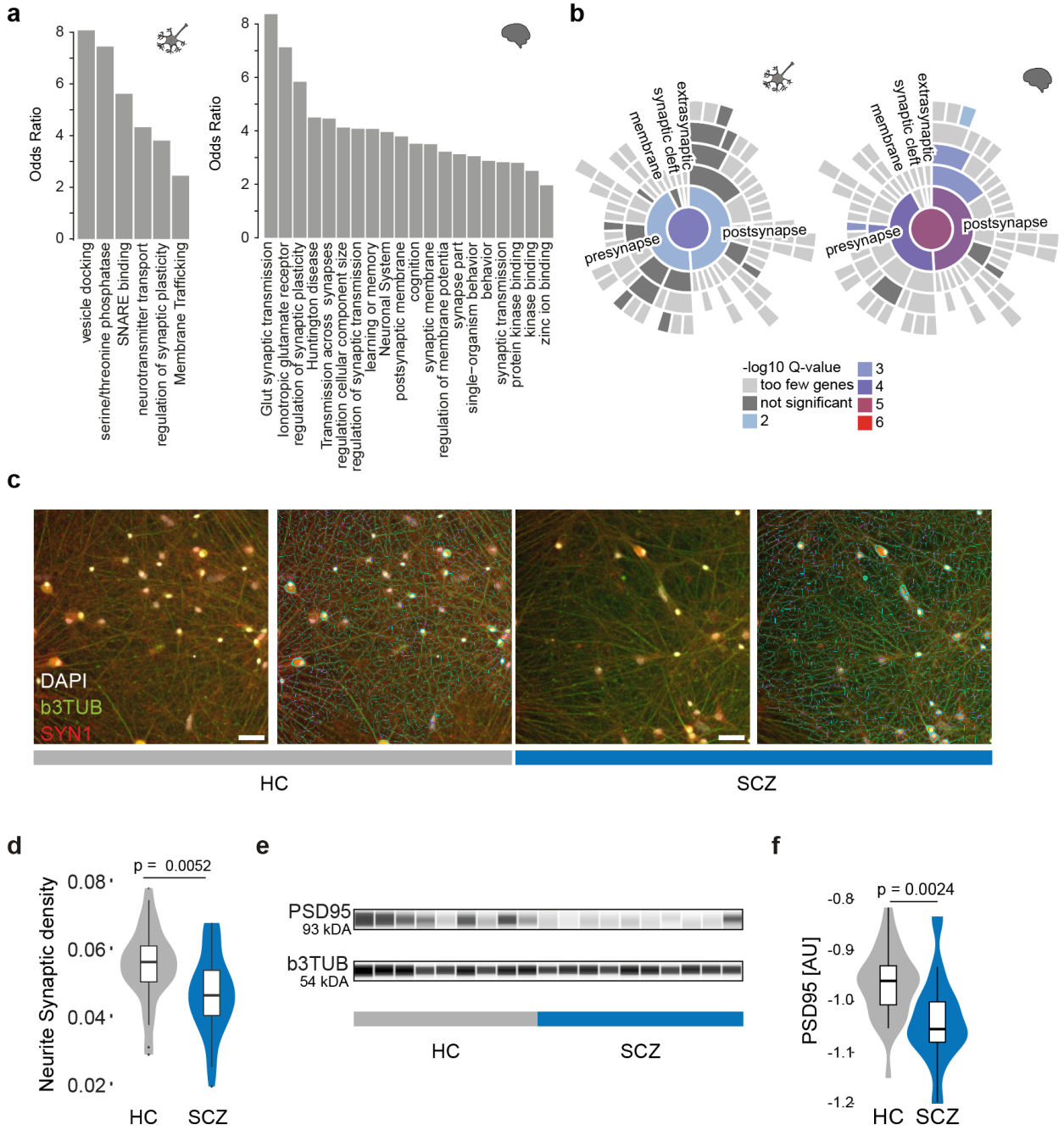

Fig. 4. Alternative polyadenylation in schizophrenia affects synaptic pathways.

a, Pathway enrichment (odds-ratio y-axis) for transcripts subject to dAPA between ISCZ and HC in iNs (left) or adult postmortem PFC (right).

b, Enrichment of for transcripts subject to dAPA (between ISCZ and HC) in iNs (left) or adult PFC (right) in synapse related biological processes based on SYNGO.[46]

c, Representative images from high content imaging (HCI) analysis of SYN1 (red), b3TUBB (green), and DAPI (white) ICC signal without (left) and with (right) neurite segmentation mask shown in iNs from HC and ISCZ. Scale bar indicates 50 µm.

d, Distribution of normalized SYN1 punctae density overlapping with neurites in iNs derived from HC and ISCZ donors at day 49. Density was assessed by HCI across n=10 HC and n=10 ISCZ iN

samples across 66 wells in total and two independent differentiation batches. P-value indicates two-tailed significance level of linear mixed model based comparison between ISCZ and HC punctae density distributions.

e, Representative visualization of digital quantitative western blot for PSD-95 protein abundance and b3TUB across 10 HC and 10 ISCZ iN samples at day 49 with b3TUB loading control.

f, Distribution of normalized PSD-95 protein abundance levels in HC and ISCZ iNs at day 49 of differentiation using quantitative western blot based on the $\log_2$ ratio of PSD95 and bTUBB signal intensity. P-value indicates two-tailed significance level of linear mixed model based comparison of n=28 (11 donors) HC and n=26 (14 donors) SCZ samples from three independent iN differentiation batches.

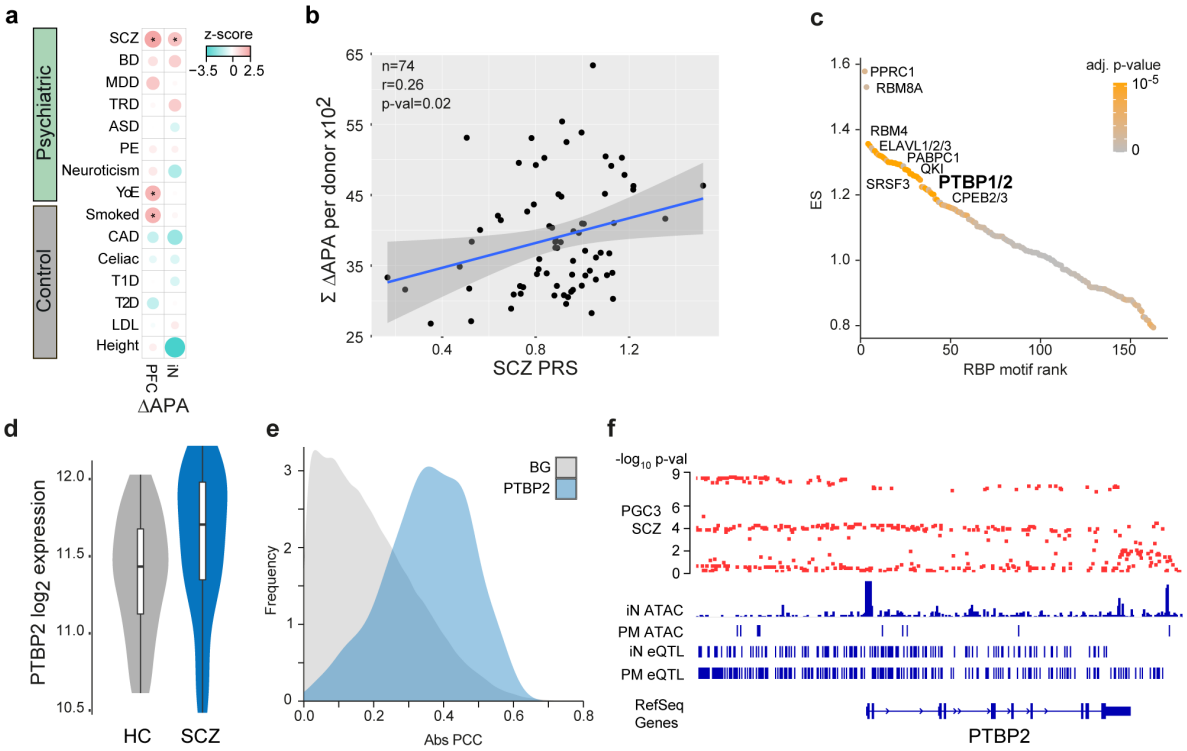

Fig. 5. Association of dAPA with cis- and trans-acting SCZ genetic risk factors.

a, Enrichment of trait heritability for genomic loci of genes subject to dAPA between HC and ISCZ in adult PFC and iNs for a collection of psychiatric diseases and control traits based on GWAS summary statistics and partition heritability analysis. Diseases/traits as indicated (SCZ = schizophrenia, BD = bipolar disorder, MDD = major depressive disorder, TRD = treatment resistant depression, ASD = autism spectrum disorder, PE = any psychotic experience, YoE = years of education, CAD = coronary artery disease, T1D/T2D = Type 1/2 diabetes, LDL = Levels of low-density lipoprotein). Dot size indicates enrichment levels as z-scores and * indicates significance (p-value≤0.05).

b, Relationship of SCZ PRS (x-axis) and cumulated APA (between HC and ISCZ) in iNs across all transcripts showing differential APA (n=628) for each donor (n=74, black dots). P-value indicates significance of linear model fit (blue line) and r the corresponding pearson correlation coefficient. Grey shading signifies standard error of the fit.

c, Distribution of RBP binding motif enrichment enrichment score (ES, y-axis) in the 3'UTR of transcripts subject to dAPA between HC and ISCZ in iNs with increased usage of the distal PAS in SCZ ordered by RBP motif enrichment rank (x-axis). Color code indicates significance of enrichment. Labeling indicates a subset of significantly enriched RBP binding motifs after multiple testing correction (adjusted p-value ≤0.1).

d, Distribution of log2 transformed variance stabilized expression level of PTBP2 in iNs from HC and ISCZ at day 49. P-value/FDR indicate significance of differential expression based on Wald-test.

e, Frequency (y-axis) of absolute pearson correlation coefficient (PCC, x-axis) between APA level of each transcript subject to dAPA (between HC and ISCZ) in iNs (n=628) and respective PTBP2 expression level across all iN samples (blue). For comparison, results from the same analysis for all other expressed RBPs are shown as background (BG, grey).

537 **f**, Functional genomic characterization of the PTBP2 locus in the human genome. From top to
538 bottom: Distribution of SCZ association -$\log_{10}$ p-values based on the PGC wave 3 GWAS for all
539 included common variants, ATAC-Seq read count histogram in iNs and PFC from postmortem
540 (PM) human tissue, eQTLs in iNs and eQTLs in PFC.

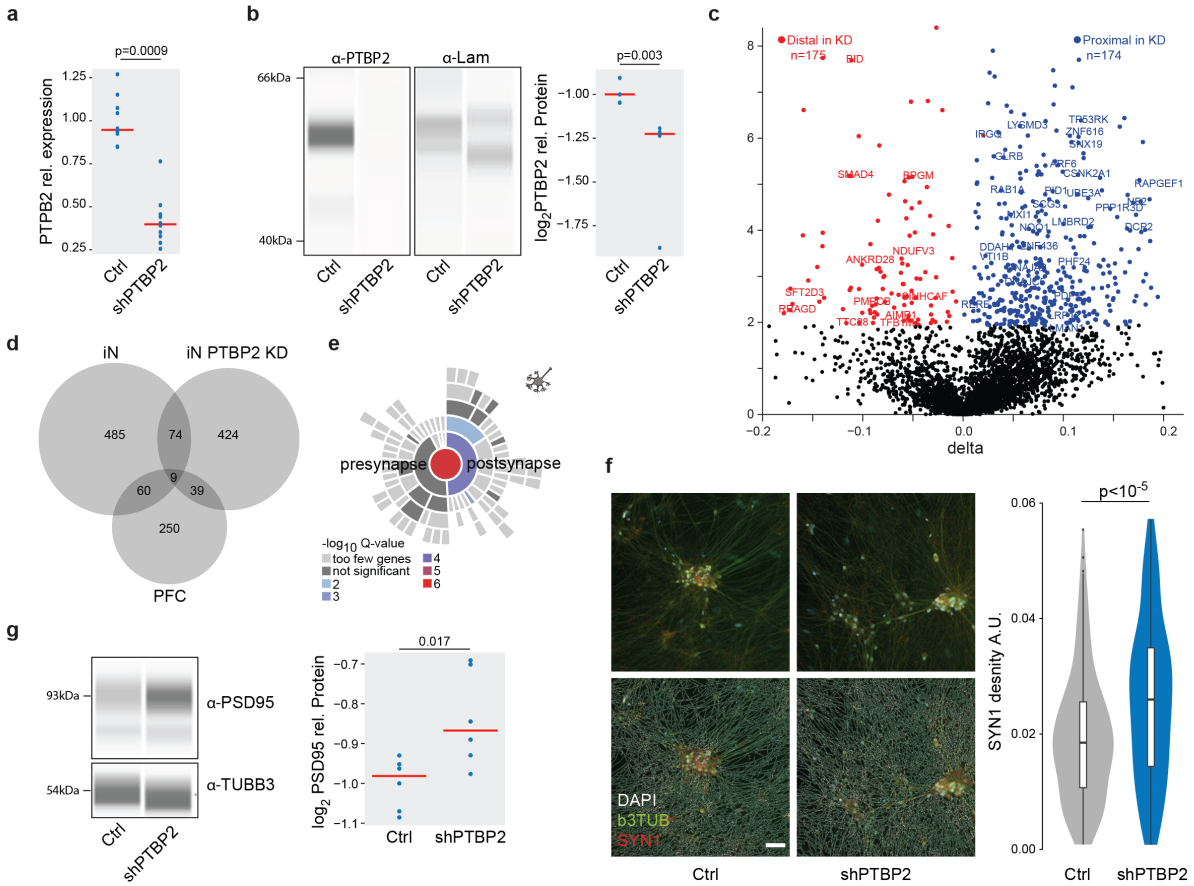

Fig. 6. PTBP2 is a trans-acting genetic risk factor for SCZ mediating dAPA dependent synaptic density alterations.

a, Distribution of relative expression levels (y-axis) of PTBP2 normalized to the housekeeping gene RTF2 in HC derived iNs treated with scramble control and a pool of 4 PTBP2 shRNAs based on qPCR. P-value indicates two-tailed significance level of linear mixed model based comparison of n=20 samples from 3 distinct donors and three independent iN differentiation batches correcting for batch as random effect.

b, Left: Representative visualization of digital quantitative western blot for PTBP2 protein abundance and laminin in scramble control and PTBP2 shRNA mediated knockdown in iNs. Right: Distribution of normalized PTBP2 protein abundance levels (y-axis) in scramble control and PTBP2 shRNA mediated knockdown in iNs based on quantitative western blot. P-value indicates two-tailed significance level of linear mixed model based comparison of n=15 samples from 3 distinct donors and three independent iN differentiation batches correcting for batch as random effect.

c, Volcano plot showing the difference (ΔAPA, x-axis) and significance (y-axis) of dAPA between scramble control (n=2) and acute shRNA mediated knockdown of PTBP2 at the end of the differentiation for 5 days (n=2) in iNs. Red dots indicate transcripts with a significant (FDR≤0.05) increase in usage of the distal UTR region in the knockdown condition, whereas blue dots delineate transcripts with a significantly higher usage of the distal UTR in the scramble control.

d, Overlap of transcripts subject to dAPA between HC and ISCZ in iN or PFC or between scramble control and PTBP2 knockdown in iNs.

563 **e**, Enrichment for transcripts subject to dAPA between scramble control and PTBP2 knockdown
564 in iNs in synapse related biological processes based on SYNGO[46].
565 **f**, Left: Representative image of SYN1 (red) distribution in iNs infected with scramble control
566 shRNA or PTBP2 knockdown alongside with bTub (green) and DAPI (white) signal without
567 (upper line) and with (top line) neurite segmentation mask. Right: Distribution of SYN1 punctae
568 area density (arbitrary units) in neurites of iNs with scramble control or PTBP2 knockdown in iNs
569 from 3 different donors each, 23 wells and 291 fields of view. P-value indicates two-tailed
570 significance level of linear mixed model based testing correcting for donor as random effect. Scale
571 bar indicates 50 µm.
572 **g**, Left: Representative visualization of digital quantitative western blot for PSD-95 protein
573 abundance and b3TUB in scramble control and PTBP2 shRNA mediated knockdown in iNs. Right:
574 Distribution of normalized PSD-95 protein abundance levels for high molecular weight (95 kDa)
575 (y-axis) in scramble control and PTBP2 shRNA mediated knockdown in iNs based on quantitative
576 western blot. P-value indicates two-tailed significance level of linear mixed model based
577 comparison of n=10 samples from 3 distinct donors and three independent iN differentiation
578 batches correcting for batch as random effect.

Extended Data Figures

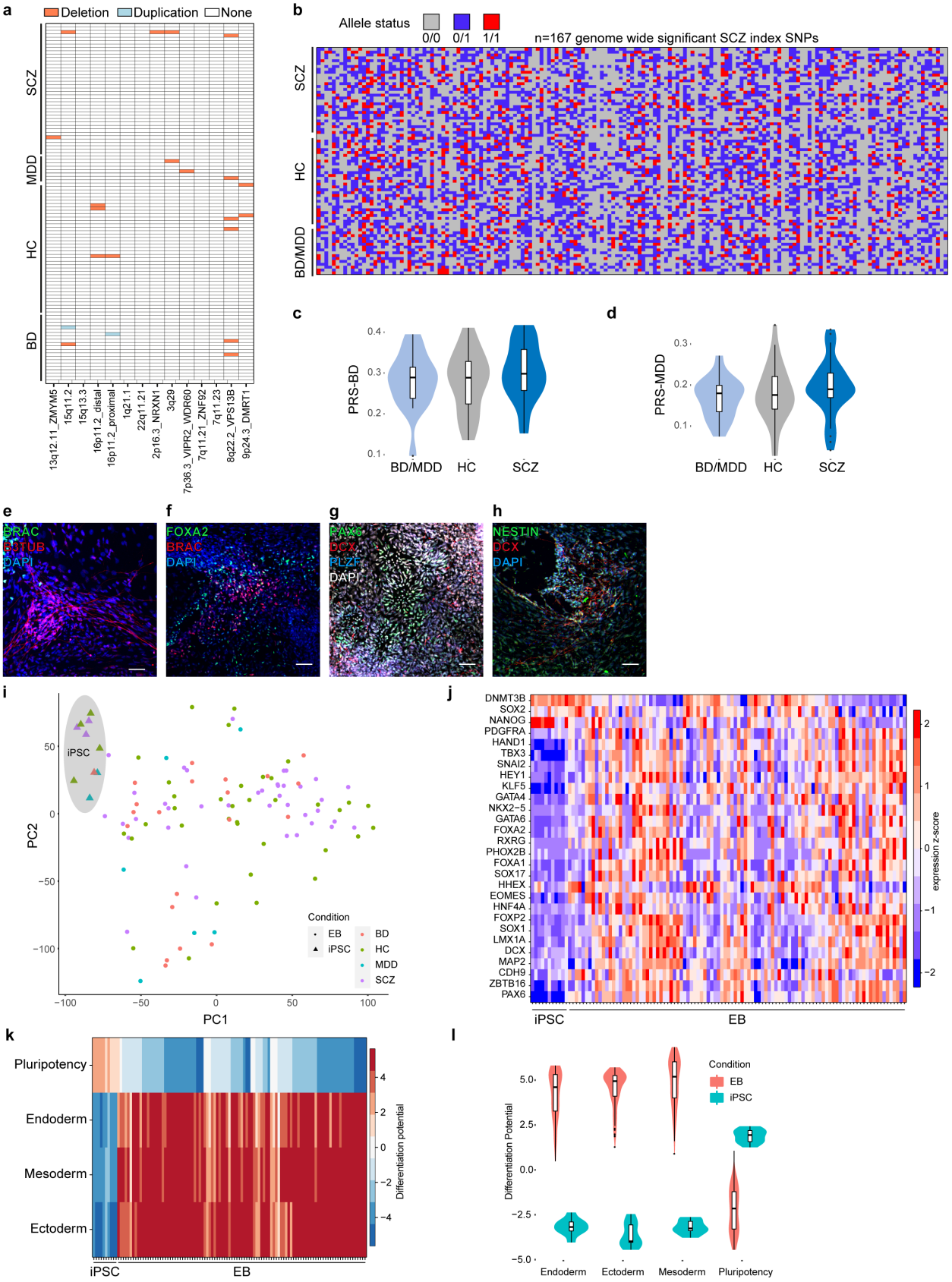

581 **Extended Data Fig. 1. Quality control of iPSCs, and genetic characterization.**

582 **a**, Distribution of previously identified CNVs associated with SCZ (x-axis) across all iPSC lines
583 ordered by diagnosis group (y-axis).
584 **b**, Distribution of index-SNP allele status (color-code) for 167 genome wide significant SCZ
585 associated loci (x-axis) across all iPSC donors.
586 **c**, Distribution of the individual polygenic risk score for bipolar disorder for the different diagnosis
587 groups of hiPSC donors.
588 **d**, Distribution of the individual polygenic risk score for major depressive for the different
589 diagnosis groups of hiPSC donors.
590 **e**, Representative immunofluorescence image of an embryoid body section at day 15 of
591 differentiation colored for mesodermal marker Brachury (BRAC) and ectodermal marker beta-3-
592 tubulin (B3TUB). Scale bar indicates 50 µm.
593 **f**, Representative immunofluorescence image of an embryoid body section at day 15 of
594 differentiation colored for endodermal marker FOXA2 and mesodermal marker BRAC. Scale bar
595 indicates 50µm.
596 **g**, Representative immunofluorescence image of an embryoid body section at day 15 of
597 differentiation colored for ectodermal markers PAX6, DCX and PLZF. Scale bar indicates 50µm.
598 **h**, Representative immunofluorescence image of an embryoid body section at day 15 of
599 differentiation colored for ectodermal markers NESTIN and DCX. Scale bar indicates 50µm.
600 **i**, PCA analysis results for RNA-Seq profiles from EBs derived from all iPSC lines (stars) and a
601 subset of iPSC analyzed in the pluripotent state (triangles) colored by diagnosis group.
602 **j**, Heatmap of key lineage marker gene expression (y-axis) across all EBs and iPSCs analyzed in
603 this study (y-axis) as z-scores (color scheme) based on RNA-Seq.
604 **k**, Cumulated differentiation potential for each germ layer and pluripotency signature assessed (y-
605 axis) by RNA-Seq for EBs (see methods for details) across iPSC lines (x-axis).
606 **l**, Distribution of cumulated differentiation potential signature (y-axis) for each germ layer and the
607 pluripotency signature and (x-axis) across iPSC-derived EBs (red) and a subset of iPSCs (blue).

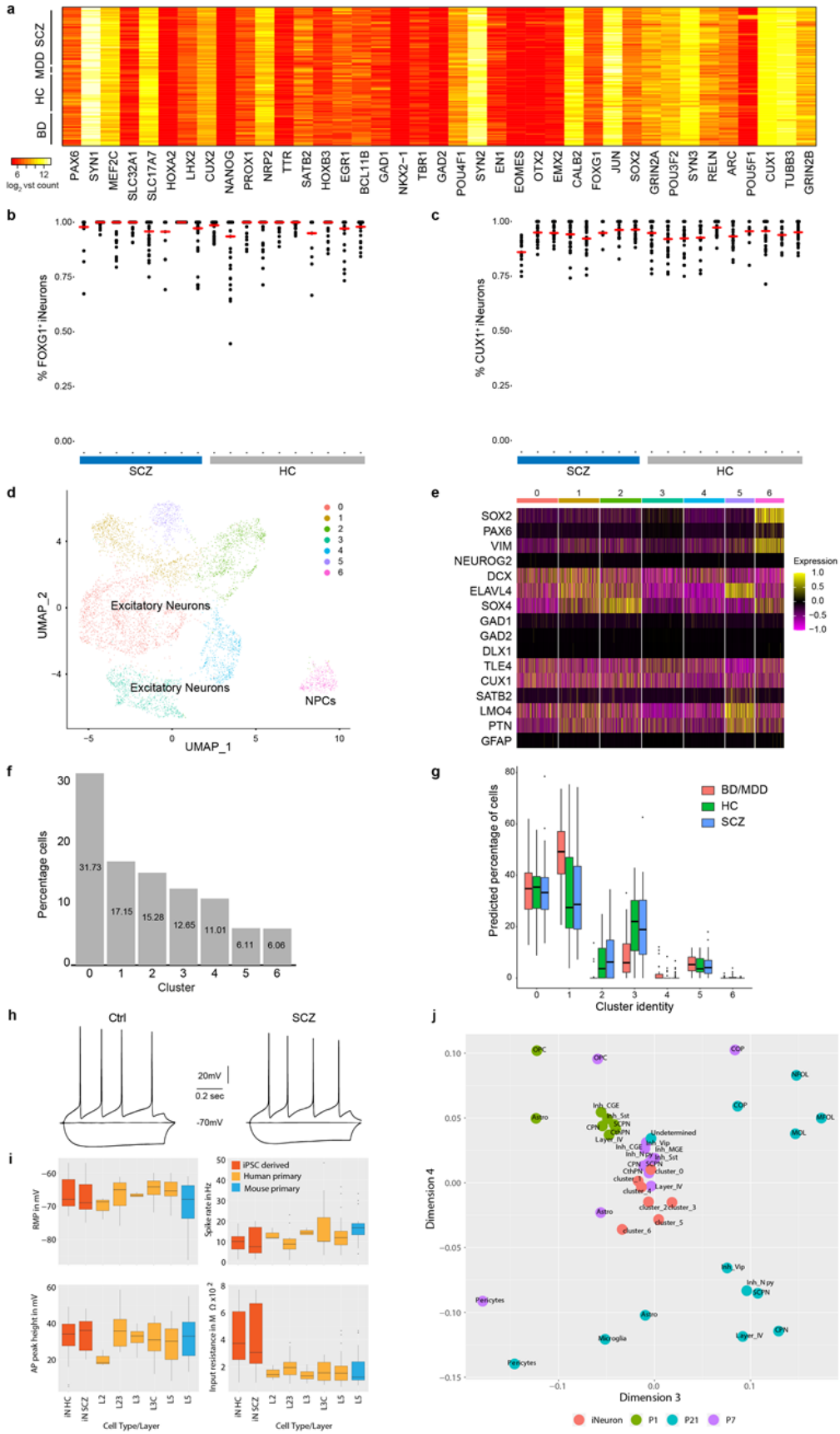
a
SCZ
MDD
HC
BD
log2 vst count
PAX6
SYN1
MEF2C
SLC32A1
SLC17A7
HOXA2
LHX2
CUX2
NANOG
PROX1
NRP2
TTR
SATB2
HOXB3
EGR1
BCL11B
GAD1
NKX2-1
TBR1
GAD2
POU4F1
SYN2
EN1
EOMES
OTX2
EMX2
CALB2
FOXG1
JUN
SOX2
GRIN2A
POU3F2
SYN3
RELN
ARC
POU5F1
CUX1
TUBB3
GRIN2B
b
% FOXG1+ iNeurons
SCZ
HC
c
% CUX1+ iNeurons
SCZ
HC
d
UMAP_2
UMAP_1
Excitatory Neurons
Excitatory Neurons
NPCs
e
SOX2
PAX6
VIM
NEUROG2
DCX
ELAVL4
SOX4
GAD1
GAD2
DLX1
TLE4
CUX1
SATB2
LMO4
PTN
GFAP
Expression
f
Percentage cells
Cluster
31.73
17.15
15.28
12.65
11.01
6.11
6.06
g
Predicted percentage of cells
Cluster identity
BD/MDD
HC
SCZ
h
Ctrl
SCZ
20mV
0.2 sec
-70mV
i
RMP in mV
Spike rate in Hz
iPSC derived
Human primary
Mouse primary
AP peak height in mV
Input resistance in MΩ x10^2
Cell Type/Layer
Cell Type/Layer
j
Dimension 4
Dimension 3
iNeuron
P1
P21
P7

608

Extended Data Fig. 2. Characterization and quality control of multi-omics iPSCderived neuron profiles.

a, Expression of key neuronal marker genes (x-axis) across all interrogated iPSC lines (y-axis) in iPSC derived neurons at day 49 based as $\log_2$ transformed RNA-Seq counts.

b, Dot plot showing FOXG1+ iNs after 49 days of differentiation from HC (n=10, grey) and SCZ (n=8, blue) based on ICC analysis. Each dot represents one FOV. Red lines indicate median of FOXG1+ iNs per cell line.

c, Dot plot showing CUX1+ iNs after 49 days of differentiation from HC (n=10, grey) and SCZ (n=8, blue) based on ICC analysis. Each dot represents one FOV. Red lines indicate median of CUX1+ iNs per cell line.

d, Umap representation of iNs single-cell RNA-Seq profiling. Cell type identities were assigned based marker gene expression. Cluster 6 represent neural progenitor cells (NPCs).

e, Heatmap for subsampled 1000 cells from a. showing the SCT scaled expression of selected marker genes across iN clusters (x-axis). Note, the increased expression of NPC markers(SOX2, PAX6, VIM) in cluster 6 and the absence of interneuronal marker gene expression (GAD1/2, DLX1) and GFAP expression in all clusters.

f, Percentage of cells (y-axis) per cluster (x-axis) from single-cell RNA-Seq of iNs from a.

g, Distribution of predicted cell identity proportion (y-axis) per single cell RNA-Seq cluster (x-axis) for each iN bulk RNA-Seq dataset splitted by diagnoses (colored boxplots). Predicted proportions were determined through in silico deconvolution analysis using the scRNA-Seq dataset from iNs as reference. Boxes indicate 25th and 75th quantiles, black bar median, lines demarcate 1.5 IQR from the median in either direction.

h, Representative traces for HC and SCZ iNs of the electrophysiological basic characterization by patch-clamp recordings.

i, Comparison of basic electrophysiological properties from single cell patch-clamp recordings of iNs from HC or ISCZ (red) to previously published data[28] from primary human (orange) or mouse neurons (blue). X-axis indicates layer of origin of patched cells. RMP – resting membrane potential in mV, AP peak height – peak height of action potential relative to baseline (overshoot) in mV, Spike rate – frequency of action potentials in Hz calculated from 700/800ms measurement windows, Input resistance – whole cell input resistance in mega Ω. L2/3/5 indicates layer of neuron origin.

j, Multidimensional scaling analysis comparing pseudo-bulk profiles of scRNA-Seq from the developing mouse cortex at developmental stages P1, P7 and P21 and individual transcriptomic profiles of all clusters detected in the iN dataset. OPC – oligodendrocyte precursor; COP, NFOL, MFOL, MOL – distinct stages of oligodendrocytes; CPN, ScPN, CThPN - excitatory neuronal projection neuron subtypes, Inh- interneuron subtypes. Cluster indicate iNeuron clusters from a.

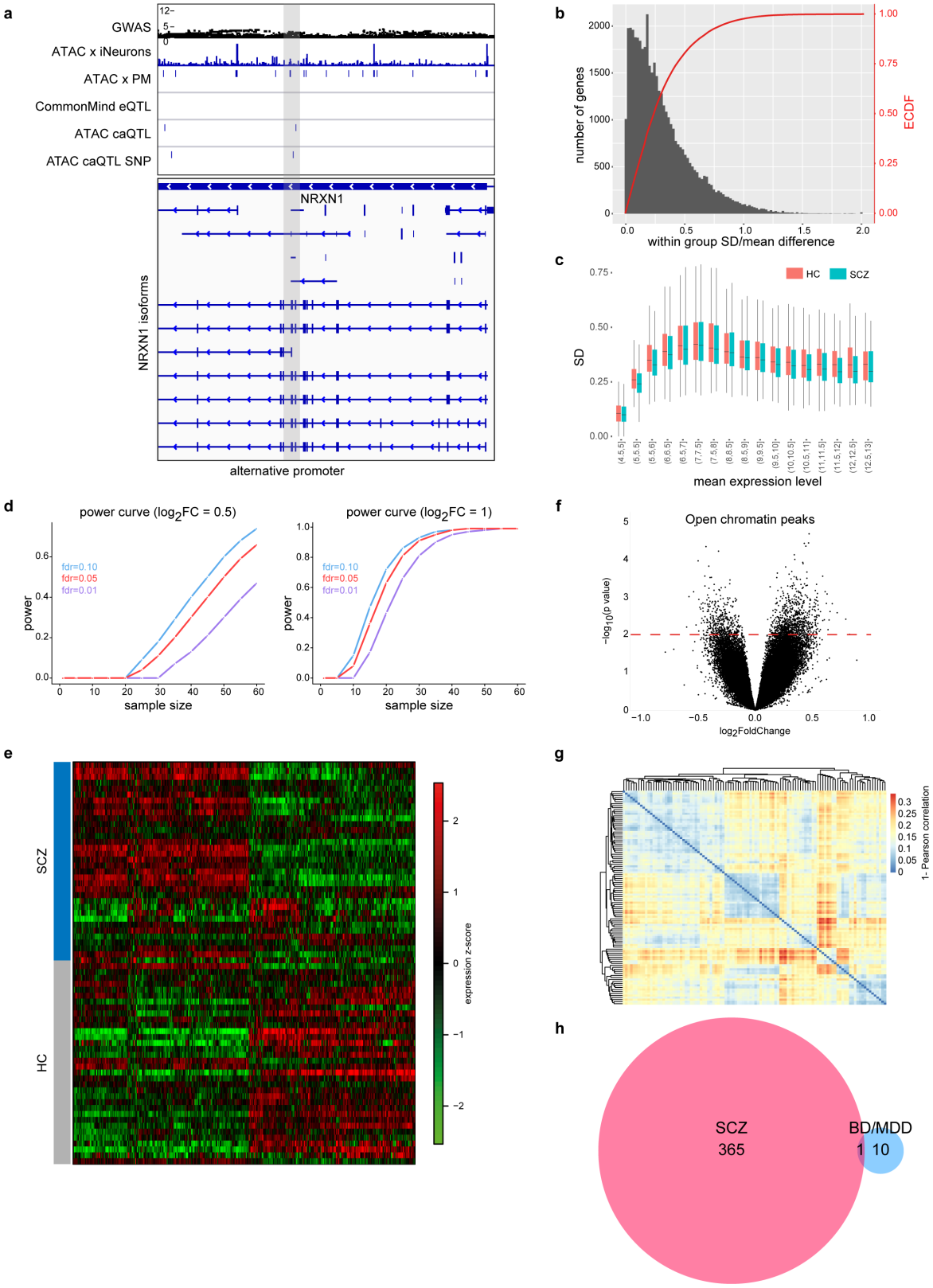
a
GWAS
ATAC x iNeurons
ATAC x PM
CommonMind eQTL
ATAC caQTL
ATAC caQTL SNP
NRXN1
NRXN1 isoforms
alternative promoter
b
number of genes
ECDF
within group SD/mean difference
c
HC
SCZ
SD
mean expression level
d
power curve (log2FC = 0.5)
power curve (log2FC = 1)
fdr=0.10
fdr=0.05
fdr=0.01
power
sample size
e
SCZ
HC
expression z-score
f
Open chromatin peaks
−log10(p value)
log2FoldChange
g
1- Pearson correlation
h
SCZ
365
BD/MDD
1
10

645

Extended Data Fig. 3. Differential expression analysis and power calculations of iPSC-derived neurons.

a, Representative example of genomic annotations and distinct qTL types at the intronic region of NRXN1 locus, from top to bottom: Association strength of imputed SNPs at the locus with SCZ based on SCZ GWAS, ATAC-Seq profile of representative iPSC derived neuron at day 49, eQTLs detected at the locus in iNs, caQTLs detected at the locus co-localizing with open chromatin regions. Grey vertical bar indicated an alternative promoter region of NRXN1 in which a caQTL is located.

b, Frequency of genes (y-axis left) characterized by a particular ratio of within group standard deviation (SD) over mean group difference (HC vs SCZ, x-axis) as well as empirical cumulative density function (ECDF) of genes (red-curve, y-axis right).

c, Distribution of standard deviation (y-axis) for all genes within a certain mean expression level interval (x-axis) per sample group (color code). Boxes indicate 25th and 75th quantiles, black bar median, lines demarcate 1.5 IQR from the median in either direction.

d, Power estimation (y-axis) to detect differentially expressed genes between two sample groups with individual sample size per group indicated on the x-axis at distinct FDR thresholds indicated by colored lines. Power estimates were conducted using a negative binomial model with empirically inferred dispersion parameters using the iPSC iN RNA-Seq profiles and a minimum effect size of $\log_2$ fold-change 0.5 (left) or 1 (right).

e, Heatmap showing differentially expressed genes (DEG) (FDR≤0.01 and $|\log_2 FC| \geq 0.4$ x-axis) between HC and ISCZ iNs (y-axis) as z-scores (color code).

f, Volcano plot showing the $\log_2$ fold change (x-axis) and significance (p-value) of differential open chromatin signal between SCZ and HC iNs at day 49. No peaks pass the significance threshold (FDR≤0.05). Dashed red line indicates nominal significance.

g, Clustered heatmap of ATAC-Seq peak profiles of all iNs from this study using 1-pearson correlation coefficient as metric (color code).

h, Overlap of DEGs between SCZ vs HC iNs (red) and BD/MDD vs HC iNs (blue).

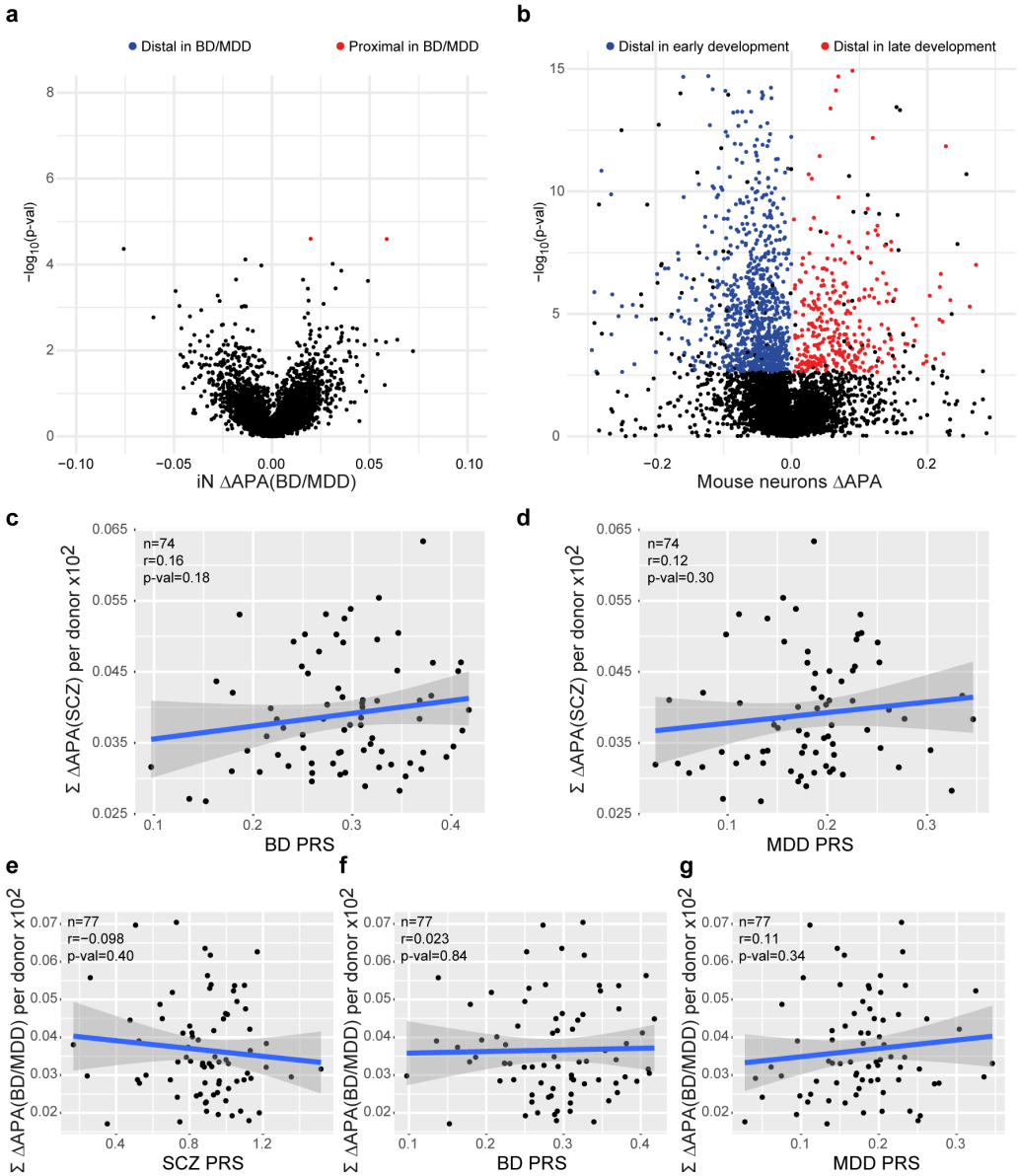

Extended Data Fig. 4. dAPA in bipolar disorder, mouse neurons, and its associations with genetic risk

a, Volcano plot showing the difference (ΔAPA, x-axis) and significance (y-axis) of differential in 3'APA between BD/MDD and HC derived iNs at day 49. Red dots indicate transcripts with a significant (FDR≤0.05) increase in usage of the distal UTR region in HC (higher usage of the proximal UTR in SCZ), whereas blue dots delineate transcripts with a significantly higher usage of the distal UTR in the BD/MDD.

b, Volcano plot showing the difference (ΔAPA, x-axis) and significance (y-axis) of dAPA between mouse callosal projection neurons during early development (E18.5- P1) and late developmental stages (P21-P48). Red dots indicate transcripts with a significant (FDR≤0.05) increase in usage of the distal UTR region in at late developmental stages, whereas blue dots delineate transcripts with a significantly higher usage of the distal UTR during the early phases of postnatal development

c, Relationship of BD PRS (x-axis) and cumulated APA (between HC and ISCZ) in iNs across all transcripts showing differential APA (n=628) for each donor (n=74, black dots). P-value

688 indicates significance of linear model fit (blue line) and r the corresponding pearson correlation
689 coefficient. Grey shading signifies standard error of the fit.
690 **d**, Relationship of MDD PRS (x-axis) and cumulated APA (between HC and ISCZ) in iNs across
691 all transcripts showing differential APA (n=628) for each donor (n=74, black dots). P-value
692 indicates significance of linear model fit (blue line) and r the corresponding pearson correlation
693 coefficient. Grey shading signifies standard error of the fit.
694 **e**, Relationship of SCZ PRS (x-axis) and cumulated APA (between HC and BD/MDD) in iNs
695 across all transcripts showing differential APA (n=20) for each donor (n=77, black dots). P-value
696 indicates significance of linear model fit (blue line) and r the corresponding pearson correlation
697 coefficient. Grey shading signifies standard error of the fit.
698 **f**, Relationship of BD PRS (x-axis) and cumulated APA (between HC and BD/MDD) in iNs across
699 all transcripts showing differential APA (n=20) for each donor (n=77, black dots). P-value
700 indicates significance of linear model fit (blue line) and r the corresponding pearson correlation
701 coefficient. Grey shading signifies standard error of the fit.
702 **g**, Relationship of MDD PRS (x-axis) and cumulated APA (between HC and BD/MDD) in iNs
703 across all transcripts showing differential APA (n=20) for each donor (n=77, black dots). P-value
704 indicates significance of linear model fit (blue line) and r the corresponding pearson correlation
705 coefficient. Grey shading signifies standard error of the fit.

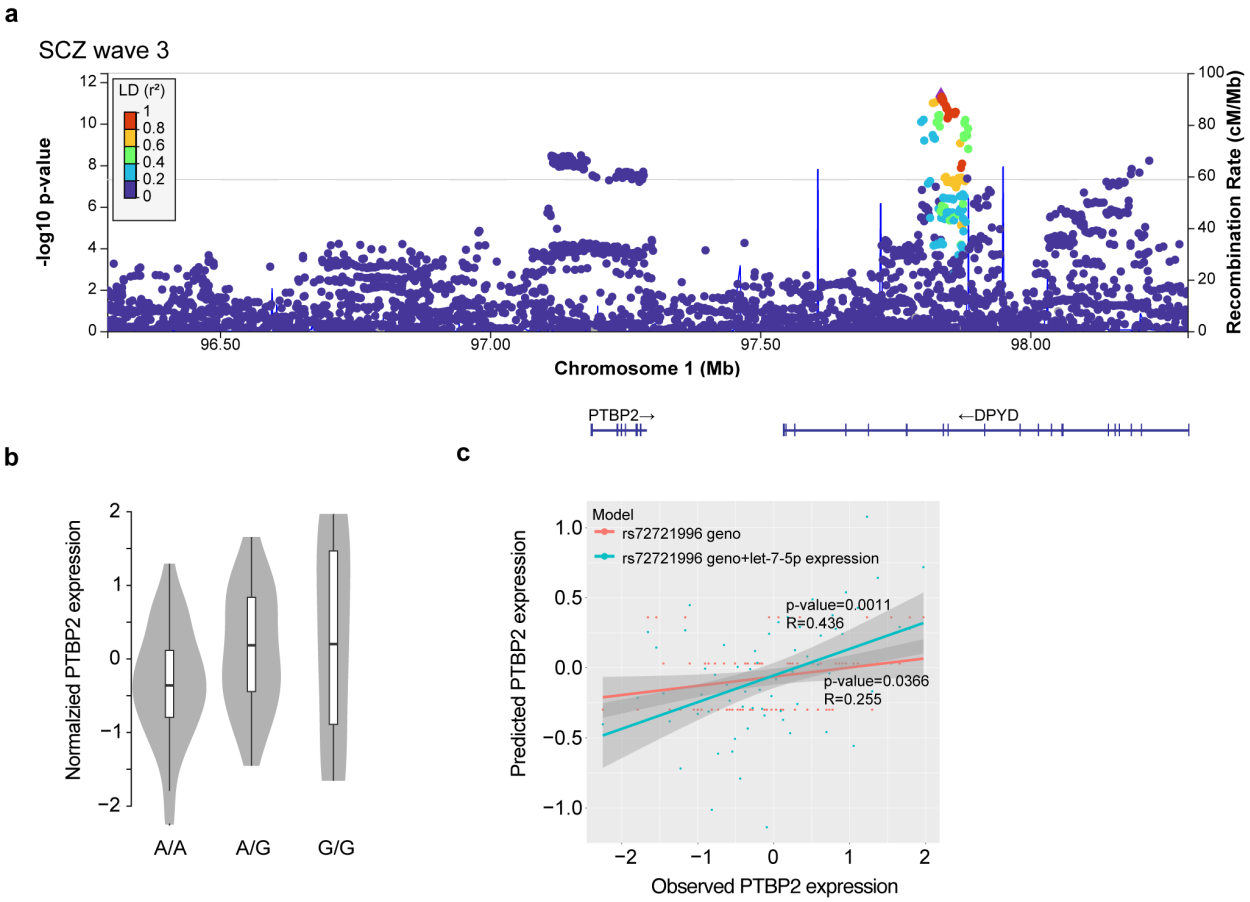

Extended Data Fig. 5. Characterization of the PTBP2 gene.
a, Locus zoom plot of PTBP2 locus showing linkage disequilibrium (LD) scores and -$\log_{10}$ p-value based on SCZ GWAS from the PGC wave 3.
b, Normalized PTBP2 expression levels in iNs from all donors as a function of allele status at the PTBP2 eQTL rs72721996 at the SCZ risk locus PTBP2.
c, Results of linear model-based regression of PTBP2 expression levels in iNs on donor genotype only (red) or donor genotype + miR-let-7-5p expression in the same donors across n=67 samples. X-axis depicts measured PTBP2 expression levels while y-axis shows predicted expression values based on the respective model. P-values indicate significance of the respective model while R values show overall correlation of measured and predicted expression values.

Supplementary Tables

Supplementary Table 1. Overview of included cell lines

Explanation of the columns from left to right: Classifier of diagnosis; Treatment information indicates recorded lithium treatment in BD patients and if patients with SCZ received clozapine treatment or treatment with other antipsychotic medication (noClozapin); Sex indicates male (M) and female (F) donors; age at timepoint of donation; Age at (recorded) onset of diseases; hiPSC generator; donor tissue; reprogramming method; RNAseq, ATAC-Seq and microRNA-Seq. Separate Excel file.

Supplementary Table 2. Summary of eQTL, caQTL and microRNA qTLs identified in this study

Separate Excel file.

Supplementary Table 3. Summary of differentially expressed genes (DEGs), microRNAs (DiffmicroRNA) and differential APA analysis (dAPA)

Separate Excel file.

Supplementary Table 4. Summary of iN endophenotyping data used for statistical analysis

Separate Excel file.

Supplementary Table 5. Summary of key reagents used

Separate Excel file.

Supplementary Data

Supplementary Data 1. Quality control of iPSC genotype

This data summarizes the digital karyotyping results of all iPSC lines used in this study using GSA genotyping array. For each line, a pairwise CNV analysis was conducted comparing the iPSC genotype to that of the original donor derived from a donor's blood sample. The top plot for each donor summarizes detected CNVs between iPSC and blood based genotype, where blue lines indicate a CNV. The two plots below show the CNV status in the donor sample (top) and iPSC line (bottom), where the color code indicates the type of CNV found in each sample. Separate PDF file.

Supplementary Data 2. Quality control of iPSC pluripotency markers

This data figures summarizes representative immunocytochemistry images for the key pluripotency markers OCT4, TRA1-60, NANOG, SOX2 as well as differentiation related markers PAX6, SOX1, NESTIN and KI-67 across all iPSC lines used in this study, highlighting robust pluripotency marker presence and absence of differentiation related markers. Pages 1-13, scale bar indicates 100µm; pages 14-24, scale bar indicates 50µm; pages 25 and 26, scale bar indicates 100µm. Separate PDF file.

Supplementary Data 3. Raw quantitative western blot images.

Fully pictured digital quantitative western blot performed with WES protein simple. Western blot for each epitope was performed in 3 independent iNeuron differentiation batches from Ctrl (grey) and SCZ (blue) at day 49. Test lanes for subsequent assay optimization, e.g. concentration optimization, are not excised but marked with black bars above the respective WB lane. Abundance of PSD95 and b3tub for normalization, is illustrated in classical WB-like lane view above the graph view with detected chemiluminescence on the y-axis and molecular weight (MW) on the x-axis, which is the base for digital quantification. Standardized ladders illustrate the molecular weight of 12, 40, 66, 116, 180, 230 kDA. Separate PDF file.

References

1. Charlson, F.J. *et al.* Global Epidemiology and Burden of Schizophrenia: Findings From the Global Burden of Disease Study 2016. *Schizophr Bull* **44**, 1195-1203 (2018).
2. Hilker, R. *et al.* Heritability of Schizophrenia and Schizophrenia Spectrum Based on the Nationwide Danish Twin Register. *Biol Psychiatry* **83**, 492-498 (2018).
3. Trubetskoy, V. *et al.* Mapping genomic loci implicates genes and synaptic biology in schizophrenia. *Nature* **604**, 502-508 (2022).
4. Singh, T. *et al.* Rare coding variants in ten genes confer substantial risk for schizophrenia. *Nature* **604**, 509-516 (2022).
5. Howard, D.M. *et al.* Genome-wide meta-analysis of depression identifies 102 independent variants and highlights the importance of the prefrontal brain regions. *Nat Neurosci* **22**, 343-352 (2019).
6. Mullins, N. *et al.* Genome-wide association study of more than 40,000 bipolar disorder cases provides new insights into the underlying biology. *Nat Genet* **53**, 817-829 (2021).
7. The Network and Pathway Analysis Subgroup of the Psychiatric Genomics Consortium. Psychiatric genome-wide association study analyses implicate neuronal, immune and histone pathways. *Nat Neurosci* **18**, 199-209 (2015).
8. Wang, D. *et al.* Comprehensive functional genomic resource and integrative model for the human brain. *Science (New York, N.Y.)* **362**, eaat8464 (2018).
9. Schrode, N. *et al.* Synergistic effects of common schizophrenia risk variants. *Nat Genet* **51**, 1475-1485 (2019).
10. Sekar, A. *et al.* Schizophrenia risk from complex variation of complement component 4. *Nature* **530**, 177-83 (2016).
11. Fromer, M. *et al.* Gene expression elucidates functional impact of polygenic risk for schizophrenia. *Nat Neurosci* **19**, 1442-1453 (2016).
12. Bryois, J. *et al.* Evaluation of chromatin accessibility in prefrontal cortex of individuals with schizophrenia. *Nat Commun* **9**, 3121 (2018).
13. Gandal, M.J. *et al.* Transcriptome-wide isoform-level dysregulation in ASD, schizophrenia, and bipolar disorder. *Science* **362**(2018).
14. Dobbyn, A. *et al.* Landscape of Conditional eQTL in Dorsolateral Prefrontal Cortex and Co-localization with Schizophrenia GWAS. *Am J Hum Genet* **102**, 1169-1184 (2018).
15. Mayr, C. What Are 3' UTRs Doing? *Cold Spring Harb Perspect Biol* **11**(2019).
16. Li, L. *et al.* An atlas of alternative polyadenylation quantitative trait loci contributing to complex trait and disease heritability. *Nat Genet* **53**, 994-1005 (2021).
17. Park, C.Y. *et al.* Genome-wide landscape of RNA-binding protein target site dysregulation reveals a major impact on psychiatric disorder risk. *Nat Genet* **53**, 166-173 (2021).
18. Kircher, T. *et al.* Neurobiology of the major psychoses: a translational perspective on brain structure and function-the FOR2107 consortium. *Eur Arch Psychiatry Clin Neurosci* **269**, 949-962 (2019).
19. Bruckl, T.M. *et al.* The biological classification of mental disorders (BeCOME) study: a protocol for an observational deep-phenotyping study for the identification of biological subtypes. *BMC Psychiatry* **20**, 213 (2020).
20. Krcmar, L. *et al.* The multimodal Munich Clinical Deep Phenotyping study to bridge the translational gap in severe mental illness treatment research. *Front Psychiatry* **14**, 1179811 (2023).
21. Budde, M. *et al.* A longitudinal approach to biological psychiatric research: The PsyCourse study. *Am J Med Genet B Neuropsychiatr Genet* (2018).

22. Lee, P.H. *et al.* Genomic Relationships, Novel Loci, and Pleiotropic Mechanisms across Eight Psychiatric Disorders. *Cell* **179**, 1469-1482.e11 (2019).
23. Anttila, V. *et al.* Analysis of shared heritability in common disorders of the brain. *Science* **360**(2018).
24. Hoffmann, A., Ziller, M. & Spengler, D. Childhood-Onset Schizophrenia: Insights from Induced Pluripotent Stem Cells. *Int J Mol Sci* **19**(2018).
25. Brennand, K.J. *et al.* Modelling schizophrenia using human induced pluripotent stem cells. *Nature* **473**, 221-5 (2011).
26. Nehme, R. *et al.* Combining NGN2 Programming with Developmental Patterning Generates Human Excitatory Neurons with NMDAR-Mediated Synaptic Transmission. *Cell Rep* **23**, 2509-2523 (2018).
27. Baron, M. *et al.* A Single-Cell Transcriptomic Map of the Human and Mouse Pancreas Reveals Inter- and Intra-cell Population Structure. *Cell Syst* **3**, 346-360 e4 (2016).
28. Howard, D. *et al.* An in vitro whole-cell electrophysiology dataset of human cortical neurons. *Gigascience* **11**(2022).
29. Yuan, W. *et al.* Temporally divergent regulatory mechanisms govern neuronal diversification and maturation in the mouse and marmoset neocortex. *Nat Neurosci* **25**, 1049-1058 (2022).
30. Geaghan, M. & Cairns, M.J. MicroRNA and Posttranscriptional Dysregulation in Psychiatry. *Biol Psychiatry* **78**, 231-9 (2015).
31. Forrest, M.P. *et al.* Open Chromatin Profiling in hiPSC-Derived Neurons Prioritizes Functional Noncoding Psychiatric Risk Variants and Highlights Neurodevelopmental Loci. *Cell Stem Cell* **21**, 305-318 e8 (2017).
32. Flaherty, E. *et al.* Neuronal impact of patient-specific aberrant NRXN1alpha splicing. *Nat Genet* **51**, 1679-1690 (2019).
33. Pardinas, A.F. *et al.* Common schizophrenia alleles are enriched in mutation-intolerant genes and in regions under strong background selection. *Nat Genet* **50**, 381-389 (2018).
34. Hauberg, M.E., Roussos, P., Grove, J., Borglum, A.D., Mattheisen, M. & Schizophrenia Working Group of the Psychiatric Genomics, C. Analyzing the Role of MicroRNAs in Schizophrenia in the Context of Common Genetic Risk Variants. *JAMA Psychiatry* **73**, 369-77 (2016).
35. Yao, Y. *et al.* Cell type-specific and cross-population polygenic risk score analyses of MIR137 gene pathway in schizophrenia. *iScience* **24**, 102785 (2021).
36. You, X. *et al.* Investigating aberrantly expressed microRNAs in peripheral blood mononuclear cells from patients with treatmentresistant schizophrenia using miRNA sequencing and integrated bioinformatics. *Mol Med Rep* **22**, 4340-4350 (2020).
37. Yu, H.-c. *et al.* Alterations of miR-132 are novel diagnostic biomarkers in peripheral blood of schizophrenia patients. *Progress in Neuro-Psychopharmacology and Biological Psychiatry* **63**, 23-29 (2015).
38. Nanou, E. & Catterall, W.A. Calcium Channels, Synaptic Plasticity, and Neuropsychiatric Disease. *Neuron* **98**, 466-481 (2018).
39. Tian, B. & Manley, J.L. Alternative polyadenylation of mRNA precursors. *Nat Rev Mol Cell Biol* **18**, 18-30 (2017).
40. Shah, A., Mittleman, B.E., Gilad, Y. & Li, Y.I. Benchmarking sequencing methods and tools that facilitate the study of alternative polyadenylation. *Genome Biol* **22**, 291 (2021).
41. Lopez-Murcia, F.J., Reim, K., Jahn, O., Taschenberger, H. & Brose, N. Acute Complexin Knockout Abates Spontaneous and Evoked Transmitter Release. *Cell Rep* **26**, 2521-2530 e5 (2019).
42. Mitok, K.A., Keller, M.P. & Attie, A.D. Sorting through the extensive and confusing roles of sortilin in metabolic disease. *J Lipid Res* **63**, 100243 (2022).
43. Finucane, H.K. *et al.* Heritability enrichment of specifically expressed genes identifies disease-relevant tissues and cell types. *Nat Genet* **50**, 621-629 (2018).
44. Hwang, H.W. *et al.* cTag-PAPERCLIP Reveals Alternative Polyadenylation Promotes Cell-Type Specific Protein Diversity and Shifts Araf Isoforms with Microglia Activation. *Neuron* **95**, 1334-1349 e5 (2017).
45. Zheng, S., Gray, E.E., Chawla, G., Porse, B.T., O'Dell, T.J. & Black, D.L. PSD-95 is post-transcriptionally repressed during early neural development by PTBP1 and PTBP2. *Nat Neurosci* **15**, 381-8, S1 (2012).
46. Koopmans, F. *et al.* SynGO: An Evidence-Based, Expert-Curated Knowledge Base for the Synapse. *Neuron* **103**, 217-234 e4 (2019).

Methods

Methods – Table of contents

Experimental Model and Subject details **36**
Key reagents and resources used in this study **36**
PBMC collection and iPSC reprogramming **36**
PBMC collection at LMU 36
Reprogramming of PBMCs to iPSCs at LMU 37
PBMC collection at MPIP 37
Reprogramming of PBMCs to iPSCs at MPIP 37
Reprogramming of fibroblasts to iPSCs **38**
Culturing of iPSCs **38**
iPSC characterization: Digital karyotyping **38**
DNA extraction and genotyping 38
Analysis digital karyotyping 39
Genotype imputation, PRS calculation, and CNV analysis **40**
Whole genome imputation of human genotyping data 40
PRS calculation 40
CNV analysis 41
iPSC characterization: Immunocytochemistry (ICC) **41**
iPSC characterization: Embryoid body (three germ layer) differentiation **41**
Embryoid body production 41
RNA-Seq library production (from EBs) 42
Characterization of germ layer differentiation potential 42
Differentiation of excitatory cortical neurons from iPSCs **42**
Lentivirus production 42
Mouse astrocyte preparation 43
Neuronal differentiation 43
Endophenotyping of iPSC-derived neurons **44**
BulkRNAseq – preparation **44**
RNA sample collection 44
RNA-Seq library preparation 45
BulkRNAseq – analysis **45**
RNA-Seq data processing and analysis 45
Identification of novel polyadenylation sites in the 3'UTR in iNs 46
3'APA analysis of iNs RNA-Seq and post mortem RNA-Seq data 47
Association analysis APA-PRS 47
LD-score regression and partition heritability analysis of transcripts subject to dAPA 47
Transcript Pathway analysis 48
Power analysis 48
Single-cell RNA-Seq from iNs **48**
Sample preparation and sequencing 48
Data processing and analysis 49
Deconvolution analysis of RNA-Seq profiles of iNs 49
Comparison of iN scRNA-Seq profiles to human and murine primary cortical snRNA-Seq 49
miRNAseq **50**
Sample collection 50
Library preparation 50
Data processing 50
Analysis 50
ATAC-Seq **50**
Sample collection and library preparation 50
ATACseq analysis 51
Identity verification of sequencing libraries **52**
qPCR **52**
Sample collection 52

919 *cDNA synthesis* ... 52
920 *Analysis* ... 52
921 **Western blot** ... **53**
922 *Harvesting* ... 53
923 *Protein extraction* ... 53
924 *Digital western blotting* ... 53
925 *Analysis* ... 53
926 **Immunocytochemistry (ICC)** ... **54**
927 *Fixation and staining* ... 54
928 *iNs maturity analysis* ... 54
929 *Synapse count analysis* ... 54
930 **PTBP2 knockdown** ... **55**
931 *Synaptic density analysis in PTBP2^{KD}* ... 55
932 **Electrophysiology** ... **56**
933 *Patch clamp* ... 56
934 **Quantitative trait analysis** ... **57**
935 *Expression quantitative trait (eQTL) analysis* ... 57
936 *microRNA quantitative trait (mirQTL) analysis* ... 57
937 *Chromatin quantitative trait (caQTL) analysis* ... 57
938 **Overlap of QTLs with human post mortem and GWAS data** ... **58**
939 **RBP binding motif analysis in 3'UTR sequences** ... **58**
940

941 Experimental Model and Subject details

942 All tissue donations from patients with schizophrenia (SCZ), bipolar disorder (BD) and depression
943 (MDD) and neurotypical controls (Ctrls) were conducted according to the guidelines of the
944 Declaration of Helsinki. Informed consent was obtained from all subjects involved in the study.
945 Human iPSC cell lines were obtained from cohort studies at the Department of Psychiatry and
946 Psychotherapy, University Hospital, LMU Munich, 80336 Munich, Germany (approved by the
947 local ethics committee of the Faculty of Medicine, LMU Munich, Project 17-880, 29.03.2018;
948 project 18-716, 15.10.2020) and at the MPI for Psychiatry (approved by the local ethics committee
949 of the Faculty of Medicine, LMU Munich, project numbers 350-14, 19-310, 20-314,19-678 and
950 18-393 and from ThermoFisher, NIMH, Helmholtz Zentrum Munich and the Coriell Biobank.
951 From the latter, we also included a cohort of Amish individuals suffering from BD/MDD and
952 respective controls, see **Supplementary Table 1**.

953 Key reagents and resources used in this study

954 **Supplementary Table 5**

955 PBMC collection and iPSC reprogramming

956 *PBMC collection at LMU*

957 Blood samples (18-36 ml) were collected in EDTA or natrium heparin tubes. PBMCs were isolated
958 by Ficoll-Paque gradient according to manufacturer's instructions. After washing with PBMC
959 medium (RPMI1640, 10% FBS, and 1 mM sodium pyruvate), cells were counted, and resuspended
960 ($1x10^7$ cells/ml) in freezing medium (RPMI1640, 20% FBS, 1 mM sodium pyruvate, and 10%
961 DMSO). Cryotubes were placed immediately into a freezing container, stored at -80°C for 24 hr,
962 and thereafter under liquid nitrogen.

963 *Reprogramming of PBMCs to iPSCs at LMU*

964 Reprogramming was carried out by modification of a previously published protocol[47]. PBMCs
965 were thawed in pre-warmed StemPro34 medium (StemCell Technologies™) and cultivated in
966 uncoated 6 well plates for 5 days (D). Half media change was performed on D 1 and D 4.
967 After 2 washes with DPBS, PBMCs (2 x 10^6) were resuspended in 100 µl nucleofection buffer
968 (Human CD34+ Nucleofector Kit™), episomal vectors[47] were added (pCE-hOCT3/4 (#41813),
969 pCE-hSK (#41814), pCE-hUL (#41855), pCE-mp53DD (#41856); and pCXB-EBNA1 (#41857);
970 all from Addgene) and nucleofection carried out with Amaxa Nucleofector II™. PBMCs were
971 recovered in StemPro34 medium and transferred to 2 wells of a vitronectin-coated 6 well plate
972 containing each 2 ml StemPro34 medium. On the next day (D 1), 1 ml of N2B27 medium
973 supplemented with bFGF (50 ng/ml) and sodium butyrate (NaB, 0.25 mM) was added to each well.
974 Until D 7, daily half media change and on D 8 full media change with supplemented N2B27 was
975 performed. On D 9, medium was replaced by Essential 8 Flex and nascent colonies grown for
976 about 3 weeks. Cultures were supplemented with 5 µM ROCK inhibitor before single colonies
977 were picked (n=8-12) under microscopic control using 25 gauge 1 ½ inch needle and 100 µl tips.
978 Remaining colonies were pooled and both singly isolated and pooled colonies were separately
979 expanded on vitronectin-coated plates. Finally, iPSC populations were purified using Tra1-60
980 microbeads according to manufacturer's instructions (Miltenyi Biotec™, see also 1.3.2).

981 *PBMC collection at MPIP*

982 PBMCs were isolated from blood sampling (see above) using SepMate-50 tubes (StemCell
983 Technologies™) according to manufacturer's instructions. Cell pellets were resuspended in 1-5
984 ml Erythroid Expansion Medium (EEM)[48], expanded for reprogramming (see below), or
985 resuspended in EEM containing 10% DMSO (5 x 10^6 cells/ml) for storage under nitrogen.

986 *Reprogramming of PBMCs to iPSCs at MPIP*

987 Reprogramming was carried out by modification of a previously published protocol[48]. Briefly,
988 PBMCs were enriched and expanded for erythroid progenitors in EEM across 10-15 days, when
989 either nucleofection was performed or stocks were made (freezing medium 90% FBS/10%
990 DMSO).
991 Nucleofection was performed with Human CD34+ Nucleofector Kit (Lonza™) and Amaxa
992 Nucleofector II. Erythroid progenitors (2 x 10^6) were resuspended in 100 µl nucleofection buffer
993 and episomal vectors (4 µg MOS, 4 µg MMK, and 2 µg GBX) **were added**. Following pulse
994 application (program T-016), cells were transferred into a single well of a 12 well plate (D 0)
995 containing 2 ml EEM. At D 2, cells were collected in a 15 ml conical tube and centrifuged at 200
996 g for 5 minutes (min). Supernatant was carefully descanted, cells resuspended in 1 ml DMEM/F12
997 supplemented with 10% FBS, and transferred into a single well of a 12 well plate coated with
998 vitronectin (5 µg/ml diluted in DPBS). Plate was sealed with parafilm, centrifuged at 200 g for 30
999 min at 25 °C, and returned to the incubator. After 24 hr, medium was carefully removed,
1000 transferred into a 15 ml conical tube, and centrifuged (300 g for 5 min). Meanwhile, Essential8
1001 (E8) medium (0.5 ml) supplemented with NaB (0.25 mM) was added to the emptied well to prevent
1002 drying of already adherent cells. Pelleted cells were resuspended in 0.5 ml supplemented E8 and
1003 reseeded in the original well. From D 5 onward, medium was replenished every other day until
1004 single cells were grown to sizeable colonies. These were isolated singly or as pool (see above) and
1005 expanded onto Matrigel-coated 48 wells with E8 medium supplemented with Revita Cell (E8/RC).
1006 Tra-1-60 selection was performed after 3-4 additional passages. Cells were washed once with
1007 DPBS, dissociated with accutase for 5 min at 37°C, and centrifuged at 300 g for 5 min. After

1008 resuspension in 80 µl E8/RC, 20 µl Tra-1-60-labelled magnetic beads (Miltenyi™) were added
1009 and selection of Tra1-60 positive cells conducted according to manufacturer's instructions.
1010 Selected cells were seeded in E8/RC until the next day when medium was replaced by E8 only.
1011 Around passage 4-7, iPSCs were adapted to StemMACS iPS Brew XF by culturing with an equal
1012 mixture of both media for one passage before replacing by StemMACS iPS Brew XF only. For
1013 storage, iPSCs were resuspended in freezing medium (50% FBS, 40% DMEM/F12, and 10%
1014 DMSO), transferred in a freezing box to -80°C for 24 hr, and thereafter to liquid nitrogen.

1015 Reprogramming of fibroblasts to iPSCs

1016 Life cultures of primary human skin fibroblasts from were obtained from Coriell. After overnight
1017 recovery, medium was replaced by FBM (DMEM, 10 % FCS, 1x MEM-NEAA) and renewed
1018 every 3-4 days. When cells reached 90 % confluency, fibroblasts were washed with DPBS and
1019 pretreated at room temperature (RT) with 0.5 mM EDTA (UltraPure™) for 5 min before cells were
1020 dissociated with 1x Trypsin/EDTA. Dislocated cells were centrifugated in FBM (300 g for 5 min
1021 at RT), reseeded, and expanded for 3-5 passages.
1022 Reprogramming of fibroblasts was conducted by modification of a previously published
1023 protocol[49]. Briefly, fibroblasts (2 x 10^6), freshly plated 24 hr before nucleofection, were
1024 resuspended in 100 µl nucleofection buffer (Nucleofector Kit R (VCA-1001, Lonza™). Following
1025 addition of 20 µg CoMiP 4in1 plasmid (#63726, Addgene), fibroblasts were nucleofected (Amaxa
1026 Nucleofector II, program U-023). Recovered fibroblasts were plated on Matrigel in 2 wells of a 6-
1027 well plate (D 0). On the following day, media was replaced by FBM supplemented with 50 µg/ml
1028 ascorbic acid and a cocktail of inhibitors (0.3 mM PFT□, 3 mM EPZ 4777, and 0.2 mM NaB).
1029 Medium was replenished on D 2 and half-changed to supplemented E7 media on D3. From D 4
1030 onward, supplemented E7 was replaced daily over 5 days. Media was half changed to
1031 supplemented E8 media on D 10 and fully replenished with supplemented E8 from D 11 onward
1032 until the first iPSCs colonies appeared around D 16 to 25. Only then, supplements were omitted.
1033 Colonies were isolated singly or as pool, expanded, and Tra-1-60 selected as described above.
1034 Throughout this study, iPSC cell lines derived from pools of 25-45 individual colonies were used.

1035 Culturing of iPSCs

1036 Frozen iPSCs were thawed in the water bath, collected in DMEM/F12 and centrifuged at 300 g for
1037 5 min. Pellet was resuspended in StemMACS iPS Brew XF supplemented with 100x RevitaCell
1038 Supplement and seeded on plates that were coated with Matrigel (diluted 1:100 in DMEM/F12)
1039 for at least 30 min. Medium was changed every day by fresh StemMACS iPS Brew XF and cells
1040 were passaged twice per week. For passaging, cells were dissociated with gentle cell dissociation
1041 reagent for 5 min at 37°C, collected in DMEM/F12, centrifuged at 300 g for 5 min and seeded 1:6
1042 in StemMACS iPS Brew XF on Matrigel-coated plates.

1043 iPSC characterization: Digital karyotyping

1044 *DNA extraction and genotyping*

1045 In order to characterize the original as well as the generated cell type by digital karyotyping, DNA
1046 of PBMCs or iPSCs from each donor was extracted using the QIAamp DNA Blood Mini Kit from
1047 Qiagen. To that end, cells were collected in a 15 ml conical tube, pelleted by centrifugation at 300
1048 g for 5 min and placed on ice. Medium was removed, pellet was dissolved in 200 µl DPBS and
1049 transferred into a 1.5 ml reaction tube prepared with 20 µl Proteinase K (from the kit). 4 µl RNase
1050 (from the kit) was added per tube and suspension was mixed by pipetting up and down. After

1051 adding 200 µl AL Buffer and vortexing for 15 seconds (sec), mixture was incubated at 56 °C for
1052 20 min. 200 µl 100% EtOH were added and mixed with the rest by pipetting up and down.
1053 Suspension was transferred to a column provided from the kit and vacuum was applied to let the
1054 fluid pass through. After washing the membrane with 500 µl AW1 Buffer and another application
1055 of vacuum, membrane was washed with 500 µl AW2 Buffer and vacuum was applied another
1056 time. Columns were transferred into a collection tube and centrifuged at 13000 g for 1 min. Flow-
1057 through was discarded and tubes were centrifuged at 13000 g for 30 sec. After transferring the
1058 column into a new 1.5 ml tube, DNA was eluted by adding 80 µl H_2O and centrifuging at 13000
1059 g for 1 min. Extracted DNA from PBMCs or iPSC cells were hybridized to the Illumina Global
1060 Screening Array-24 (GSA).

1061 *Analysis digital karyotyping*

1062 In order to detect de novo copy number abnormalities (CNA) arising in cultured cell lines or
1063 general screening for copy number variation status (CNV), we implemented a comprehensive
1064 pipeline which includes a developed digital karyotyping method developed[50] and freely available
1065 in BCFtools package[51] as "cnv" command. In addition, our pipeline (available at
1066 https://gitlab.mpcdf.mpg.de/luciat/cnv_detection.git) includes also quality control for genotype
1067 and sample calls as well as sample label mismatch detection and correction. The goal is to
1068 determine possible differences between cell lines and starting material of derivation in term of
1069 copy number variation using genotyping arrays. This genomic screening for chromosomal
1070 abnormalities is used as a quality control to establish and maintain stem cell lines. We indicate
1071 with line the single probe/sample and with donor the individual from which multiple lines can be
1072 derived (e.g. iPSCs and fibroblast).
1073 Following raw data acquisition, Genotyping (GT) module of GenomeStudio software provided by
1074 Illumina was used to call genotypes. For each probe, GT module estimates Log R ratio (LRR) and
1075 B-allele frequency (BAF) using a clustering module applied to the distribution of signal intensities.
1076 Samples quality is evaluated and quality control of genotype calls are curated. In particular, SNPs
1077 statistics from GenomeStudio are reviewed and filtered based on the protocols[52]. For autosomal
1078 chromosomes and pseudoautosomal regions in chromosomes X and Y, variants with any of the
1079 following conditions are excluded: cluster separation ≤ 0.3, AA R Mean ≤ 0.2, AB R Mean ≤ 0.2,
1080 BB R Mean ≤ 0.2, AB T mean ≤ 0.1 or > 0.9, Het Excess < -0.9 or > 0.9, MAF > 0 and AB Freq
1081 = 0, AA Freq = 1 and AA T Mean > 0.3, AA Freq = 1 and AA T Dev > 0.06, BB Freq = 1 and BB
1082 T Mean < 0.7, BB Freq = 1 and BB T Dev > 0.06. Finally, we also excluded variants with call
1083 frequency < 0.98 if the total number of probes is higher than 500, otherwise lower or equal than
1084 $f(n) = 0.0004 * n + 0.7804$ with n the number of probes in the chip considered, so that a study
1085 with a small number of samples is not excessively penalized. For variants in the haploid
1086 chromosomes instead, we initially inferred the sex of each sample. If (i) percentage of genotype
1087 called as AB in chromosome X < 0.01 and (ii) percentage of not called (NC) genotypes in
1088 chromosome Y is < 0.7 then the sample is assigned as "male". Instead, if both conditions (i) and
1089 (ii) are not satisfied the sample is assigned as "female" and if only one of the two conditions is met
1090 then the sample is assigned as "undefined". Afterwards, a variant in chromosome X is excluded if
1091 the fraction of AB calls in males with respect to the total number of males is higher than 0.5 and a
1092 variant in chromosome Y is excluded if the fraction of assigned calls with R > 0.2 in females with
1093 respect to the total number of females is higher than 0.5. In chromosome Y, variants such that the
1094 call frequency in males is lower than 0.98 or the function f previously defined depending on the
1095 number of samples are additionally excluded. The final set of variants is used to compute sample
1096 call rates with should be > 0.98 to be considered reliable.

1097 Then, sample mismatches or mislabelling are checked using genotype assignment (AA, AB or BB)
1098 and a percentage of matching genotypes for each pair of the available lines is computed as the
1099 percentage of variants with the same call. Lines from same donor should show genotype match
1100 around 99%. If the match is lower than 97% for the same donor or there is one or more lines that
1101 match a certain donor but are not assigned to it, then the matching samples are reassigned with a
1102 new name.
1103 Finally, copy number differences between starting material (e.g. PBMC) and derived lines (e.g.
1104 iPSC) from the same donor are inferred using a hidden Markov model algorithm implemented in
1105 BCFtools (cnv command)[50]. The program is run in the pairwise mode with the default parameters.
1106 For the CNV detection of a single line instead, the program is run on single mode based on a
1107 single-sample hidden Markov model. CNA calls are then filtered to reduce the number of false
1108 calls (see Methods section[53]) and only CNA with the following characteristics are retained: length
1109 higher or equal than 0.2 Mb, quality score higher than 2, number of markers and heterozygous
1110 markers for copy number 1 and 3 respectively higher than 10.

1111 Genotype imputation, PRS calculation, and CNV analysis

1112 *Whole genome imputation of human genotyping data*

1113 GSA array genotyping data for 184 human samples corresponding to the case/control cohort used
1114 in this study was processed by Illumina Genome Studio <> PLINK1.9 and PLINK2 were used for
1115 all quality control assessments; first a per SNP and per sample missingness count was performed
1116 with parameters set at --maf 0.01 --geno 0.02 --mind 0.02. The dataset was then filtered for sample
1117 repeats, identity by descent was used to identify close relatives which were temporarily removed
1118 (PI HAT threshold = 0.0625) to assess population stratification and identify population outliers.
1119 The latter was done by first pruning the SNPs by --geno 0.02 --hwe 1e-3 --indep-pairwise 200 100
1120 0.2 --maf 0.05 —set-hh-missing and excluding the major histocompatibility complex (MHC) as
1121 well as the interstitial inverted duplication INV8, this was followed by creating an
1122 multidimensional scaling (MDS) clustering using the following parameters: —cluster --mds-plot
1123 10 eigendecomp. Outliers were discarded using a threshold of 4 standard deviations and relatives
1124 were added back to the dataset. SNPs were evaluated and filtered based on Hardy-Weinberg
1125 equilibrium with a threshold of 1e-6. SNP names were updated to match those of the 1000
1126 Genomes Phase 3 which was the reference panel used for imputing the samples. Duplicated SNPs
1127 were removed and remaining SNPs were checked and strand orientation corrected if needed. The
1128 dataset was phased using shapeit v2.r837 and windows of 5Mb were imputed using IMPUTE
1129 version 2.3.2 using the parameters -pgs_miss -filt_rules_l -buffer 500. Post-imputation quality
1130 control was applied by identifying empty or low SNP count blocks which were either discarded or
1131 reimputed by moving the window location and/or size. In order to filter high quality imputed SNPs,
1132 an info score great than 0.8 and minor allele frequency threshold of 0.01 were used to select the
1133 final SNPs.

1134 *PRS calculation*

1135 We calculated PRS for schizophrenia based on prior GWAS of schizophrenia using the PGC3
1136 release[3], Mullins et al. for BD[6] and Wray et al. for MDD[54]. PRS-CS[55] was used to infer posterior
1137 SNP effect sizes under continuous shrinkage priors and estimate the global shrinkage parameter
1138 (φ) using a fully Bayesian approach with genotype dosage data.

1139 *CNV analysis*

1140 Bipolar disorder, Major Depressive disorder and Autism associated Copy Number Variations
1141 (CNV) were obtained from Zarrei et. al.[56], only CNVs labeled as high confidence were used. CNVs
1142 were called in all our samples and later compared to the known disease associated CNVs
1143 mentioned above by overlapping their genomic coordinates, this was done using bedtools intersect
1144 v2.26.0, a match was only called when a minimum overlap of 90% of both CNVs being compared
1145 was covered. The same overlapping procedure was applied to SCZ CNVs obtained from Marshall
1146 et al.[57], which were first lifted over from hg18 to hg19 genome assembly using UCSC[58] liftover
1147 tool (http://genome.ucsc.edu/cgi-bin/hgLiftOver).

1148 iPSC characterization: Immunocytochemistry (ICC)

1149 Initially, attached cells were washed 1x with DPBS. DPBS was removed and fixation was
1150 performed with 4% PFA in DPBS for 10 min at RT. After removal of fixation solution, 3x washing
1151 steps with DPBS were performed. Samples were stored up to 2 weeks at 4°C for subsequent steps.
1152 After permeabilization with 0.1% Trition-X-100 in PBS for 10 min at RT blocking was performed
1153 with blocking solution of 0.1% Trition-X-100 and 1% BSA in PBS for 60 min at RT. Primary
1154 antibodies were added in blocking solution and incubated overnight at 4°C. At the next day,
1155 primary antibody solution was removed with 3x washing with PBS. Respective secondary
1156 antibodies in PBS were added and incubated for 60 min at RT. Secondary antibody solution was
1157 removed with 3x washing with PBS, Finally, samples were washed 1x with water and mounted
1158 onto microscope slides. If mounting medium did not contain DAPI, nuclei counterstaining was
1159 performed with DAPI, supplemented during the 2nd washing step. At the LMU Munich, imaging
1160 was performed on an Axio Observer.Z1 (Zeiss) inverted microscope and image analysis was
1161 performed with ZEN (Version 3.3, Zeiss) and Fiji[59].

1162 iPSC characterization: Embryoid body (three germ layer) differentiation

1163 *Embryoid body production*

1164 In order to confirm the differentiation potential into all three germ layers, embryoid body (EB)
1165 formation was performed for each reprogrammed cell line[60]. To that end, iPSCs were seeded in
1166 iPS Brew medium in one well of a 6well plate coated with Matrigel and grown until 90 %
1167 confluency. Medium was aspirated and cells were washed once with 1 ml DPBS before being
1168 dissociated by 1 ml Gentle Cell Dissociation Reagent for 5 min at RT. 1 ml iPS Brew was added
1169 and cell suspension was transferred into a 15 ml conical tube without disrupting the dissociated
1170 colonies. After centrifugation at 300 g for 5 min, pellet was solved in 5 ml EB medium consisting
1171 of Knockout-DMEM (88%), Knockout Serum Replacement (10%), Non-essential amino acids
1172 (1%) and L-Glutamine (1%) by pipetting up and down maximally 3 times, transferred into a 60
1173 mm dish and incubated at 37°C. Medium was changed on Day 2 and Day 4 by transferring the EB
1174 suspension gently into a 15 ml conical tube and adding 2 ml EB medium into the dish in order to
1175 avoid drying of remaining EBs. After letting EBs sediment in the conical tubes for 10-15 min,
1176 supernatant was aspirated, EBS resuspended with 3 ml fresh EB medium and transferred back into
1177 the 60 mm dish. While changing the medium on Day 5 in the same way as before for 4 ml of EB
1178 suspension, remaining 1 ml suspension was transferred into a separate 15 ml conical tube, cells
1179 were sedimented separately and resuspended in 2 ml EB medium for being plated into two wells
1180 of a 24well plate coated with Matrigel (1ml/well). Medium was changed every other day until Day
1181 12-15. For harvesting the cells in the dish, EBs were transferred gently into 15 ml conical tube and
1182 centrifuged at 300 g for 5 min. After removing supernatant, pellet was frozen at -80°C. Attached

1183 cells in the 24well plate were fixed in 16% Paraformaldehyde and were stored at 4°C until being
1184 stained.

1185 *RNA-Seq library production (from EBs)*

1186 QuantSeq 3' mRNA-Seq Library Prep Kits (Lexogen) was used to prepare Illumina sequencing
1187 libraries. Based on manufacturer's protocol 500 ng of RNA from each sample was used to prepare
1188 the RNA-Seq libraries. Library's size distribution and quality were quantified by high-sensitivity
1189 DNA chip (Agilent Technologies).

1190 *Characterization of germ layer differentiation potential*

1191 In order to assess iPSC differentiation potential into cells from the three embryonic germ layers
1192 ectoderm, mesoderm and endoderm, we followed a similar strategy previously implemented in the
1193 iPSC Scorecard concept and its derivatives[60], relying on 15 days long random differentiation of
1194 iPSCs into embryoid bodies, followed by bulk RNA-Seq of the respective EBs. In addition, we
1195 generated representative RNA-Seq profiles from a subset of the iPSC lines. Subsequently, we used
1196 established markers for pluripotent, ectodermal, mesodermal and endodermal cells and computed
1197 the "differentiation potential" of each iPSC line into these germ layers based on the RNA-Seq
1198 profiles of the EBs, following the same approach as implemented by Tsankov et al.[61]. Briefly, to
1199 analyze the germ layer marker gene expression in each EB sample, we computed the one-sided t-
1200 statistic comparing the gene's expression against its distribution across the iPSC lines. As negative
1201 control, we also computed the one-sided t-statistic for each marker in each iPSC line compared to
1202 its expression in all other iPSC lines. In addition, we computed the $\log_2$ fold change of each marker
1203 gene between the average EB and average iPSC expression level as weight for each marker gene
1204 and calculated the germ layer differentiation potential based on the marker gene sets for each germ
1205 layer, analogous to the approach employed by Tsankov et al.[61] and display the results in **Extended**
1206 **Data Fig. 1k,l**.

1207 Differentiation of excitatory cortical neurons from iPSCs

1208 In order to investigate potential differences in neurons derived from patients with mental illness
1209 and healthy controls, iPSC from 106 different donors were differentiated into induced cortical
1210 glutamatergic neurons (iNs) according to previous protocols[26,62] by using doxycycline-inducible
1211 overexpression of the transcription factor NGN2 and cultured those neurons, together with murine
1212 astrocytes after seven days, for a period of 49 days.

1213 *Lentivirus production*

1214 Human embryonic kidney cell line HEK293 was cultured in DMEM (high glucose, pyruvate)
1215 supplemented with 10% FBS. Around 80 % confluency, cells were dissociated with 2x Trypsin
1216 and collected in DMEM/10% FBS. After centrifugation at 300 g for 5 min and counting with
1217 Neubauer Chamber, 5 x 10^6 cells were seeded in 8 ml DMEM/10% FBS into a cell culture dish
1218 (8.7 cm^2) and incubated for 20-24 hours at 37°C. Cells were washed once with 5 ml DMEM/F12
1219 and afterwards cultured in 8 ml DMEM/F12. Two mixes forming the plasmid mix and the
1220 transfection reagent mix were prepared. For each cell culture dish 6 µg psPAX2, 3 µg pMD2.G
1221 (VSVG) and 9 µg pTet-O_Ngn2-puro or FUW-M2rtTA were prepared in 0.5 ml DMEM/F12
1222 forming the plasmid mix. In a second mix 54 µl transfection reagent LipoD293 DNA was added
1223 in 0.5 ml DMEM/F12. After vortexing both mixes briefly, LipoD293 DNA mix was added to the
1224 plasmid mix, vortexed briefly again and incubated for ten min at RT. After adding 1 ml transfection
1225 mix dropwise to the cells and incubating for 18 hours at 37 °C, medium was replaced by 20 ml
1226 DMEM/10% FBS and incubated for further 48 hours at 37 °C. Medium was collected, filtered

1227 through 0.45 µm sterile Acrodisc syringe filter in a 50 ml conical tube and supplemented with 5
1228 ml Peg-it Virus Precipitation Solution. After inverting the tubes five to ten times, mixture of viral
1229 particles and Peg-it Virus Precipitation Solution was incubated for 72 hours at 4 °C. After
1230 incubation time, mixture was centrifuged at 1500 g for 30 min at 4°C. The supernatant was
1231 discarded, pellet with precipitated viral particles resuspended in 250 µl cold DMEM/F12 (1:100),
1232 aliquoted on ice and stored at -80 °C.

1233 *Mouse astrocyte preparation*

1234 25-35 P1 mice were sacrificed in each batch and cerebral cortices were isolated in PBS
1235 supplemented with 2.5% FBS. Dissected cortices were transferred into a 15 ml conical tube and
1236 centrifuged briefly to remove the remaining PBS/10% FCS. After washing the pellet twice with 5
1237 ml PBS, 2 ml 1% DNAse in PBS was added and incubated for 5 min at 37°C in the water bath
1238 followed by adding 2 ml 2.5x trypsin and further incubation for 5 min at 37°C. Enhancing
1239 enzymatic dissociation, cell suspension was pipetted up and down 15 times starting with a 10 ml
1240 serological pipette, incubating for 5 min at 37 °C, pipetting up and down 15 times with a 5 ml
1241 serological pipette, incubating for 7 min at 37 °C, ending in pipetting up and down 10 times with
1242 the 1 ml filter tip. After dissociation single cells were filtered through a 100 µm filter mesh and
1243 collected in a 50 ml conical tube containing DMEM (high glucose, pyruvate) supplemented with
1244 10% horse serum (HS). Filter mesh was washed twice with DMEM/10% HS and cell suspension
1245 was centrifuged for 10 min at 300g. Supernatant was discarded carefully, cell pellet was
1246 resuspended in 5 ml DMEM/10% HS and filtered through a 40 µm filter mesh into a new 50 ml
1247 conical tube containing DMEM/10% HS. Filter mesh was washed twice with DMEM/10% HS and
1248 cells were seeded into four 75 cm^2 flasks that were coated with Attachment Factor Protein (1x) for
1249 at least 30 min at 37°C. Medium was changed to fresh DMEM/10% HS after two days and
1250 subsequently twice per week. Astrocytes were passaged after seven to nine days by incubating the
1251 cells with 2x Trypsin for 10 min at 37°C, collecting in DMEM/10% HS, centrifuging at 300 g for
1252 5 min and seeding the cells 1:2 to 1:2.5 on Attachment Factor-coated flasks. To end up always in
1253 the same passage number (P.3), astrocytes were either passaged another time after seven more
1254 days or were frozen transiently. To that end, cells were dissociated with 2x Trypsin, collected in
1255 DMEM/10% HS, centrifuged at 300 g for 5 min and either frozen in 90% DMEM/10% HS
1256 combined with 10% DMSO or seeded again 1:2 to 1:2.5 in DMEM/10% HS on Attachment Factor
1257 Protein-coated flasks.

1258 *Neuronal differentiation*

1259 At Day 0, 10cm dishes were coated with Matrigel (Matrigel in DMEM/F12; 5 ml/ 10cm dish for
1260 at least 1 hour at 37°C. iPSCs were separated with Accutase for 5 min at 37°C, diluted 1:1 in
1261 DMEM/F12 supplemented with 1% BSA, centrifuged at 300g for 5 min and resuspended in
1262 StemMACS iPS Brew XF supplemented with Polybrene (6µg/ml) and 1x RevitaCell. Cells were
1263 counted, cell suspension was adjusted to a concentration of 500,000 cells/ml) and lentiviral
1264 infection with pTet-O_Ngn2-puro and FUW-M2rtTA was performed. After incubation for 10 min
1265 at RT, subsequent seeding (25,000 cells/cm^2) on Matrigel-coated plates was performed.
1266 At the next day (Day 1), media was replaced by KSR media, which consists of KO DMEM with
1267 15% Knockout Serum Replacement, 1x NEAA, 1x Glutamax and 50 µM beta-mercaptoethanol,
1268 supplemented with 10 µM SB431542, 2 µM XAV939, 0.1 µM LDN-193189 and 2 µg/ml
1269 doxycycline to start neuronal patterning and directed differentiation. At Day 2, KSR media
1270 replaced by a 1:1 mixture of KSR media and N2 media, which consists of DMEM/F-12, 1x
1271 Glutamax, 3mg/ml glucose and 1x N-2, supplemented with 5 µM SB431542, 1 µM XAV939, 0.05
1272 µM LDN-193189, doxycycline and 10 µg/ml puromycin to select for successfully co-infected

1273 cells. At Day 3, media was replaced by N2 media supplemented with doxycycline and a final day
1274 with puromycin.
1275 At the following day (Day 4), young iNs were dissociated by treatment with Accutase for 5 min at
1276 37°C. After diluting cell suspension in Accutase in doubled volume of 1%BSA in DMEM/F12,
1277 cells were triturated by pipetting up and down 3x with an 1ml tip. After centrifugation, cells were
1278 seeded with 60.000 cells/cm² (200,000 cells/glass coverslip in a 24well for Patch Clamp
1279 Recording, 150.000 cells/well for MEA recordings) in NBM media, which consists of Neurobasal
1280 medium, 1x Glutamax, 1x NEAA, 1xB27 without vitamin A, 3 mg/ml glucose, 2% fetal bovine
1281 serum (FBS), freshly supplemented with 10 ng/ml BDNF, 10 ng/ml CNTF, 10 ng/ml GDNF and
1282 2 µg/ml doxycycline, on dishes that were coated with Poly-L-Ornithine (15 µg/ml) overnight at
1283 37°C and after 3x washing with DPBS at least 6 hours at 37°C with Laminin (1µg/ml) and
1284 Fibronectin (2 µg/ml). Regarding functional assays as patch clamp and MEA recordings, glass
1285 coverslips or glass plates were coated with Poly-L-Ornithine (20 µg/ml) in borate buffer (100 mM
1286 boric acid, 25mM Sodium Tetraborate in deionized H_2O) for 6 hours at 37°C, Wells were washed
1287 3x with H_2O (WFI), dried overnight at RT and coated the next day with Laminin (10 µg/ ml) and
1288 Fibronectin (20 µg/ ml) for at least 6 hours at 37°C.
1289 At Day 7, murine astrocytes were added by full media change with a density of 5000 mouse
1290 astrocytes/cm² on the iNs. After three days, last full media change was performed and 4 µM AraC
1291 was added to NBM media to stop glial cell division. Subsequently, half media changes were
1292 performed twice a week. Doxycycline was removed from NBM media after 21 days and replaced
1293 by 1µg/ml laminin. At Day 24, NBM media was replaced by BrainPhys media, which consists of
1294 BrainPhys Neuronal Medium, 1x Glutamax, 1x NEAA, 1xB27 without vitamin A, 3 mg/ml
1295 glucose, 3% fetal calf serum (FCS), freshly supplemented with 10 ng/ml BDNF, 10 ng/ml CNTF,
1296 10 ng/ml GDNF and 1µg/ml laminin to foster neuronal maturation. At Day 49 experiments for
1297 endophenotyping were performed.

1298 Endophenotyping of iPSC-derived neurons

1299 Investigating differential expression of genes between iNs derived from individuals with
1300 schizophrenia (ISCZ) or bipolar disorder (BD) compared to iNs derived from Ctrls, various
1301 experimental approaches were performed.

1302 BulkRNAseq – preparation

1303 *RNA sample collection*

1304 iNs were collected after 49 days of differentiation and RNA was isolated by using the RNA Clean
1305 and Concentrator-5 Kit (Zymo Research). Whole network was detached and collected in 1.4 ml
1306 cold DPBS in a 1.5 ml reaction tube. Cells were centrifuged at 300 g for 10 min at 4°C. PBS was
1307 removed and 500 µl QIAzol Lysis Reagent (Qiagen) was added per tube. Sample was incubated
1308 for 10 min at RT and subsequently either stored at -80 °C or further processed directly. After
1309 adding 100 µl chloroform, sample was vortexed, incubated for 2 min at RT and afterwards
1310 centrifuged at 10000 g for 15 min at 4 °C. Upper phase was collected in a new 1.5 ml reaction tube
1311 and same volume 100% ethanol was added and mixed by pipetting up and down. Sample was
1312 loaded on the Zymo-column provided by the kit and centrifuged for 30 sec at 10000 g. After adding
1313 400 µl RNA Prep Buffer and further centrifugation for 30 min at 10000 g, sample was washed
1314 with 700 µl RNA Wash Buffer and centrifuged for 1 min. Flow through was discarded and sample
1315 was centrifuged again for 30 min at 10000 g to remove residual Wash Buffer. After transferring
1316 column into new 1.5 ml collection tube, RNA was eluted by adding 15 µl DNA/RNAse free water

1317 and centrifuging for 1 min at 13000 g. In order to increase the outcome, the last step was repeated
1318 by adding eluted 15 µl again on column and centrifuging again for 1 min at 13000 g.
1319 RNA was treated with DNAse using DNA-*free*™ DNA Removal Kit (Invitrogen®). Therefore 8
1320 µl RNA was mixed with 1 µl 10x DNase I Buffer and 1 µl recombinant DNase I (rDNase I), and
1321 incubated for 30 min at 37 °C. 2 µl DNAse Removal Buffer was added and mixed with sample,
1322 and further incubated for 2 min at RT. The inactivation beads were spined down by centrifugation
1323 for 30", supernatant was transferred into a new tube and RNA was quantified by using RNA
1324 ScreenTape on 2200 TapeStation from Agilent Technologies and assessed with 2200 TapeStation
1325 Controller Software. For that purpose, 5 µl RNA Buffer were mixed with 1 µl RNA sample by
1326 vortexing for 1 min. Sample was centrifuged briefly, incubated for 3 min at 72 °C and subsequently
1327 incubated for 2 min on ice before being loaded on the TapeStation. Samples with a RIN above 8
1328 were further processed.

1329 *RNA-Seq library preparation*

1330 Full length: RNA was retrotranscribe and amplified using the SMART-Seq v4 Ultra Low Input
1331 RNA Kit for Sequencing (Clonotech). In particular, 2 ng of high quality RNA was mix with 0.3
1332 µl 10x Reaction buffer (prepared following the manufacturer's instructions) and 0.5 µl SMART-
1333 Seq CDS Primer II A. RNA secondary structures were destabilized at 72°C for 3 min. Afterwards,
1334 a mix containing 1 µl 5x First-Strand Buffer, 0.3 µl SMART-seq v4 Oligo, 0.2 µl RNase Inhibitors
1335 and 0.5 µl SMARTScribe enzyme was added to each reaction. Reverse transcription was was
1336 performed at 42°C for 90 min and the reverse transcriptase was inactivated by 10 min at 70°C. For
1337 the cDNA amplification step, to the last reaction a mix of 7.7 µl containing 6.3 µl 2x SeqAmp
1338 Buffer, 0.3 µl PCR Primer IIA and 0.3 µl SeqAmp Polymerase was added.
1339 The amplified double-strand cDNA was purified using 1.0X AMPure XP beads (Beckman
1340 Coulter), washed twice with 80% EtOH and eluate in 13 µl Elution Buffer (from Clonotech kit)
1341 and quantified on BioAnalyzer, (Agilent) using the High Sensitivity DNA chip.
1342 Forty picograms of the purified double-strand cDNA were fragmented using the Nextera XT DNA
1343 Library Preparation Kit (Illumina). The reaction was carried out in 5.1 µl adding to the appropriate
1344 volume of sample 2.5 µl Tagment DNA Buffer and 1.3 µl Amplicon Tagment Mix. The reaction
1345 was incubated at 55°C for 5 min and rapidly cooled down at 10°C. The tagmentation was
1346 inactivated incubating the samples at room temperature for 5 min with 1.3 µl Neutralize Tagment
1347 buffer.
1348 A different combination of index oligo from the Nextera XT Index Kit v2 Set A (Illumina) was
1349 used for each sample and amplified in a 12.8 µl reaction using 3.8 µl Nextera PCR Master Mix.
1350 Indexed libraries were purified using 1.8X AMPure XP beads (Beckman Coulter), washed twice
1351 with 80% EtOH and eluate in 23 µl.
1352 The final libraries were quantified on the BioAnalizer using the High Sensitivity DNA chip,
1353 multiplexed in equimolar pools and sequenced on HiSeq4000 (Illumina).

1354 <u>BulkRNAseq – analysis</u>

1355 *RNA-Seq data processing and analysis*

1356 Paired-End raw RNA-Seq read sequences were aligned against the GRCh38 genome assembly
1357 with the GENCODE version 27 transcriptome definition using the STAR aligner[63] version 2.7.3a
1358 with the following parameters: --outFilterType BySJout --outFilterMultimapNmax 20 --
1359 outFilterMismatchNmax 999 --outFilterMismatchNoverReadLmax 0.04 --alignIntronMin 20 --
1360 alignIntronMax 1000000 --alignMatesGapMax 1000000 --alignSJoverhangMin 8 --
1361 alignSJDBoverhangMin 1 --sjdbScore 1 --readFilesCommand zcat --outSAMtype BAM Unsorted

1362 SortedByCoordinate --quantMode GeneCounts --outSAMstrandField intronMotif. Subsequently,
1363 duplicates were marked and library quality metric were computed using picard tools
1364 (http://broadinstitute.github.io/picard/). In addition, reads were also aligned to GRCh37 and
1365 GENCODE version 27 for detailed comparison analysis with human post mortem data and eQTL
1366 calling, which was performed on GRCh37. Following quality control, gene level read counts
1367 were obtained using the Rsubread package, collapsing exon level reads onto gene level features
1368 based on GENCODE version 27 with the following parameters:
1369 countMultiMappingReads=FALSE,ignoreDup=FALSE,sGTFAnnotationFile=TRUE,
1370 isPairedEnd=T. Quantitative expression analysis was performed with DESeq2 version 1.22.2.
1371 Following size factor estimation, we excluded genes with total read counts across all samples
1372 below the 20th and above the 99th percentile as well as mitochondrial genes. Finally, we performed
1373 standard differential expression analysis testing for effect of diagnosis using differentiation site
1374 and sex as covariate including only one RNA-Seq sample per donor. Genes showing an adjusted
1375 p-value ≤0.01 and a minimal absolute $\log_2$ fold-change ≥ 0.5 between Ctrl and SCZ or Ctrl and
1376 BD (adjusted p-value ≤0.05) were defined as differential and used in subsequent analysis. To
1377 account for potential technical confounders originating from the library preparation etc., we
1378 performed PCA on the following technical parameters determined for each library using picard
1379 tools: PF_BASES, PERCENT_DUPLICATION, PCT_CODING_BASES, PCT_UTR_BASES,
1380 PCT_INTRONIC_BASES, PCT_INTERGENIC_BASES, MEDIAN_5PRIME_BIAS,
1381 MEDIAN_3PRIME_BIAS. PF_BASES was log2 transformed prior to PCA. We then included the
1382 first principal component (TechnicalPC1) from this analysis as covariate in all downstream
1383 analyses.

1384 *Identification of novel polyadenylation sites in the 3'UTR in iNs*

1385 To identify alternative polyadenylation sites and quantify differential polyadenylation site usage,
1386 we followed the recommendations from a recent benchmarking study comparing different
1387 experimental and computational approaches[40]. To that end, we first detected all polyadenylation
1388 sites (PAS) in use in iNs using 3'RNA-Seq in iNs at day 49 from 6 distinct donors[64] by mapping
1389 their 3'UTRs. We then detected all polyadenylated transcribed regions within the union of these
1390 RNA-Seq libraries using the R package transcriptR[65] in the following manner: We built a reference
1391 collection of candidate 3'transcript fragments using the constructTDS function with fragment size
1392 set to 250 and the swap.strand option set. Next, we overlapped the transcript fragment collection
1393 with all genes from Gencode version 27 and estimated the background distribution of detected
1394 fragments across the genome using the estimateBackground function with an FDR cutoff of 0.01.
1395 Subsequently, we identify polyadenylated transcripts using the detectTranscript function with a
1396 gap distance of 75, followed by merging neighboring candidate transcripts fragments within 100bp
1397 of each other. Finally, we only retain transcripts with a minimum size of 50bp, a maximum size of
1398 2kb, supported by at least 10 independent sequenced fragments, an FPKM of greater than 3 and
1399 overlapping with a known Gencode gene. The resulting transcript collection represents transcript
1400 fragments detected based on their polyadenylated 3'-end region. Finally, we use the APA analysis
1401 software QAPA to identify those transcripts with end-coordinates located within or beyond known
1402 3'UTRs of Gencode genes using the *qapa build* command. The 3'UTR end-coordinates correspond
1403 to novel and known PAS sites in iNs. All internal PAS are not considered further. We next defined
1404 coordinates of all individual 3'UTRs based on the coding sequence end-coordinate of each
1405 transcript and the PAS end-coordinate for each detected individual transcript fragment.
1406 Given that many Gencode transcripts harbored more than two PAS within a single known 3'UTR,
1407 we next reduced this complexity to two PAS sites/UTR variants for each transcript, selecting the

most distal PAS and the dominant proximal PAS. To that end, we segmented the entire 3'UTR region of each gene, extending from the CDS end-coordinate to the most distal PAS, into non-overlapping 3'UTR fragments based on all PAS located within the UTR. Subsequently, we quantified the number of overlapping read fragments from our full-length RNA-Seq data in iNs across 100 RNA-Seq samples and defined the UTR fragment with the highest mean normalized read count as the dominant proximal UTR/PAS site. These analyses gave rise to a maximum of two 3'UTR regions for each gene that were used for all subsequent analyses (**Supplementary Table 3**, APA sites). For differential APA analysis, we next quantified the normalized read count in all full-length RNA-Seq samples for each of the non-overlapping 3'UTR regions for each gene, counting all reads overlapping with the proximal or distal UTR region respectively. From these values, r_{prox} and r_{dist}, we computed the percentage of distal 3'UTR used for each gene *j* and each iN donor *I,* analogous to previous studies[66,67] as $R_{ij}= r_{distij}/(r_{proxij}+r_{distij})$. To quantify differential PAS site usage between HC and SCZ in iNs, we employed a beta regression approach as reported previously using a logit link function for the mean model, the identity function for the precision model as well as a maximum likelihood estimator[66], correcting for gender, batch and TechnicalPC1 (see the RNA-Seq analysis), testing for diagnosis status. Similarly, we also corrected the R_{ij} values for gender, batch and TechnicalPC1 using beta regression and used the residuals to compute the average difference in R values between the groups (ΔAPA, **Supplementary Table 3**). P-value were adjusted using the q-value method[68] and filtered based a q-value ≤0.05.

3'APA analysis of iNs RNA-Seq and post mortem RNA-Seq data

Analysis of differential APA in human postmortem samples was performed in a similar manner to dAPA analysis, quantifying normalized read counts across all CommondMind RNA-Seq libraires for samples with HC or SCZ status using the same 3'UTR library that was employed in iNs. dAPA analysis was conducted as before using beta regression adjusting for the following covariates: institution, gender, age of death, post mortem interval, RIN, RIN2, clustLIB, the first 5 genotype PCs capturing ancestry as well as the first 3 TechnicalPCs derived from the PCA of all RNA-Seq library quality parameter of the corresonding libraries. All dAPA events with a q-value ≤0.1 were considered significant.

Association analysis APA-PRS

To enable gene expression or APA association analysis with PRS, we first computed a cumulative measure of gene expression or APA across all differentially expressed or polyadenylated genes between SCZ and HC or MDD/BD and HC by averaging over their z-score normalized gene expression or R values for each sample separately. Following outlier filtering using Tukey's criterion for the averaged values, we performed association testing using a linear model to estimate the association between cumulated differential gene expression or cumulated dAPA with PRS for SCZ, BD and MDD separately.

LD-score regression and partition heritability analysis of transcripts subject to dAPA

To estimate whether or not genomic loci with transcripts that are subject to APA are enriched for psychiatric disease associated heritability, we performed LDscore regression and partition heritability analysis as previously described[43]. To that end, UTR regions extended by xx subject to APA in iNs or human postmortem PFC were intersected with the LDSC annotation files using bedtools[69] Version: v2.27.1-1-gb87c465. and formatted as input to the S-LDSC software[70]. LD scores were then calculated separately for each category (using LD Score Regression (LDSC) Version 1.0.1). Partition heritability analysis was performed according to current recommendation using the baseline model version 1.2[43]. For all annotation categories, a cell-type-specific analysis

1453 was performed using the *--h2-cts* flag to estimate disease association for the following traits: Major
1454 Depressive Disorder, Antidepressant treatment resistant, Any psychotic experience,
1455 Schizophrenia, Ever Smoked, Autism Spectrum Disorder, Bipolar Disorder, Major Depression,
1456 Psychotic Experience, Coronary Artery, Disease, Height, Type 1 Diabetes, Type 2 Diabetes,
1457 Neuroticism, LDL, Celiac, Years of Education. This was carried out using each disease's
1458 corresponding publicly available GWAS summary statistics obtained from
1459 https://alkesgroup.broadinstitute.org/LDSCORE/all_sumstats/.
1460 Finally, we report the cell and condition specific enrichment of all by traits P-value of tau and z-
1461 scores based on the regression coefficient and coefficient standard error.

1462 *Transcript Pathway analysis*

1463 In order to annotate transcripts subject to APA in iNs from ISCZ, we performed pathway and
1464 ontology enrichment analysis of this gene set using the enrichR meta-database[71] and SYNGO[46].

1465 *Power analysis*

1466 For detailed power analysis, we utilized the R-framework RnaSeqSampleSize[72], relying on a
1467 negative binomial model to simulate read count distributions from individual sample groups. We
1468 followed the standard protocol for power estimation based on RNA-Seq samples from the Ctrl and
1469 SCZ sample group, including only one sample per donor and using the same samples employed
1470 for the differential expression analysis in the main manuscript. Subsequently, genes were filtered
1471 based on raw read counts including only genes with at least 11 reads (20th percentile) and less than
1472 478780.4 (99th percentile) total reads per gene across the entire dataset. Power estimation analysis
1473 was conducted based the remaining gene set. Subsequently, we used the "est_count_dispersion"
1474 function of the RnaSeqSampleSize package with a 2 group design to estimate the dispersion,
1475 resulting in disp = 0.28525. We rounded this to the nearest digit and subsequently worked with a
1476 dispersion estimate of 0.3 We then used this estimate and a maximal sample size of 60 samples
1477 per group to compute power curves for different fold-change and FDR combinations using the
1478 "est_power_curve" function with lambda0 = 200, phi0 = 0.3, n = 60, f = 0.1 or 0.05 or 0.01 and
1479 rho = 1.5 or rho=2. The results are shown in **Extended Data Fig. 3d**.

1480 Single-cell RNA-Seq from iNs

1481 *Sample preparation and sequencing*

1482 Multiplexed scRNA-Seq profling involved iNs from 4 distinct donors per library. Neuronal
1483 networks were dissociated 49 days after differentiation with papain (10 units/ml) and DNAse (100
1484 units/ml) diluted in DMEM/F12 for 10 min at 37 °C to facilitate generation of a single cell
1485 suspension. Afterwards, the network was mechanically sheared with a P1000 pipette tip.
1486 DMEM/F12 supplemented with 20% FCS was added for centrifugation at 400 g for 5 min at RT.
1487 Cells were resuspended in DMEM/F12 supplemented with 1% BSA and 1x RC and pelleted for a
1488 final resuspension in 1 % BSA in DPBS supplemented with RNAse Inhibitor, 1x RC, 3 mM
1489 $Mg(Ac)_2$, and 5 mM $CaCl_2$. After removal of network debris with filters, cells were counted.
1490 12,000 cells (3,000 per donor) were loaded on the 10X Chromium machine (10X Genomics).
1491 scRNASeq libraries were prepared following manufacturer's instructions of the Chromium™
1492 Single Cell 3' Library & Gel Bead Kit v3 (10X Genomics). The scRNA-Seq library was
1493 subsequently sequenced/processsed on a NovaSeq 6000 S1 flowcell.

1494 *Data processing and analysis*

1495 For scRNA-Seq read alignment, pre-build GRCh37 genome reference files for 10X cellranger
1496 were downloaded from https://www.10xgenomics.com/. Subsequently, cellranger count (version
1497 3.1.0) was used for raw data processing giving rise to feature count matrices. In order to
1498 deconvolute the distinct cells from individual donors, we utilized demuxlet supplemented with the
1499 relevant donor genotypes to assign the most likely genotype of origin to each cell, following the
1500 standard protocol for this approach[73]. More specifically, we created a vcf containing relevant SNPs
1501 from the 3'UTR of hg19 transcripts using cftools (version 0.1.17) and the gencode 3'UTR hg19
1502 BED file (downloaded 09.02.2021 from http://genome.ucsc.edu/cgi-bin/hgTables). The resulting
1503 vcf encompassed ~ 98,000 sites. The genotype deconvolution was conducted in demuxlet setting
1504 the parameters to demuxlet --alpha 0.0 --alpha 0.0 --vcf
1505 vcf_ips_christine_hg19.filtered.recode.sorted.vcf --field GT.
1506 Subsequently, scRNA-Seq data analysis was continued in R (R version 3.6.1)[74] and Seurat package
1507 version 3.2.2 [75]. A Seurat object was created from the aggregated filtered count matrix, keeping
1508 cells with at least 800 and less than 10000 detected features as well as less than 15% mitochondrial
1509 RNA reads.
1510 Subsequently, count correction, regression of mitochondrial content, log normalization and
1511 pearson residuals were computed according to Seurats SCTransform. PCA on 3,000 most variable
1512 features and elbow plot analysis indicated the first 20 principal components to be relevant. These
1513 components were then selected for UMAP (min_dist=0.2), nearest neighbour graph construction
1514 and clustering analysis (resolution = 0.3, nn.eps = 0.5) using Seurat standard workflow, during
1515 which 7 clusters were identified. Subsequently, marker genes were plotted to identify cellular
1516 identities (**Extended Data Fig. 2d-f**).

1517 *Deconvolution analysis of RNA-Seq profiles of iNs*

1518 Marker gene sets for deconvolution analysis were defined with Seurat (version 3.2.2)[75] using the
1519 iN scRNA-Seq dataset including all 7 clusters and all donors. The RNA assay of the scRNA-Seq
1520 count object was log normalized, scaled and the percentage of mitochondrial gene expression was
1521 regressed out. FindAllMarkers was run in order to identify representative genes for each of the 7
1522 clusters setting the following parameters: assay = "RNA", slot = "data", test.use = "MAST",
1523 only.pos = TRUE, return.thresh = 0.01. 2,143 hits were significant at adjusted p value ≤0.01, which
1524 included 1,875 genes in total. The cluster specificity tau was calculated for each gene[76] and the
1525 resulting sets of markers were filtered to keep all hits with average logFC > 0.35 and tau > 0.6.
1526 Consequently, 214 hits covering 210 different genes were used for the deconvolution analysis of
1527 115 RNA-Seq samples of iPSC derived neurons. The deconvolution was implemented using
1528 CIBERSORT based R package bseqsc (version 1.0). The bulk counts were CPM normalized and
1529 the base matrix of reference gene expression profiles was built on the identified marker genes and
1530 the iN scRNA-Seq expression counts. The cluster proportions for the bulk samples were estimated
1531 running bseqsc_proportions on the CPM normalized counts and the base matrix. The distribution
1532 of resulting cluster proportions for all samples in each diagnoses group was then plotted in
1533 **Extended Data Fig. 2g**.

1534 *Comparison of iN scRNA-Seq profiles to human and murine primary cortical snRNA-Seq*

1535 In order to determine the cortical neuronal subtypes and developmental stage that were most
1536 closely related to iN cellular identity, we compared previously published[29] scRNA-Seq data from
1537 the developing mouse cortex at developmental stage P1, P7 and P21. For similarity analysis, we
1538 first determined all genes expressed in 5% or more of all cells in iNs and mouse samples.

1539 Subsequently, we mapped all murine genes to their human orthologs using the ensemble database.
1540 We then aggregated all raw counts per cell identity/cluster and performed VST normalization on
1541 the pseudo-bulk samples followed by pearson correlation analysis and multidimensional scaling.
1542 Since the first two dimensions primarily captured technical variables (e.g. species and lab of
1543 origin), we retained dimension 3 and 4 that separated samples by time points and cellular identity.

1544 miRNAseq

1545 In order to study miRNA-dependent regulation of genes, miRNAseq was performed.

1546 *Sample collection*

1547 Samples were collected and prepared following the same procedure as for the RNAseq. Isolated
1548 and DNAse treated RNA was further processed at Telethon Institute of Genetics and Medicine.

1549 *Library preparation*

1550 Total RNA was quantified using the Qubit 2.0 fluorimetric Assay (Thermo Fisher Scientific) and
1551 sample integrity, based on the RIN (RNA integrity number), was assessed using an RNA
1552 ScreenTape assay on TapeStation 4200 (Agilent Technologies).
1553 Libraries were prepared from 250 ng of total RNA using the smallRNAseq sequencing service
1554 (Next Generation Diagnostics srl) which included, library preparation, quality assessment and
1555 sequencing on a NovaSeq 6000 sequencing system using a single-end, 50 cycle strategy (Illumina
1556 Inc.).

1557 *Data processing*

1558 The raw data were analyzed by Next Generation Diagnostics srl proprietary SmallRNA-seq
1559 pipeline (v 1.0)[77]. Illumina NovaSeq 6000 base call (BCL) files were converted in fastq file
1560 through bcl2fastq. Then, trimming and cleaning with Trimgalore
1561 (https://github.com/FelixKrueger/TrimGalore) was followed by alignment on the hg19 reference
1562 genome using Bowtie[78]. Detection counts were determined with SAMtools[79]. The miRNA genome
1563 was build using miRBase v22. Finally, exported tab-delimited text files included the raw counts
1564 for subsequent analysis.

1565 *Analysis*

1566 microRNA-Seq data was analyzed using with DESeq2 version 1.22.2. Following size factor
1567 estimation, we excluded microRNAs with total read counts less than 100 across all samples.
1568 Subsequently, we performed standard differential expression analysis testing for effect of
1569 diagnosis using differentiation site and sex as covariate including only one microRNA sample per
1570 donor. microRNAs below an adjusted p-value ≤ 0.05 between Ctrl and SCZ were defined as
1571 differential and used in subsequent analysis.

1572 ATAC-Seq

1573 Chromatin structure was assessed by the assay for transposase-accessible chromatin (ATAC).

1574 *Sample collection and library preparation*

1575 iNs were dissociated at D 49 with 135 U Papain and 1,180 U Deoxyribonuclease I (Worthington)
1576 dissolved in 7.5 ml DMEM/ F12 using 1 ml per 6well for 10 min at 37°C. After enhancing
1577 enzymatic dissociation by pipetting up and down, cell suspension was collected in DMEM/F12
1578 supplemented with 10% FBS and RevitaCell Supplement (1:100). After centrifugation at 300 g for
1579 5 min, each pellet was resuspended in 1 ml DMEM/F12/10% FBS/RC and counted with Neubauer

1580 Chamber. 7 x 10^4 cells were centrifuged at 500 g for 5 min at 4 °C and supernatant was discarded
1581 carefully. After resuspending pellet in cold ATAC-Resuspension Buffer I (RSB I) consisting of
1582 1M Tris-HCl (pH 7.4), 5M NaCl and 1M $MgCl_2$ in sterile H_2O containing 0.1% NP40, 0.1%
1583 Tween-20 and 0.01% Digitonin by pipetting up and down 3 times, suspension was incubated for
1584 3 min on ice. 1 ml cold ATAC-RSB II consisting of 1M Tris-HCl (pH 7.4), 5M NaCl and 1M
1585 $MgCl_2$ in sterile H_2O containing 0.1% Tween-20 only was added to each sample on ice and the
1586 tube was inverted 3 times. Nuclei were pelleted by centrifugation at 500g for 10 min at 4°C.
1587 Supernatant was discarded carefully and pellet was resuspended in 52 µl transposition mix
1588 consisting of 25 µl 2x TD buffer, 2.5 µl transposase, 16.5 µl DPBS (+Mg, +Ca), 0.5 µl 1%
1589 Digitonin, 0.5 µl 10% Tween-20 and 5 µl H_2O by pipetting up and down 6 times. Reaction was
1590 incubated in a thermomixer at 1000 rpm for 30 min at 37 °C and was subsequently cleaned up by
1591 using the DNA Clean and Concentrator-5 Kit (Zymo Research). For that purpose, 250 µl DNA
1592 Binding Buffer provided from the kit was added to each 50 µl sample and either stored at -20°C
1593 or further processed. Sample warmed to RT was added to the column and was centrifuged at 10000
1594 g for 30 sec. After washing with 200 µl Wash Buffer, sample was centrifuged again at 10000 g for
1595 30 sec and washing and centrifugation was repeated once. Sample was eluted in 22 µl Elution
1596 Buffer by centrifugation at 10000 g for 30 sec. Eluted DNA was either stored at -20 °C t or
1597 amplified by mixing 20 µl transposed sample with 25 µl 2x NEBNext Master Mix, 2.5 µl 25 µM
1598 Primer Forward (Ad1) and 2.5 µl 25 µM Primer Reverse (Ad2.1, Ad2.3-Ad2.24) and following
1599 the protocol 72 °C for 5 min, 98 °C for 30 s, 6x [98 °C for 10 s, 63 °C for 30 s, 72 °C for 1 min].
1600 Amplified samples were purified by double sided AMPure Beads clean up. To that end, 2x
1601 concentrated Agencourt AMPure XP beads were mixed and warmed to RT for at least 30 min. 2x
1602 concentrated beads were mixed again and 27.5 µl (0.55x) was added to 50 µl PCR reaction. After
1603 mixing by pipetting up and down 10 times, sample was incubated for 10 min at RT and was
1604 subsequently placed on a magnet for 5 min to separate the beads from the solution. Cleared solution
1605 was transferred into a new tube and 17.5 µl (0.35x) 2x concentrated beads were added and mixed
1606 by pipetting up and down 10 min. After incubating 10 min at RT, sample was placed again on a
1607 magnet for 5 min. Cleared solution was discarded this time and pellet was washed with 200 µl
1608 80% ethanol for 1 min at RT. Ethanol was discarded and washing was repeated once. After
1609 removing ethanol completely, sample was dried for 5-10 min at RT while being placed on the
1610 magnet. Off the magnet, pellet was resuspended in 20 µl low TE Buffer by pipetting up and down
1611 10 times and incubated for 5 min at RT. After incubation, reaction was placed on the magnet for
1612 5 min to separate the beads from the sample. 19 µl sample was transferred into a new tube and
1613 quantified by using D1000 ScreenTape on 2200 TapeStation. For that purpose, 3 µl D1000 Sample
1614 Buffer was mixed with 1 µl sample and loaded on the TapeStation. 4 ng of each sample was pooled
1615 together with samples being labelled with different barcodes due to different reverse primers [80]
1616 resulting in pools containing 23 samples each. Each pool was quantified again on a DNA high
1617 sensitivity bioanalyzer chip to confirm properly tagmented libraries showing a nucleosome-like
1618 banding pattern and a minimum concentration of 2 ng/µl. Lower concentrated pools were cleaned
1619 up by using the double sided AMPure Beads clean up as described above and were eluted in 17 µl
1620 low TE Buffer. Quantification on DNA high sensitivity bioanalyzer chip was repeated and 15 µl
1621 library was sent for ATAC sequencing.

1622 *ATACseq analysis*

1623 Paired-end raw ATAC-Seq reads were aligned against the GRCh38 genome using bowtie 2 [81]
1624 (version 2.3.5). Subsequently, duplicates were removed using picard tools and peak calling was
1625 performed using macs2 and standard human genome size (hs parameter). Resulting peak files of

1626 all samples were then merged using diffbind, only retaining those peaks that were present in at
1627 least 6 samples, giving rise to the union peak set employed in all further analyses. Next, bedtools
1628 multicov function was used to count fragments overlapping with peaks by at least one base. The
1629 resulting matrix peak x fragment count matrix was then further analyzed with DESeq2, using the
1630 effective library size (counting only reads overlapping with at least one peak of the union peak set)
1631 for sequencing depth normalization/size factor estimation. Subsequently, dispersions were
1632 estimate using DESeq2's function: estimateDispersions(obj,fitType='local'). Differential peak
1633 enrichment analysis was then performed again using a paired design in DESeq2 with the design
1634 formula ~sex+batch+Factor and the nbinomWaldTest function. No peaks were detected
1635 differentially open between diagnosis groups below an adjusted p-value < 0.1.

1636 Identity verification of sequencing libraries

1637 In order to confirm donor identity of each RNA-Seq, ATAC-Seq and microRNA-Seq library, we
1638 utilized the software verifyBam[82], providing it with the raw bam file and a vcf file containing the
1639 genotypes of all donors. For microRNA-Seq, fastq files were re-aligned to the whole genome using
1640 STAR[63]. Identified swaps were corrected and correct labels were used in subsequent analyses. For
1641 scRNA-Seq data of iNs, we used demuxlet[73] in combination with the aforementioned vcf file to
1642 assign individual cells to one of the four donors that were included in this experiment.

1643 qPCR

1644 Realt-time PCR was performed for experiments in manuscript. For a detailed primer list see **key**
1645 **resources table**.

1646 *Sample collection*

1647 Samples were prepared as described above (4.1.1) and further processed for cDNA synthesis by
1648 using RevertAid H Minus First Strand cDNA Synthesis Kit (Thermo Fisher Scientific).

1649 *cDNA synthesis*

1650 Oligo(dT)18 primer (1µl from 100 µM stock) was added to 500 ng RNA filled up to 11 µl with
1651 DNA/RNAse-free H_2O. After incubation for 5 min at 65 °C, the reaction was kept on ice. 4 µl 5x
1652 Reaction Buffer, 1 µl RiboLock RNase Inhibitor (20 U/ µl), 2 µl 10 mM dNTP Mix and 1 µl
1653 RevertAid H Minus Reverse Transcriptase (200U/ µl) was added to each reaction, incubated for 1
1654 hr at 42 °C and stored at -20 °C or directly used for qPCR. For that purpose, 5 µl 2x SSO Advanced
1655 Biorad Mastermix, 0.25 µl 10 µM Primer Forward, 0.25 µl 10 µM Primer Reverse and 3.5 µl H_2O
1656 were mixed with 1 µl cDNA diluted 1:10 in H_2O and loaded on LightCycler 480 II from Roche or
1657 BIO-RAD CFX thermal cycler following the protocol 95 °C for 2 min, 35x [95 °C for 10 s, 62 °C
1658 for 15 s, 72 °C for 5 s], 60°C for 1 s (2.5 °C/ s), 95 °C continuous (0,11 °C/ s), 45 °C for 1 s.

1659 *Analysis*

1660 For qPCR analysis, CT-values of target gene and reference (e.g. MAP2, RTF2 or Distal/Proximal
1661 UTR, **Supplementary Table 4**) were used to calculate target specific relative expression as 2^(-
1662 $(CT_{target}-CT_{Reference})$) giving rise to normalized transcript levels.
1663 The distal/proximal 3'UTR fold change for the dAPA locus specific analysis was calculated as the
1664 arithmetic ratio between the relative expression of the two different 3'UTR regions belonging to
1665 the same gene locus.
1666 The normalized transcript levels were analyzed by linear mixed models as implemented in the
1667 lme4 R package[83] modeling diagnosis as fixed effect and batch as well as donor (for APA
1668 comparison) as random effect. Significance of the fixed effect was assessed using the two-tailed t-

1669 test as implemented lmerTest package relying Satterthwaite's method for approximating degrees
1670 of freedom[84]. qPCR value distribution as visualized as violin or boxplot. For visualization
1671 purposes, we normalized transcript values for each batch by dividing the respective transcript
1672 abundance levels by the mean across all control samples from entire batch plotted the results.

1673 Western blot

1674 *Harvesting*

1675 iNs were collected at D 49 in 1.4 ml cold DPBS in a 1.5 ml reaction tube and centrifuged at 300 g
1676 for 5 min. Supernatant was discarded and cell pellet was stored at -80 °C until further use.

1677 *Protein extraction*

1678 Cell pellets were thawed on ice and centrifuged for 5 min at 500 x g and 4°C. Remaining DPBS
1679 supernatant was removed by pipetting. Then pellets were washed once with ice-cold DPBS. After
1680 complete aspiration of the supernatant (DPBS), ice-cold lysis buffer/RIPA buffer containing 150
1681 mM NaCl, 1% NP-40, 0.1% SDS, 50 mM Tris Ph8.1, 0.5% sodium deoxycholate and proteinase
1682 inhibitor was added and incubated 5 min on ice. After homogenization by pipetting up and down
1683 5x, samples were incubated additional 30 min with brief vortexing every 5 min. Lysated samples
1684 were then centrifuged for 15 min at 14,000 x g and 4°C. Immediately after centrifugation,
1685 supernatant was transferred to a clean microfuge tube and the concetration was analyzed by
1686 Bradford assay (Biorad) using a BSA standard-curve as reference. Protein extract concentrations
1687 were uniformed to 1µg/µl in lysis buffer and 5µg aliquots were stored at -80°C.

1688 *Digital western blotting*

1689 Sample preparation for digital western blotting using Wes™ (ProteinSimple, USA, PSD95
1690 experiments) or Abby (ProteinSimple, USA, PTBP2 KD experiments) was performed according
1691 to manufactures instructions. First, 400mM DTT solution from EZ Standard Pack 1 was prepared
1692 by addition of 40µl H20 and Fluorescent 5X Master Mix was prepared by addition of 20µl 10X
1693 Sample Buffer and 20µl 400mM DTT solution. Primary antibody dilutions were prepared using
1694 Antibody Diluent 2 (PSD95 1:200, b3TUB 1:50). For each sample, one part (1µl) of 5X
1695 Fluorescent Master Mix and four parts of protein lysates (adjusted with 0.1X Sample Buffer to a
1696 total protein amount of: b3TUB, 0.1µg; PSD95, 1.6µg) were gently mixed, vortexed, denaturated
1697 at 95°C for 5 min, vortexed, spined down, and stored on ice before loading. Pre-filled Plates (12-
1698 230 kDa) were loaded with Antibody Diluent 2, Streptavidin-HRP, Anti-Mouse Secondary HRP
1699 Antibody or Anti-Rabbit Secondary HRP Antibody according to primary antibody application,
1700 Biotinylated Ladder, freshly prepared mix of Luminol-S and Peroxide, and Wash Buffer according
1701 to manufacturer's instructions. Plates were centrifuged for 5 min at 1000g at RT. Digital western
1702 blotting with prepared 12-230 kDa plates and 25-Capillary cartridges for Size based Separation at
1703 Wes™ was performed with default settings.Subsequent analysis were performed with the
1704 "Compass" software (Compass for SW 5.0.1 Mac Beta), on the best exposure time for each
1705 individual run, selected based on to chemiluminescence intensity linearity. determination of the
1706 peak area was performed using 'Dropped line'. Data were exported as Excel files for subsequent
1707 statistical analysis.

1708 *Analysis*

1709 PSD95 intensity values for the high molecular weight (90-95 kDa) were divided by b3Tub
1710 intensity from the same protein extract and $\log_2$ transformed, giving rise to the normalized intensity
1711 ratio (NRI). For PTBP2, intensity values were divided by the intensity of histone 3 (H3) from the

1712 same nuclear extracts. Statistical testing of NRIs (**Supplementary Table 4**) was conducted using
1713 by linear mixed models as implemented in the lme4 R package[83] modeling diagnosis or treatment
1714 as fixed effect and batch as well as donor (for PSD95 analysis) as random effect. Significance of
1715 the fixed effect was assessed using the t-test as implemented lmerTest package relying
1716 Satterthwaite's method for approximating degrees of freedom[84]. Prior to analysis, outliers were
1717 filtered using Tukey's outlier test (including only values within 1.5 x inter-quartile range) in a
1718 batch specific manner for each variable separately.
1719 For visualization purposes, we normalized the NRI values for each batch by dividing the respective
1720 NRI values by the mean NRI from control samples across the entire batch and plotted the results.

1721 Immunocytochemistry (ICC)

1722 In order to investigate differential gene expression on protein level regarding quantity and
1723 localization, immunofluorescent stainings were performed.

1724 *Fixation and staining*

1725 Samples were washed twice with DPBS, fixed with 4% Paraformaldehyde for 15 min at RT and
1726 washed again twice with DPBS. After permeabilization with 0.1% Triton-X-100 in DPBS for 15
1727 min at RT, cells were blocked with 1% BSA and 1% donkey serum in 0.1% Triton-X-100 for 45
1728 min at RT. Primary antibody was added in blocking solution over night at 4 °C. Cells were washed
1729 three times with 0.1% Triton-X-100, and incubated with secondary antibody in blocking solution
1730 for 2.5 hr in the dark at RT. Cells were washed twice with 0.1 Triton-X-100, once with DPBS and
1731 mounted in Aqua-Poly/Mount from Polysciences™.

1732 *iNs maturity analysis*

1733 iNs from Ctrls (n=10) and ISCZ (n=8) were fixed and stained with DAPI, FOXG1, and CUX1 as
1734 described above. Primary image analysis and segmentation was performed using CellInsight CX5
1735 High-Content Screening System and HCS Navigator™ Version 6.6.1 Software from Thermo
1736 Scientific™. Briefly, 3 wells per donor (2 donors with 2 wells, 2 donors with 1 well per donor)
1737 were investigated and 9 fields of view (FOV) were taken at randomly defined but fixed positions
1738 for each well at 20X magnification. Subsequently each image was segmented for the imaging
1739 analysis using Fiji[59] and the BIOVOXXEL toolbox[85], see also https://github.com/biovoxxel, based
1740 on ImageJ, Version 1.15f51. First, nuclei, FOXG1 and CUX1 segmentation masks were separately
1741 applied using the appropriate fluorescent channels. Then, expression of FOXG1 or CUX1 within
1742 a certain cell was defined by an overlap of the FOXG1 or CUX1-segmentation mask with the
1743 DAPI-based nuclei segmentation-defined regions of interests. Number of total cells (DAPI-based
1744 segmentation) and number of cells that express FOXG1 (overlap DAPI segmentation and FOXG1
1745 segmentation) and CUX1 (overlap DAPI segmentation and CUX1 segmentation) were exported
1746 per field of view. Results are shown in **Extended Data Fig. 2b,c**.

1747 *Synapse count analysis*

1748 To measure synapse number in iNs from Ctrls (n=10) and ISCZ (n=10), iNs were fixed and stained
1749 as described above. Synapses were defined by pixel overlaps of the synaptic markers Synapsin
1750 (SYN1) and the neurite/neuronal marker βTubulin. Primary image analysis and segmentation was
1751 performed using CellInsight CX5 High-Content Screening System and HCS Navigator™ Version
1752 6.6.1 Software from Thermo Scientific. Briefly, 30 fields of view (FOV) were taken at randomly
1753 defined but fixed positions for each well at 20X magnification. Subsequently, each image was
1754 segmented into cell body and neurite compartments using the DAPI and βTubulin channel in

1755 combination with morphological and intensity parameters such as size, shape and differences in
1756 pixel intensities.
1757 For that purpose, nuclei were recognized in the DAPI channel while cell bodies were identified by
1758 βTubulin staining overlapping with tagged nuclei at a minimum of 10 %. Neurite segmentation
1759 mask was generated by using βTubulin channel as well. SYN1 spots were identified by
1760 aforementioned parameter settings and one additional channel showing SYN1 staining was
1761 determined. Overlap of puncta was defined as a minimal intersection of 10 % within the cell body
1762 or neurite segmentation masks defined by βTubulin staining[86].
1763 The detailed protocol for segmentation and analysis of CellInsight software is available upon
1764 request as XML file.
1765 Following primary feature segmentation, definition of relevant SYN1 puncta was performed by
1766 intersecting the latter feature masks with those of detected cell bodies and neurites. Only puncta
1767 overlapping with the latter were considered for further analysis. Next, measurements were
1768 collapsed for each FOV, computing the SYN1 puncta density in neurites and cell bodies separately,
1769 by dividing the total number or area of the former puncta per FOV by the total area of either cell
1770 bodies or neurites. Prior to further analysis, FOV were filtered for a minimal and maximal detected
1771 cell body and neurite area, excluding FOVs at the extremes of the distribution (excluding empty
1772 FOVs and high cell body density FOVs). Finally, the resulting density values per FOV were
1773 averaged for each well and used for subsequent statistical analysis.
1774 For latter, we used linear mixed models as implemented in the lme4 R package[83] modeling
1775 diagnosis as fixed effect and batch as well as donor as random effect. Significance of the fixed
1776 effect was assessed using the t-test as implemented lmerTest package relying Satterthwaite's
1777 method for approximating degrees of freedom[84]. Model fit, residual distribution and diagnostics
1778 were evaluated using the R package DHARMa[87]. All well level density values used can be found
1779 in **Supplementary Table 4**.

1780 PTBP2 knockdown

1781 To functionally assess the contribution of PTBP2 to the dAPA in iNs from ISCZ, PTBP2
1782 repression was modulated using shRNAs. To that end, lentiviral particles containing 4 different
1783 shRNAs (**key resources table**) targeting the human PTBP2 transcript (TRC database) or a non-
1784 targeting control lentivirus were produce using the protocol described above. In order to limit the
1785 effect the effects of PTBP2 knockdown on neuronal development/maturation and rather assess its
1786 relevance for o neuronal physiology under steady state conditions, we performed an acute
1787 knockdown towards the end of the differentiation timeline. We evaluated distinct transduction
1788 time-points and duration between day 30 and 65 testing 5, 10 and 15 days of culture under
1789 knockdown conditions to exclude any dependency of the silencing effect on the differentiation
1790 stage, collecting iNs at day 44, 49, 62 and 70. Evaluation of PTBP2 knockdown magnitude and
1791 impact on PSD95 protein levels showed no dependency on transduction time point or duration and
1792 data points for PTBP2 knockdown or PSD95 were pooled into a Ctrl and PTBP2 knockdown
1793 condition. Based on these observations, we selected 15 days of knockdown duration and collection
1794 at day 49 for synapse density analysis, considering the possibility of a lag in PTBP2 knockdown
1795 effect on synapse turnover. Accordingly, iNs were infected in BrainPhys media supplemented with
1796 6µg/ml Polybrene and cultured following the regular protocol.

1797 *Synaptic density analysis in PTBP2^{KD}*

1798 To determine synaptic density changes induced by the downregulation of PTBP2, iNs were fixed
1799 with 4% PFA in DPBS for 10 min at RT, permeabilized with 0.2% Triton-X in DPBS for 10 min

1800 and unspecific epitope recognition was blocked using 0.5% Tween-20 and 1% BSA in DPBS for
1801 60 min. Primary antibody (anti-Syn1 and anti-Tubb3) were incubated in the blocking solution
1802 supplemented with 1% normal donkey serum overnight at 4°C, the excess of antibody was washed
1803 3 times with 0.5% Tween-20 in DPBS for 5 min each wash. Secondary antibodies were incubated
1804 in blocking solution supplemented with 1% normal donkey serum for 60 min at room temperature.
1805 Stained cells were maintained in Aqua-Poly/Mount media at 4°C.
1806 Imaging acquisition was automatized on the CellInsight CX5 High-Content Screening system
1807 using 20x magnification objective (20 field/well, 4 well/condition) with 2048dpi. TIFF file were
1808 exported and analyzed using CellProfiler 4.2.1. Nuclei were detected based on the DAPI channel
1809 using the Adaptive Otsu thresholding method for intensities between 0.5 and 0.9. iN nuclei were
1810 detected and distinguished from the co-cultured mouse astrocytes based on size (diameter between
1811 24 and 70 pixels) and on the absence of chromocenter structures (FilterObjects by
1812 Texture_Correlation and by AreaShape_Compactness). The identified nuclei were then further
1813 used for the identification of the soma as secondary objects (Distance – B method, with 60 pixels
1814 as maximum distance) using the Tubb3 signal.
1815 To avoid any exclusion of soma regions, primary object identification was also performed on the
1816 TUBB3 channel using the Adaptative Otsu thresholding method with intensities between 0.48 and
1817 0.9 and a permissive size interval between 30 and 300 pixels. The two independently detected
1818 soma maks were then combined into a final comprehensive soma mask. Neurite tubeness was
1819 enhanced with a smoothing scale of 1 for features with 20 pixels of maximum size to facilitate the
1820 identification of a partial network (including some soma regions) using the Adaptative with Robust
1821 background thresholding method for intensities between 0.0115 and 0.04 with a typical diameter
1822 between 6 and 400 pixels. Removing from the latter mask the final soma mask we obtained the
1823 Neurite compartment mask. The enhancement of speckles with max size of 5 pixel facilitated the
1824 primary objects identification for Syn1 signals(Adaptative Otsu, intensity 0.04,0.3) Detected
1825 Synapsin objects within the different compartments (Soma and Neurites) were counted, and the
1826 occupied area of all the masks and sub-masks was calculated.

1827 Electrophysiology

1828 *Patch clamp*

1829 Whole-cell current- and voltage-clamp recordings (-70 mV holding potential, >1 GΩ seal
1830 resistance, <20 MΩ series resistance, 8 mV liquid junction potential correction, 3 kHz low-pass
1831 filter, 15 kHz sampling rate) from cultured neurons were conducted at room temperature (23-25°C)
1832 using an EPC9 amplifier (HEKA). Cells were superfused (2-3 ml/min flow rate) with a carbogen
1833 gas (95% O2/5% CO2)-saturated solution containing (in mM): 121 NaCl, 4.2 KCl, 29 NaHCO3,
1834 0.45 NaH2PO4, 0.5 Na2HPO4, 1.1 CaCl2, 1 MgSO4, and 20 D-glucose (Bardy et al., 2015). This
1835 solution additionally contained NBQX (5 µM) and picrotoxin (100 µM) for current-clamp
1836 measurements. For current-clamp measurements, patch pipettes (3-5 MΩ open tip resistance) were
1837 filled with a solution consisting of (in mM): 135 KMeSO4, 8 NaCl, 0.3 EGTA, 10 HEPES, 2 Mg-
1838 ATP, and 0.3 Na-GTP. Current injections were used to depolarize or hyperpolarize the neuron
1839 under investigation. Offline analysis was performed using the Mini Analysis Program (version
1840 6.0.7, Synaptosoft).

1841 Quantitative trait analysis

1842 *Expression quantitative trait (eQTL) analysis*

1843 For eQTLs analysis, RNA-Seq reads were re-aligned to hg19 using the same strategy as outlined
1844 in the section RNA-Seq processing, since all genotype-based analyses were conducted on hg19.
1845 We utilized the gtex-pipeline implemented by the Broad institute for the analysis to preprocess the
1846 data before identifying the eQTLs by linear regression with FastQTL[88]. We only included genes
1847 with ≥ 0.1 TPM and ≥ 6 unnormalized reads in ≥ 20% of the samples. Thereafter each of the
1848 remaining 24,799 genes was inverse normal transformed across samples. We calculated 15 PEER
1849 factors from the resulting expression data, which were used as the covariates, as well as the sex
1850 and differentiation site of each sample for FastQTL.
1851 We identified cis-EQTLs within a 200 kb window of the Transcription Start Site of each included
1852 gene and by performing both a nominal and an adaptive permutation pass, running between 1000
1853 and 10000 permutations, of FastQTL on the data. We also computed the allelic Fold Change as a
1854 comparative measurement of effect size of cis-eQTLs[89]. Subsequently, eQTLs with a multiple
1855 testing corrected permutation based p-value below 0.05 were defined as significant and considered
1856 for further analysis consistent with the GTEx approach.

1857 *microRNA quantitative trait (mirQTL) analysis*

1858 The mirQTL analysis was done analogous to the eQTL analysis, using the GTEx preprocessing
1859 pipeline and FastQTL. We kept genes with ≥ 0.1 TPM and ≥ 3 unnormalized reads in ≥ 10% of
1860 samples, resulting in 832 remaining mature miRNAs. The covariates consisted of the first 3 PEER
1861 factors, omitting the remaining, colinear factors, 3 genotype PCs, 3 miRNA PCs and the sex and
1862 differentiation site of each sample. We ran both a nominal and adaptive permutation pass on the
1863 data, keeping the parameters of the eQTL analyses, but setting the FDR to 0.2.

1864 *Chromatin quantitative trait (caQTL) analysis*

1865 For caQTLs analysis, ATAC-Seq reads were re-aligned to hg19 using the same strategy as outlined
1866 in the section ATAC-Seq processing since all genotype based analyses were conducted on hg19.
1867 Newly aligned bam files were then used for caQTL mapping in combination with RASQUAL[90].
1868 To that end, we created a fragment count table based on the previously identified union peak set
1869 lifted over to hg19 using the UCSC liftover tool (http://genome.ucsc.edu/cgi-bin/hgLiftOver)[91] and
1870 bedtools multicov (see ATAC-Seq data processing). Subsequently, we created a modified VCF
1871 file containing the allele-specific counts derived from the master VCF file using the RASQUAL
1872 toolbox script createASVCF.sh. We only included variants in a 200 kb *cis* window of the
1873 transcription starting sites of each peak and added the -z flag to convert the genome imputation
1874 quality score to allelic probability and the –force flag to include fitting the model for large numbers
1875 of fSNPs and rSNPs, accepting the added computational effort. As covariate, we included sex,
1876 differentiation site and the first PC of the genotype PCA. In addition, we ran RASQUAL with the
1877 -r flag to generate a random permutation of each feature and obtain empirical null distribution of
1878 p-values. Both the original and permuted output values were further processed using eigenMT[92]
1879 to adjust for multiple testing and compare the experimental p-values to the null distribution. To
1880 that end, RASQUAL based p-values were Bonferroni corrected for each peak, using the number
1881 of SNPs tested for each peak. Subsequently, different Bonferroni corrected p-value thresholds
1882 were used to assess the number of peas with at least one significant caQTL in the original and
1883 permuted dataset. Based on this analysis, we selected a Bonferroni corrected p-value threshold of
1884 0.01 yielding an empirical FDR of 0.16 to define the set of significant caQTL peaks.

1885 Overlap of QTLs with human post mortem and GWAS data

1886 For overlap analysis with GWAS data, we downloaded the SCZ GWAS summary statistics from
1887 Pardinas et al.[33] from the PGC website and intersected genomic coordinates of
1888 eQTLs/caQTLs/mirQTLs on hg19. The results are shown in **Fig. 1**. For intersection with eQTLs
1889 from post mortem brain material, we downloaded eQTL summary results[93] from the common mind
1890 consortium[11] (https://www.synapse.org/#!Synapse:syn2759792/wiki/69613) and intersected the
1891 genomic coordinates.

1892 RBP binding motif analysis in 3'UTR sequences

1893 For RBP motif enrichment with the UTR of transcripts subject to APA, we performed
1894 computational motif enrichment using *Transite*[94]. The latter that leverages a large collection of
1895 available RBP and expression data from the ENCODE project. We performed *Transite* analysis
1896 for transcript with increased or decreased distal APA site usage in SCZ separately, using the entire
1897 set of 3'UTR from all gencode genes as background. Resulting enrichment scores and p-values for
1898 the set of transcripts with increased usage of the distal PAS are depicted in **Fig. 5c** with p-values
1899 corrected for multiple testing using the q-value method and listed in **Supplementary Table 3**.
1900 Enrichment analysis for RBP binding site in the set of transcripts with more proximal UTR usage
1901 in SCZ yielded no significant results.

1902 **Data availability**

1903 The data for this project have been deposited in GEO under accession [TBA] or the European
1904 genome phenome archive, accession number [TBA] for privacy protected data.

1905 **Materials & Correspondence**

1906 Materials used in this manuscript are available through Michael J. Ziller (ziller@uni-muenster.de)
1907 and Moritz J. Rossner (Moritz.Rossner@med.uni-muenchen.de), conditional on proper ethics
1908 approval from the requesting institution. A subset of iPSC lines is subject to sharing constraints
1909 due to limited donor consent.

1910 **Methods-only references**

1911 1. Charlson, F.J. *et al.* Global Epidemiology and Burden of Schizophrenia: Findings From the Global Burden
1912 of Disease Study 2016. *Schizophr Bull* **44**, 1195-1203 (2018).
1913 2. Hilker, R. *et al.* Heritability of Schizophrenia and Schizophrenia Spectrum Based on the Nationwide Danish
1914 Twin Register. *Biol Psychiatry* **83**, 492-498 (2018).
1915 3. Trubetskoy, V. *et al.* Mapping genomic loci implicates genes and synaptic biology in schizophrenia. *Nature*
1916 **604**, 502-508 (2022).
1917 4. Singh, T. *et al.* Rare coding variants in ten genes confer substantial risk for schizophrenia. *Nature* **604**, 509-
1918 516 (2022).
1919 5. Howard, D.M. *et al.* Genome-wide meta-analysis of depression identifies 102 independent variants and
1920 highlights the importance of the prefrontal brain regions. *Nat Neurosci* **22**, 343-352 (2019).
1921 6. Mullins, N. *et al.* Genome-wide association study of more than 40,000 bipolar disorder cases provides new
1922 insights into the underlying biology. *Nat Genet* **53**, 817-829 (2021).
1923 7. The Network and Pathway Analysis Subgroup of the Psychiatric Genomics Consortium. Psychiatric genome-
1924 wide association study analyses implicate neuronal, immune and histone pathways. *Nat Neurosci* **18**, 199-
1925 209 (2015).
1926 8. Wang, D. *et al.* Comprehensive functional genomic resource and integrative model for the human brain.
1927 *Science (New York, N.Y.)* **362**, eaat8464 (2018).
1928 9. Schrode, N. *et al.* Synergistic effects of common schizophrenia risk variants. *Nat Genet* **51**, 1475-1485
1929 (2019).
1930 10. Sekar, A. *et al.* Schizophrenia risk from complex variation of complement component 4. *Nature* **530**, 177-83
1931 (2016).

11. Fromer, M. *et al.* Gene expression elucidates functional impact of polygenic risk for schizophrenia. *Nat Neurosci* **19**, 1442-1453 (2016).
12. Bryois, J. *et al.* Evaluation of chromatin accessibility in prefrontal cortex of individuals with schizophrenia. *Nat Commun* **9**, 3121 (2018).
13. Gandal, M.J. *et al.* Transcriptome-wide isoform-level dysregulation in ASD, schizophrenia, and bipolar disorder. *Science* **362**(2018).
14. Dobbyn, A. *et al.* Landscape of Conditional eQTL in Dorsolateral Prefrontal Cortex and Co-localization with Schizophrenia GWAS. *Am J Hum Genet* **102**, 1169-1184 (2018).
15. Mayr, C. What Are 3' UTRs Doing? *Cold Spring Harb Perspect Biol* **11**(2019).
16. Li, L. *et al.* An atlas of alternative polyadenylation quantitative trait loci contributing to complex trait and disease heritability. *Nat Genet* **53**, 994-1005 (2021).
17. Park, C.Y. *et al.* Genome-wide landscape of RNA-binding protein target site dysregulation reveals a major impact on psychiatric disorder risk. *Nat Genet* **53**, 166-173 (2021).
18. Kircher, T. *et al.* Neurobiology of the major psychoses: a translational perspective on brain structure and function-the FOR2107 consortium. *Eur Arch Psychiatry Clin Neurosci* **269**, 949-962 (2019).
19. Bruckl, T.M. *et al.* The biological classification of mental disorders (BeCOME) study: a protocol for an observational deep-phenotyping study for the identification of biological subtypes. *BMC Psychiatry* **20**, 213 (2020).
20. Krcmar, L. *et al.* The multimodal Munich Clinical Deep Phenotyping study to bridge the translational gap in severe mental illness treatment research. *Front Psychiatry* **14**, 1179811 (2023).
21. Budde, M. *et al.* A longitudinal approach to biological psychiatric research: The PsyCourse study. *Am J Med Genet B Neuropsychiatr Genet* (2018).
22. Lee, P.H. *et al.* Genomic Relationships, Novel Loci, and Pleiotropic Mechanisms across Eight Psychiatric Disorders. *Cell* **179**, 1469-1482.e11 (2019).
23. Anttila, V. *et al.* Analysis of shared heritability in common disorders of the brain. *Science* **360**(2018).
24. Hoffmann, A., Ziller, M. & Spengler, D. Childhood-Onset Schizophrenia: Insights from Induced Pluripotent Stem Cells. *Int J Mol Sci* **19**(2018).
25. Brennand, K.J. *et al.* Modelling schizophrenia using human induced pluripotent stem cells. *Nature* **473**, 221-5 (2011).
26. Nehme, R. *et al.* Combining NGN2 Programming with Developmental Patterning Generates Human Excitatory Neurons with NMDAR-Mediated Synaptic Transmission. *Cell Rep* **23**, 2509-2523 (2018).
27. Baron, M. *et al.* A Single-Cell Transcriptomic Map of the Human and Mouse Pancreas Reveals Inter- and Intra-cell Population Structure. *Cell Syst* **3**, 346-360 e4 (2016).
28. Howard, D. *et al.* An in vitro whole-cell electrophysiology dataset of human cortical neurons. *Gigascience* **11**(2022).
29. Yuan, W. *et al.* Temporally divergent regulatory mechanisms govern neuronal diversification and maturation in the mouse and marmoset neocortex. *Nat Neurosci* **25**, 1049-1058 (2022).
30. Geaghan, M. & Cairns, M.J. MicroRNA and Posttranscriptional Dysregulation in Psychiatry. *Biol Psychiatry* **78**, 231-9 (2015).
31. Forrest, M.P. *et al.* Open Chromatin Profiling in hiPSC-Derived Neurons Prioritizes Functional Noncoding Psychiatric Risk Variants and Highlights Neurodevelopmental Loci. *Cell Stem Cell* **21**, 305-318 e8 (2017).
32. Flaherty, E. *et al.* Neuronal impact of patient-specific aberrant NRXN1alpha splicing. *Nat Genet* **51**, 1679-1690 (2019).
33. Pardinas, A.F. *et al.* Common schizophrenia alleles are enriched in mutation-intolerant genes and in regions under strong background selection. *Nat Genet* **50**, 381-389 (2018).
34. Hauberg, M.E. *et al.* Analyzing the Role of MicroRNAs in Schizophrenia in the Context of Common Genetic Risk Variants. *JAMA Psychiatry* **73**, 369-77 (2016).
35. Yao, Y. *et al.* Cell type-specific and cross-population polygenic risk score analyses of MIR137 gene pathway in schizophrenia. *iScience* **24**, 102785 (2021).
36. You, X. *et al.* Investigating aberrantly expressed microRNAs in peripheral blood mononuclear cells from patients with treatmentresistant schizophrenia using miRNA sequencing and integrated bioinformatics. *Mol Med Rep* **22**, 4340-4350 (2020).
37. Yu, H.-c. *et al.* Alterations of miR-132 are novel diagnostic biomarkers in peripheral blood of schizophrenia patients. *Progress in Neuro-Psychopharmacology and Biological Psychiatry* **63**, 23-29 (2015).
38. Nanou, E. & Catterall, W.A. Calcium Channels, Synaptic Plasticity, and Neuropsychiatric Disease. *Neuron* **98**, 466-481 (2018).

39. Tian, B. & Manley, J.L. Alternative polyadenylation of mRNA precursors. *Nat Rev Mol Cell Biol* **18**, 18-30 (2017).
40. Shah, A., Mittleman, B.E., Gilad, Y. & Li, Y.I. Benchmarking sequencing methods and tools that facilitate the study of alternative polyadenylation. *Genome Biol* **22**, 291 (2021).
41. Lopez-Murcia, F.J., Reim, K., Jahn, O., Taschenberger, H. & Brose, N. Acute Complexin Knockout Abates Spontaneous and Evoked Transmitter Release. *Cell Rep* **26**, 2521-2530 e5 (2019).
42. Mitok, K.A., Keller, M.P. & Attie, A.D. Sorting through the extensive and confusing roles of sortilin in metabolic disease. *J Lipid Res* **63**, 100243 (2022).
43. Finucane, H.K. *et al.* Heritability enrichment of specifically expressed genes identifies disease-relevant tissues and cell types. *Nat Genet* **50**, 621-629 (2018).
44. Hwang, H.W. *et al.* cTag-PAPERCLIP Reveals Alternative Polyadenylation Promotes Cell-Type Specific Protein Diversity and Shifts Araf Isoforms with Microglia Activation. *Neuron* **95**, 1334-1349 e5 (2017).
45. Beveridge, N.J. & Cairns, M.J. MicroRNA dysregulation in schizophrenia. *Neurobiol Dis* **46**, 263-71 (2012).
46. Koopmans, F. *et al.* SynGO: An Evidence-Based, Expert-Curated Knowledge Base for the Synapse. *Neuron* **103**, 217-234 e4 (2019).
47. Okita, K. *et al.* An efficient nonviral method to generate integration-free human-induced pluripotent stem cells from cord blood and peripheral blood cells. *Stem Cells* **31**, 458-66 (2013).
48. Chou, B.K. *et al.* A facile method to establish human induced pluripotent stem cells from adult blood cells under feeder-free and xeno-free culture conditions: a clinically compliant approach. *Stem Cells Transl Med* **4**, 320-32 (2015).
49. Diecke, S. *et al.* Novel codon-optimized mini-intronic plasmid for efficient, inexpensive, and xeno-free induction of pluripotency. *Sci Rep* **5**, 8081 (2015).
50. Danecek, P., McCarthy, S.A., HipSci, C. & Durbin, R. A Method for Checking Genomic Integrity in Cultured Cell Lines from SNP Genotyping Data. *PLoS One* **11**, e0155014 (2016).
51. Danecek, P. *et al.* Twelve years of SAMtools and BCFtools. *Gigascience* **10**(2021).
52. Guo, Y. *et al.* Illumina human exome genotyping array clustering and quality control. *Nat Protoc* **9**, 2643-62 (2014).
53. Kilpinen, H. *et al.* Common genetic variation drives molecular heterogeneity in human iPSCs. *Nature* **546**, 370-375 (2017).
54. Wray, N.R. *et al.* Genome-wide association analyses identify 44 risk variants and refine the genetic architecture of major depression. *Nat Genet* **50**, 668-681 (2018).
55. Ge, T., Chen, C.Y., Ni, Y., Feng, Y.A. & Smoller, J.W. Polygenic prediction via Bayesian regression and continuous shrinkage priors. *Nat Commun* **10**, 1776 (2019).
56. Zarrei, M. *et al.* A large data resource of genomic copy number variation across neurodevelopmental disorders. *NPJ Genom Med* **4**, 26 (2019).
57. Marshall, C.R. *et al.* Contribution of copy number variants to schizophrenia from a genome-wide study of 41,321 subjects. *Nat Genet* **49**, 27-35 (2017).
58. Kent, W.J. *et al.* The human genome browser at UCSC. *Genome Res* **12**, 996-1006 (2002).
59. Schindelin, J. *et al.* Fiji: an open-source platform for biological-image analysis. *Nat Methods* **9**, 676-82 (2012).
60. Bock, C. *et al.* Reference Maps of human ES and iPS cell variation enable high-throughput characterization of pluripotent cell lines. *Cell* **144**, 439-52 (2011).
61. Tsankov, A.M. *et al.* A qPCR ScoreCard quantifies the differentiation potential of human pluripotent stem cells. *Nat Biotechnol* **33**, 1182-92 (2015).
62. Zhang, Y. *et al.* Rapid single-step induction of functional neurons from human pluripotent stem cells. *Neuron* **78**, 785-98 (2013).
63. Dobin, A. *et al.* STAR: ultrafast universal RNA-seq aligner. *Bioinformatics* **29**, 15-21 (2013).
64. Rummel, C.K. *et al.* Cell type and condition specific functional annotation of schizophrenia associated non-coding genetic variants. *bioRxiv* (2023).
65. Karapetyan, A. transcriptR: An Integrative Tool for ChIP- And RNA-Seq Based Primary Transcripts Detection and Quantification. (2022).
66. Szkop, K.J., Moss, D.S. & Nobeli, I. flexiMAP: a regression-based method for discovering differential alternative polyadenylation events in standard RNA-seq data. *Bioinformatics* **37**, 1461-1464 (2021).
67. Xia, Z. *et al.* Dynamic analyses of alternative polyadenylation from RNA-seq reveal a 3'-UTR landscape across seven tumour types. *Nat Commun* **5**, 5274 (2014).

68. Storey, J.D. The positive false discovery rate: A Bayesian interpretation and the q-value. *Annals of Statistics* **31**, 2013-2035 (2003).
69. Quinlan, A.R. & Hall, I.M. BEDTools: a flexible suite of utilities for comparing genomic features. *Bioinformatics* **26**, 841-2 (2010).
70. Bulik-Sullivan, B. *et al.* An atlas of genetic correlations across human diseases and traits. *Nat Genet* **47**, 1236-41 (2015).
71. Xie, Z. *et al.* Gene Set Knowledge Discovery with Enrichr. *Curr Protoc* **1**, e90 (2021).
72. Zhao, S., Li, C.I., Guo, Y., Sheng, Q. & Shyr, Y. RnaSeqSampleSize: real data based sample size estimation for RNA sequencing. *BMC Bioinformatics* **19**, 191 (2018).
73. Kang, H.M. *et al.* Multiplexed droplet single-cell RNA-sequencing using natural genetic variation. *Nat Biotechnol* **36**, 89-94 (2018).
74. Team, R.C. R: A Language and Environment for Statistical Computing. (R Foundation for Statistical Computing, Vienna, Austria, 2019).
75. Stuart, T. *et al.* Comprehensive Integration of Single-Cell Data. *Cell* **177**, 1888-1902 e21 (2019).
76. Kryuchkova-Mostacci, N. & Robinson-Rechavi, M. A benchmark of gene expression tissue-specificity metrics. *Brief Bioinform* **18**, 205-214 (2017).
77. Krueger, F.J., F.; Ewels, P.; Afyounian, E.; Schuster-Boeckler, B. TrimGalore. (2021).
78. Langmead, B., Trapnell, C., Pop, M. & Salzberg, S.L. Ultrafast and memory-efficient alignment of short DNA sequences to the human genome. *Genome Biol* **10**, R25 (2009).
79. Li, H. *et al.* The Sequence Alignment/Map format and SAMtools. *Bioinformatics* **25**, 2078-9 (2009).
80. Buenrostro, J.D., Wu, B., Chang, H.Y. & Greenleaf, W.J. ATAC-seq: A Method for Assaying Chromatin Accessibility Genome-Wide. *Current protocols in molecular biology* **109**, 21.29.1-21.29.9 (2015).
81. Langmead, B. & Salzberg, S.L. Fast gapped-read alignment with Bowtie 2. *Nat Methods* **9**, 357-9 (2012).
82. Jun, G. *et al.* Detecting and estimating contamination of human DNA samples in sequencing and array-based genotype data. *Am J Hum Genet* **91**, 839-48 (2012).
83. Bates, D., Mächler, M., Bolker, B. & Walker, S. Fitting Linear Mixed-Effects Models Using lme4. *Journal of Statistical Software* **67**, 1 - 48 (2015).
84. Kuznetsova, A., Brockhoff, P.B. & Christensen, R.H.B. lmerTest Package: Tests in Linear Mixed Effects Models. *Journal of Statistical Software* **82**(2017).
85. Bocher, J. The BioVoxxel Image Processing and Analysis Toolbox. in *EuBIAS-Conference* (2015).
86. ThermoFisherScientificInc. Thermo Scientific Cellomics® Neuronal Profiling V4. in *V4 Version* (Thermo Fisher Scientific Inc., Pittsburgh, Pennsylvania 15219, USA).
87. Hartig, F. DHARMa: residual diagnostics for hierarchical (multi-level/mixed) regression models. (https://cran.r-project.org/, 2021).
88. Ongen, H., Buil, A., Brown, A.A., Dermitzakis, E.T. & Delaneau, O. Fast and efficient QTL mapper for thousands of molecular phenotypes. *Bioinformatics* **32**, 1479-85 (2016).
89. Mohammadi, P., Castel, S.E., Brown, A.A. & Lappalainen, T. Quantifying the regulatory effect size of cis-acting genetic variation using allelic fold change. *Genome Res* **27**, 1872-1884 (2017).
90. Kumasaka, N., Knights, A.J. & Gaffney, D.J. Fine-mapping cellular QTLs with RASQUAL and ATAC-seq. *Nat Genet* **48**, 206-13 (2016).
91. Kuhn, R.M., Haussler, D. & Kent, W.J. The UCSC genome browser and associated tools. *Brief Bioinform* **14**, 144-61 (2013).
92. Davis, J.R. *et al.* An Efficient Multiple-Testing Adjustment for eQTL Studies that Accounts for Linkage Disequilibrium between Variants. *Am J Hum Genet* **98**, 216-24 (2016).
93. Hoffman, G.E. *et al.* CommonMind Consortium provides transcriptomic and epigenomic data for Schizophrenia and Bipolar Disorder. *Sci Data* **6**, 180 (2019).
94. Krismer, K. *et al.* Transite: A Computational Motif-Based Analysis Platform That Identifies RNA-Binding Proteins Modulating Changes in Gene Expression. *Cell Rep* **32**, 108064 (2020).

Acknowledgments

First, we would like to thank the patients for their study participation and tissue donation. We would like to thank the entire Ziller and Rossner lab team as well as many colleagues from the Department of Psychiatry at the LMU Munich, Germany, and the Department of Translational Research in Psychiatry, MPIP, Germany. We acknowledge the expert help of the Douglas–Bell Canada Brain Bank staff (J. Prud'homme, M. Bouchouka and A. Baccichet), and H. Djambazian

at the MUGQIC. Moreover, we thank Jan Brocher from BioVoxxel for his excellent help with imaging analysis and Lucio Di Filippo for his support of the microRNA library preparation.
This study used data from the CommonMind consortium provided through NIMH. Data for this publication were obtained from NIMH Repository & Genomics Resource, a centralized national biorepository for genetic studies of psychiatric disorders. Data were generated as part of the CommonMind Consortium supported by funding from Takeda Pharmaceuticals Company Limited, F. Hoffman-La Roche Ltd and NIH grants R01MH085542, R01MH093725, P50MH066392, P50MH080405, R01MH097276, RO1-MH-075916, P50M096891, P50MH084053S1, R37MH057881, AG02219, AG05138, MH06692, R01MH110921, R01MH109677, R01MH109897, U01MH103392, and contract HHSN271201300031C through IRP NIMH. Brain tissue for the study was obtained from the following brain bank collections: the Mount Sinai NIH Brain and Tissue Repository, the University of Pennsylvania Alzheimer's Disease Core Center, the University of Pittsburgh NeuroBioBank and Brain and Tissue Repositories, and the NIMH Human Brain Collection Core. CMC Leadership: Panos Roussos, Joseph Buxbaum, Andrew Chess, Schahram Akbarian, Vahram Haroutunian (Icahn School of Medicine at Mount Sinai), Bernie Devlin, David Lewis (University of Pittsburgh), Raquel Gur, Chang-Gyu Hahn (University of Pennsylvania), Enrico Domenici (University of Trento), Mette A. Peters, Solveig Sieberts (Sage Bionetworks), Thomas Lehner, Stefano Marenco, Barbara K. Lipska (NIMH).
This work was supported by BMBF, eMed grant numbers 01ZX1504, 01ZX1706A (MJZ), Else-Kroener-Fresenius Stiftung, grant A54 (MJZ), Research grants provided by Boehringer Ingelheim and the BMBF (FKZ 1EK2101D) (MJR), the Näder Foundation (PF, MJR), Else Kröner-Fresenius Research School for Translational Psychiatry (FJR), Munich Clinician Scientist Program (MCSP), FöFoLe 009/2019 (FJR), German Research Foundation, grants FOR2107 DA1151/5-1 and DA1151/5-2 (UD), Intramural Research Program of the NIMH, ZIA-MH002810 (FC), Italian Ministry of Health (Piano Operativo Salute Traiettoria 3, "Genomed"), Fondazione Telethon Core Grant, Armenise-Harvard Foundation Career Development Award, European Research Council (grant agreement 759154, CellKarma), and the Rita-Levi Montalcini program from MIUR (DC), and Rita-Levi Montalcini program from MIUR (MC).

Author contributions

iPSC generation: AH, FJR., AH, MG, CR, SG, NG, SM, VS, VA; iPSC characterization: AH, FJR, RA, AH, CR, SM, LT, LJB, MRH, SP, SG, NG, VA, SS, MW; Differentiation experiments: AH, FJR, SG, NG, AH, BK; Omics profiling: AH, MG, SR, RA, AH, CR, MR, DC; Molecular biology experiments: AH, FJR, MG; Imaging and imaging analysis: AH, FJR, MG, RA, SM, AA, MJZ; Electrophysiology: AH, DM, BH, EMW, VS, ME; Bioinformatics: LT, LW, VM, LJB, MJZ; Planned experiments: AH, FJR, MG; Fibroblast collection/processing: CR, AH; Provided critical resources incl. PBMC collection and patient characterization: FR, SG, NG, IP, TOS, SDW, FJM, AS, PF, AH, UD, IN, TK, GT, EBB; Data visualization and curation: FJR, AH and MJZ with the help of all authors; Wrote the paper: MJZ, FJR, DS, AH with the help of all authors; Critically revised the manuscript: EBB, MJR; Acquired Funding: MJZ, MJR; Supervised the work: MJZ, MJR; Conceived study, designed experiments and analyses: MJZ.

Competing interests

SG and MCW are part-time employees by and shareholders of Systasy Bioscience GmbH, Munich, Germany. MJR is shareholder and consultant of Systasy Bioscence GmbH. DC is founder, shareholder, and consultant of NEGEDIA (Next Generation Diagnostic) is founder, shareholder,

2142 and consultant of Next Generation Diagnostic srl. Sara Riccardo is an employee of NEGEDIA.
2143 All other authors declare that they have no competing interests.